NTNU
Norwegian University of
Science and Technology

Dielectric response and electrical conductivity of mass impregnated HVDC cable insulation

Lars Erik Pettersen

Master of Science in Electric Power Engineering
Submission date: June 2018
Supervisor: Erling Ildstad, IEL

Norwegian University of Science and Technology
Department of Electric Power Engineering

NORGES TEKNISK-NATURVITENSKAPELIG UNIVERSITET

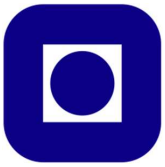

Hovedoppgave våren 2018

Student:	Lars Erik Pettersen	larsepe@stud.ntnu.no
Supervisor:	Prof. Erling Ildstad	erling.ildstad@elkraft.ntnu.no
Co-supervisor:	Stip. Gunnar Håkonseth	hakonseth@ntnu.no

Title: **Dielectric response and electrical conductivity of mass impregnated HVDC cable insulation.**

Tittel: **Dielektrisk respons og elektrisk ledningsevne i masseimpregnert HVDC kabelisolasjon.**

Today, high voltage direct current (HVDC) cables, used for long distance subsea transfer of electric energy, are designed using either XPLE or mass-impregnated non-draining (MIND) paper are used as insulation. Mass-impregnated HVDC cables, insulated with paper strips that are impregnated with viscous oil, is still the state-of-the art technology for the longest subsea cable connections. It has been in use since the early1950´s and is considered a mature type of insulation system. Recent new results from conductivity measurements and electric field calculations indicate, however, that it seems possible to increase the maximum load capacity of such cables, by increasing both the maximum current load capacity and the applied DC voltage.

The main purpose of this thesis work is to provide new data that can be used to facilitate such design improvements.

The main question addressed is:

- How does the dielectric response and DC conductivity of mass insulated HVDC insulation vary with temperature and electric stress?

In general, the electric field in HVDC cables strongly dependent on voltage level, temperature and duration of voltage application. Turning the voltage on or off, changing the load and changing the polarity strongly affect the internal electric field distribution. The steady state electric field distribution between the paper layers and the mass filled butt-gaps is of particular interest.

The thesis is mainly of experimental character and expected to constitute:

- A literature survey including previous results and theoretical models, forming the base for expected electric field distributions and the suggested test methods.
- Design and description of the laboratory setups used, including preparation of electrodes, samples with different thickness and mass content and test procedure.
- Experimental characterization of the samples with respect to dielectric response and DC conductivity versus temperature and electric stress.
- Comparison and evaluation of the experimental results with respect to previous works and existing theoretical assumptions regarding the electric field distribution within such cable insulation.
- Conclusions regarding interpretation of the results and suggestions for further work.

The details of the test program will be decided in cooperation with the supervisor.

Start: 18. Januar 2018
Innlevering: 17. Juni 2018

Preface

This thesis is a continuation of the specialization project in [1] and the final work of the 2-year MSc in Electric Power Engineering at Department of Electric Power Engineering at the Norwegian University of Science and Technology (NTNU). The work was performed during the spring semester of 2018. The purpose of this thesis is to gather data which facilitates design improvements of oil-impregnated paper insulation used in HVDC cables.

My thanks goes to my supervisor prof. Erling Ildstad and co-supervisor ph.d-candidate Gunnar Håkonseth for excellent guidance throughout the course of the semester. I would like to extend my thanks to Knut B. Liland and Torbjørn Andersen Ve at SINTEF Energy Research and the rest of the staff at the institute of Electric Power Engineering for aiding me with the laboratory work. Additional thanks goes to my fellow student Magnus Erlend Tangen for insightful discussions and feedback throughout the course of the entire study. Lastly, I want to thank my parents, Line and Jon Pettersen, sister, Annbjørg Christiane Pettersen, and girlfriend, Jeanette Marí Pedersen, for continuous support during my studies.

Trondheim, June 2018

Lars Erik Pettersen

Abstract

The main purpose of this thesis has been to gather data which facilitates design improvements of oil-impregnated paper insulation used in HVDC cables. Conductivities and loss tangents were gathered for this purpose. Several minor studies for improving the methodology was conducted throughout the thesis.

Samples of oil-impregnated paper and modified samples with oil pockets (called bulk oil samples) and butt gaps were constructed and subjected to several voltages and temperatures in order to obtain polarization and depolarization currents. These currents were then utilized to calculate the conductivity of the various samples. Conductivities of paper were obtained from literature while conductivities of oil were derived from measurements.

The method ”Polarization Depolarization Current” (PDC) was used to obtain the currents by use of a laboratory setup. The loss tangent was obtained from the Hamon approximation where the goal was to verify the applicability in paper, bulk oil and butt gap samples.

Results from the main study showed that the conductivity dependency of paper on electric field strength and temperature was in accordance with the literature. Voltage across the oil in bulk oil samples differed significantly from zero, as opposed to previous assumptions of zero voltage across the bulk oil. Steady state current in bulk oil samples were exponential with respect to voltage but turned linear with increasing oil volume. Conductivity of oil and paper were in the same range, as opposed to previous assumptions of a higher conductivity for oil. Conductivity of oil versus electric field strength in oil showed an exponential dependency.

Calculated DC currents of a bulk oil sample compared to measured values showed equal magnitudes at low voltages but different exponential rate of rise. A sensitivity analysis showed that conductivity of paper dominates the calculated DC current. The Hamon approximation was applicable for paper samples but not for bulk oil and butt gap samples.

Results from the minor studies showed that PDC is viable for monitoring the impregnation process. It showed that most of the absorption of oil into paper occurs during the first 12 hours. Currents in dried paper were 10 times higher than impregnated paper. Insufficient polarization durations significantly affects the DC currents at low voltage. The samples required at least one day to reach thermal equilibrium after a temperature drop. Sample with at least 5 sheets of paper are applicable for PDC measurements.

Sammendrag

Hovedformålet med denne denne master oppgaven har vært å samle data som muliggjør forbedringer av designet i oljeimpregnert papirisolasjon som brukes i HVDC-kabler. Ledningsevne og tapsvinkel ble målt og flere studier for å forbedre metodikken ble gjennomført gjennom hele oppgaven.

Prøver av oljeimpregnert papir og modifiserte prøver med oljelommer (kalt bulkoljeprøver) og butt gap ble konstruert og påsatt flere spenninger og temperaturer. Resulterende polarisasjon og depolarisasjonsstrømmer ble målt. Disse strømmene ble benyttet for å beregne ledningsevnen til de forskjellige prøvene. Papirledningsevnen ble hentet fra litteraturen mens oljens ledningsevne ble avledet fra måleresultater.

Metoden "Polarization Depolarization Current" (PDC) ble brukt til å måle polarisasjons- og depolarisasjonsstrømmene ved bruk av et laboratorieoppsett. Stabil strøm ved enden av polarisasjonsperioden (kalt DC strøm) var benyttet for å beregne ledningsevner. Tapsvinkelen ble beregnet ved bruk av Hamon approximasjonen hvor målet var å verifisere anvendeligheten av metoden i papir, bulkolje og butt gap prøver.

Resultatene fra hovedundersøkelsen viste at ledningsevnen av papir på elektrisk feltstyrke og temperatur var i samsvar med litteraturen. Spenning over oljen i bulkoljeprøvene var ulik null, i motsetning til tidligere antagelser om null spenning over bulkoljen. DC strømmer i bulkoljeprøver var eksponentiell med hensyn på påtrykt spenning, men ble lineær med økende oljevolum. Ledningsevne av olje og papir var i samme størrelserorden, i motsetning til tidligere antagelser om at oljen har større ledningsevne. Ledningsevnen i olje med hensyn på elektrisk feltstyrke i olje viste en eksponentiell avhengighet.

Beregnede DC strømmer av en bulkoljeprøve sammenlignet med målte verdier viste like størrelser ved lave spenninger, men forskjellig eksponensiell stigningshastighet. En sensitivitetsanalyse viste at ledningsevnen av papir dominerer beregnede DC strømmer. Hamon approximasjonen var anvendelig for papirprøver, men ikke for bulkolje og buttgapsprøver.

Resultatene fra de metodikkstudiene viste at PDC kan benyttes for overvåking av impregneringsprosessen. Det viste at det meste av absorpsjonen av olje til papir oppstår i løpet av de første 12 timene. DC strøm i tørket papir var 10 ganger høyere enn impregnert papir. Utilstrekkelig polariseringsvarighet påvirker størrelsen på DC stømmer ved lave spenninger. Prøvene krever minst én dag for å oppnå termisk likevekt etter et temperaturfall. Prøver med minst 5 lag papir kan benyttes til PDC målinger.

Table of Contents

List of Tables

List of Figures

Abbreviations

MIND = Mass Impregnated Non-Draining
PDC = Polarization Depolarization Current
HVDC = High Voltage Direct Current
AC = Alternating Current
DC = Direct Current
PEA = Piezo Electro-Acoustic
PTFE = Polytetrafluoreten

Chapter 1

Introduction

Mass-impregnated non-draining (MIND) paper insulation has been used since the 1950's and is still the choice for the longest high voltage direct current (HVDC) subsea cables [2]. These cables consist of paper strips wrapped helically around a conductor and impregnated with high-viscous mineral oil. The paper strips are wrapped in such a way that gaps, called "butt gaps", are left between adjacent strips which allows bending of the cable. During the impregnation process, oil fills the fibrous structure in the paper and butt gaps.

HVDC cables have long lifetimes but with an increasing demand for transfer of electrical energy their capacity may become insufficient. However, recent results of conductivity and electrical field distribution indicates a possibility of increasing the total capacity by increasing both maximum load current and DC voltage. The main purpose of the work in this thesis is to gather data which facilitates such capacity improvements. This thesis is a continuation of the specialization project described in [1].

It is well known from previous studies that the conductivity of oil impregnated paper insulation is heavily dependent on electrical field strength, temperature and duration of applied DC voltage [3]. However, butt gaps in combination with oil impregnated paper is less studied. Hence, the main motivation for the work in this thesis is to obtain the conductivity of oil and investigate its dependency of voltage which enables calculations of butt gaps.

Obtaining the conductivity is done utilizing the method of "Polarization Depolarization Current" (PDC). This method consists of charging a dielectric sample with a DC voltage and measure the polarization current and then discharging the sample by grounding it and measure the depolarization current. At the end of the polarization duration, the steady state current flows which is used for calculating the conductivity of the dielectric sample. This steady state current is referred to as "DC current" in this report. Oil impregnated paper is referred to as "paper".

As the focus of this thesis is obtaining conductivity of oil and calculating the DC current in butt gaps, samples of paper and samples with strips of paper are created and impregnated

in oil. The latter samples contains small channels of oil between the strips to simulate one layer of butt gaps. The volume of oil in this configuration is small, thus modified paper samples containing large pockets of oil in series with paper are created to amplify the effect of oil in the system. Samples with paper strips are called ”butt gap samples” and samples with pockets of oil are called ”bulk oil samples”.

It is of interest to verify the methodology in this thesis by comparing obtained conductivity of paper with literature and then to further study the oil in combination with paper. Previous studies have shown that conductivity in samples with only oil and bulk oil in series with few layers of paper show no clear dependency of voltage [4, 5]. Hence, both bulk oil and butt gap samples are designed with various amounts of oil to achieve a wide range of paper and oil volume combinations. Due to lack of mechanical strength in the bulk oil volumes, these samples are modified with an added mechanical support to reduce the risk of collapse in the oil volume. A separate electrode, called ”bulk oil electrode”, is created to enable PDC measurements with this modification.

Due to the amount of samples investigated in this thesis, a flexible system is implemented where stacks of paper, butt gaps and bulk oils are combined into samples. These stacks contains either a few layers of paper, only the bulk oil volume or butt gap area. This way, the stacks are re-arranged to form any desired sample. All stacks are impregnated simultaneously.

The loss tangent $\tan(\delta)$ is gathered by use of the approximation invented by Hamon [6]. In the specialization project, this approximation was found to be viable when studying paper samples [1]. Hence, the applicability and results when studying bulk oil and butt gap samples are investigated in this thesis. Paper samples are also investigated to confirm the validity found in [1].

This thesis also contains minor studies with focus to improve the methodology. Prolonged polarization and depolarization durations, PDC measurement during impregnation and distortion from injection of charges are among the studies conducted.

Chapter 2

Theoretical background

This chapter contains the relevant theory. The samples were arranged in a parallel plate configuration and is essentially a parallel plate capacitor. Hence, the content showed in this chapter focus on this configuration. Mathematical models, equations, circuit drawings and graphs are used to illustrate and explain each topic. Models of one and two dielectrics in series are presented. The main focus here is DC (direct current) conditions but AC (alternating current) condition is briefly included.

2.1 Mathematical models of a dielectric material and two dielectric materials in series

A parallel plate capacitor consist of one or more dielectric materials with an electrode on each side. First consider one dielectric material. Applying a voltage across the material results in a current *i(t)* flowing based on the voltage shape. Note that voltage has no gradients in this configuration. Under DC-voltage the dielectric is governed by its resistance, and under AC-voltage it is governed by its capacitance. The mathematical model in figure 2.1 illustrate this relation for one dielectric.

Here, U is the applied voltage, R the resistance and C the capacitance. Equations (2.1). (2.2) and (2.3) expresses these components

$$U = Ed \tag{2.1}$$

$$R = \frac{d}{\sigma A} \tag{2.2}$$

$$C = \varepsilon_0 \varepsilon_r \frac{A}{d} \tag{2.3}$$

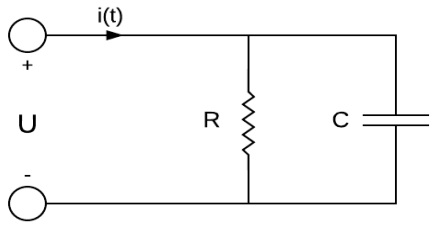

Figure 2.1: Mathematical model of a dielectric material in parallel plate configuration.

where E is the electric field strength, $\varepsilon_0 = 8.85 \times 10^{-12}$ [F/m] the permittivity of free space, ε_r the material relative permittivity, d [m] the gap distance between the plates and A [m^2] the surface area. The equations show that the current is governed by the material conductivity σ $[S/m]$ under DC conditions and its relative permittivity ε_r under AC conditions.

Considering paper and oil as the two dielectrics in series, figure 2.1 is modified into figure 2.2.

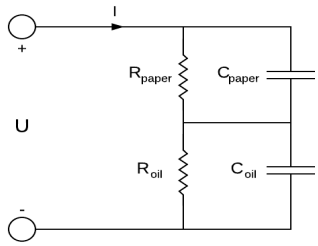

Figure 2.2: Circuit of two dielectric materials in series in parallel plate configuration. The two materials are represented by paper and oil.

This circuit is essentially a downwards extension of figure 2.1. Equations for the resistances and capacitances are the same as equations (2.2) and (2.3) but with sub-names of paper and oil for distance, permittivity and conductivity. The surface area is the same for both materials. Permittivity for paper is $\varepsilon_{paper} = 4$ and for oil $\varepsilon_{oil} = 2.5$ [7]. Conductivity is usually in the range of $10^{-15} - 10^{-8}$ S/m. The applied voltage in this circuit is across the entire insulation and is expressed as equation (2.4).

$$U = E_{paper} d_{paper} + E_{oil} d_{oil} \tag{2.4}$$

The electric field resulting from the applied voltage is the mean value across the entire insulation in this case by use of equation (2.1). Voltage is divided among paper and oil according to (2.4). If paper is present on both sides of the oil they are simply added together

and considered as one dielectric. Under DC-conditions, the capacitances are disregarded and the resistances can be combined by addition. Under AC-conditions, the resistance are disregarded and the capcitances are combined using equation (2.5).

$$\frac{1}{C_{total}} = \frac{1}{C_{paper}} + \frac{1}{C_{oil}} \tag{2.5}$$

2.2 Definition of conductivity

Conductivity is defined as the ability to conduct current in a material. An electric current consists of multiple types of charge carriers that flows through a solid, fluid or gaseous material. Among the carrier types are electrons in metals and positive ions in electrolytes. Positive ions are heavier and thus slower than electrons. Electron conduction is the dominating carrier type in wires used for electric circuits while ionic conduction is dominating in fluids such as oil. Equations (2.6) and (2.7) expresses the relation between charge carriers and current density.

$$J = \sum_i n_i v_i q_i \tag{2.6}$$

$$J = E \sum_i n_i \mu_i q_i \tag{2.7}$$

n is the concentration of charge carries, v the velocity of the carries and q the charge of each carrier. Furthermore, v can be defined as the product of charge mobility μ and electric field E. Note that μ for some carrier types may be dependent on E and/or temperature T. The equations show that current density is the sum of all charge carriers present in a material. Some charge carrier types dominate depending on the material.

2.3 Accumulation of charges in a dielectric from applying a DC voltage

A dielectric under a constant voltage accumulates different type of charges. The charges relevant for this thesis are *homo charges*, *hetero charges*, *surface charges* and *space charges*. The following two subsections contain a brief explanation of these.

2.3.1 Homo charges and hetero charges

The condition of the electrode-insulation interface plays an important role regarding how homo charges and hetero charges accumulate. Charge carriers are injected into the insulation from the anode and exits through the cathode. If the electrodes injects and removes charges faster than the insulation can conduct them, an accumulation of charges with the

same polarity occurs at both interfaces. These are called *homo charges*. In the opposite case where the insulation conducts faster than the electrodes, an accumulation of charges with the opposite polarity occurs, called *hetero charges*.

2.3.2 Surface charges and space charges

In layered dielectrics, such as oil impregnated paper, surface charges accumulate at the interfaces. Channels between paper strips within the actual cable insulation, called butt gaps, are filled with oil and experience a significant decrease in electric field strength due to these charges, [8]. From the law of Maxwell, the amount of surface charges $\rho_{surface}$ are obtained from calculating the divergence of the electric flux density D, shown in equation (2.8).

$$\rho_{surface} = divD = div(\varepsilon E) \tag{2.8}$$

E is the electric field strength and ε the permittivity of the material. Note that only the permittivitiy ε_r affect the amount of accumulated surface charges.

Space charge ρ_{space} have been generated in the dielectric bulk if a gradient of the ratio ε/σ exists. This can come from local temperature changes which are common in the insulation of HVDC cables in service. The difference from surface charges is that space charges are also dependent on conductivity σ. A study conducted on space charges are presented in chapter 3.4.

2.4 Dielectric response in time domain of a dielectric material subjected to a DC voltage

Subjecting a dielectric to a constant voltage does not result in an immediate stable current flowing through it. Instead, the current slowly declines toward a steady value due to alignment of dipoles within the dielectric. These dipoles contribute to accumulation of surface charges at all interfaces in the insulation. Electrode-insulation interfaces and, in case of several dielectrics, insulation-insulation interface affects the electric field distribution across the material and thus the current.

2.4.1 Waveform of the polarization and depolarization currents

An electric field applied to a dielectric material generates a current density $j(t)$ across its surface, expressed as equation (2.9).

$$j(t) = \sigma E(t) + \frac{\delta D(t)}{\delta t} \tag{2.9}$$

The first part of equation (2.9) relates to the steady state DC current density generated by the applied field $E(t)$ and material conductivity σ. The latter part relates to the current

generated by the change in $D(t)$, further shown in equation (2.10).

$$D(t) = \varepsilon_0 E(t) + P(t) \tag{2.10}$$

where ε_0 is the permittivity of free space and $E(t)$ the applied electric field. As $E(t)$ is constant only $P(t)$ contribute to $D(t)$. $P(t)$ relates to the process of aligning dipoles within a dielectric and is called polarization. The polarization is different for each dielectric and depends on the number of polarization mechanisms. These are divided into momentary and relaxation mechanisms. Momentary mechanisms are fast and align with the field immediately. Relaxation mechanisms are slow and require longer time and are dependent on temperature. Interfacial polarization is the most important relaxation mechanism. As polarization $P(t)$ is different for each material it is described by its response function. Equation (2.11) shows this relation [7].

$$P(t) = \varepsilon_0 \int_{-\infty}^{t} f(t-\tau) E(\tau) d\tau \tag{2.11}$$

where $f(t)$ is the dielectric response function characterized by the material and τ is the polarization time constant. Note that the $P(t)$ is dependent on the electric field. Combining equations (2.10) and (2.11) with (2.9) gives equation (2.12).

$$j(t) = \sigma E + \varepsilon_0 [\varepsilon_\infty \delta(t) + f(t)] E \tag{2.12}$$

ε_∞ is the momentary permittivity and $\delta(t)$ a step function. The graphical representation of this equation depends on $f(t)$ but a typical waveform of the current $i(t)$ is plotted in figure 2.3.

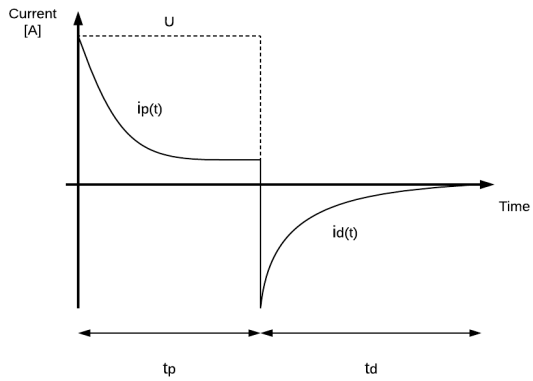

Figure 2.3: Typical waveform of polarization and depolarization currents

From figure 2.3 the polarization current $i_p(t)$ is at $0 \leq t \leq t_p$ and depolarization current $i_d(t)$ is at $t_p \leq t \leq t_d$. The polarization current occurs when the voltage U is applied and has

an initial high value before decreasing gradually towards a stable value, called the steady state current I_{DC}. Depolarization current occurs when the voltage is removed and has an initial high value of the opposite direction before gradually decreasing towards zero. This can be explained as the dielectric being charged during polarization and then discharged during depolarization.

2.4.2 Mathematical model of the dielectric response of a dielectric material

A popular way of modeling the dielectric response is using the method proposed by Debye. This method assumes that the polarization $P(t)$ follows an inverse-exponential rate of rise, as shown in equation (2.13).

$$P_d(t) = P_d(\infty)(1 - e^{-\frac{t}{\tau}}) \tag{2.13}$$

$P_d(\infty)$ is the polarization equilibrium and τ is its time constant. Subscript d relates to the active relaxation mechanism. The expressions for polarization and depolarization currents then have inverse-exponential rate of rises, as shown in equations (2.14) and (2.15).

$$i_p(t) - I_{DC} = Ae^{-\frac{t}{\tau}} \tag{2.14}$$

$$|i_d(t)| = Ae^{-\frac{t}{\tau}} \tag{2.15}$$

A is a constant and τ the same time constant as in equation (2.13). The mathematical model which represent $i_p(t)$ and $i_d(t)$ for one relaxation mechanism is an extension of the circuit in figure 2.1, illustrated in figure 2.4.

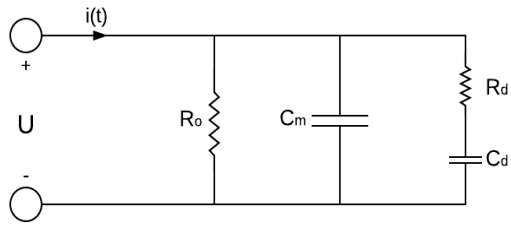

Figure 2.4: Mathematical model of a Debye-model with a dielectric and one relaxation mechanism.

An RC-branch is added which models the polarization process. A supplied voltage U charges the capacitance C_m momentary. Capacitance C_d is charged at a slower rate due to R_d which results in a current curve as in equation (2.14). When both capacitances are charged, the current only flows through R_o. Formulas for the resistances and capacitances

are shown in equations (2.16), (2.17), (2.18) and (2.19).

$$C_m = \varepsilon_m \frac{A}{d} \tag{2.16}$$

$$R_0 = \frac{d}{\sigma A} \tag{2.17}$$

$$C_d = \varepsilon_d \frac{A}{d} \tag{2.18}$$

$$R_d = \frac{\tau}{C_d} \tag{2.19}$$

ε_m is the permittivity of the momentary mechanism and ε_d and τ the permittivity and time constant of the relaxation mechanism. If more than one mechanism is present, the circuit is extended by additional RC-branches matching the number of mechanisms. This gives additional time constants and permittivities for each mechanism.

2.4.3 Expression of the conductivity

As was explained in chapter 2.4.2, the current is only flowing through R_0 when the polarization is complete (at the end of t_p in figure 2.3). Hence, when $P(t) = 0$ the current density in equation (2.9) becomes

$$j = \sigma E \tag{2.20}$$

which is recognized as Ohm's Law. If equation (2.20) is multiplied with the surface area A and combined with equation (2.17) and then expressed with respect to conductivity the expression becomes

$$\sigma = \frac{dI_{DC}}{UA} \tag{2.21}$$

I_{DC} is the steady state current obtained at $t = t_p$, U the applied voltage and d the gap distance of the dielectric. For this equation to be applicable, a sufficient polarization time is needed to obtain steady state. As the polarization is heavily dependent on temperature this may be too long in many cases. Hence, another method to calculate σ is to recognize that $i_p - i_d \approx I_{DC}$ from equations (2.14) and (2.15). This is because the amount of polarization occurring during charging is approximately equal to the depolarization during discharging. Substituting I_{DC} an approximation of the conductivity can be made, as shown in equation (2.22).

$$\sigma \approx \frac{d}{UA}(i_p(t) - i_d(t)) \tag{2.22}$$

This approximation is not dependent on reaching steady state but may be inaccurate if the polarization and depolarization currents have significant deviations.

The method used for obtaining conductivities of oil in series with paper is presented in chapter 4.6.6.

2.5 Calculating the loss tangent by use of Hamon approximation

The losses from an insulating material is characterized by its loss tangent $tan(\delta)$. The loss tangent express the losses originating from both permittivity and conductivity as these are impossible to distinguish between. The loss tangent can be expressed as in equation (2.23) [7].

$$tan(\delta) = \frac{\varepsilon_r^{''}}{\varepsilon_r^{'}} + \frac{\sigma}{w\varepsilon_r^{'}\varepsilon_0} \tag{2.23}$$

Parameters $\varepsilon_r^{'}$ and $\varepsilon_r^{''}$ are the material complex relative permittivity and loss factor, respectively. The angular velocity is expressed as $w = 2\pi f$, where f is the applied frequency of an AC-voltage.

The complex permittivites can be obtained from direct measurement using special equipment, but it is also possible to obtain the loss factor from the polarization current through calculations. The approximation invented by Hamon allows for an easy conversion of the loss factor from frequency to time domain [6]. The resulting loss tangent can then be plotted with respect to frequency.

In [6], Fourier transformation of the loss factor gives equation (2.24).

$$\varepsilon_r^{''} = \frac{G_0 + \Phi(t)}{wC_0} \tag{2.24}$$

G_0 is the steady state DC conductance and $\Phi(t)$ the relaxation function. Hamon assumes a relaxation function that follows a 'Curie von Schweindler'-curve, seen in equation (2.14), as this fits well to most measured polarization currents. Equation (2.25) expresses this relaxation function and thus the polarization current.

$$\Phi(t) = \beta C_0 t^{-n} = At^{-n} \tag{2.25}$$

where β, n and A are constants and C_0 the geometric capacitance. The transformation also results in the product of w and t, shown in equation (2.26).

$$wt = [\Gamma(1-n)cos(n\pi/2)]^{-1/n} \tag{2.26}$$

where $\Gamma(1-n)$ is the gamma-function and n the same parameter as in equation (2.25). The gamma-function is not required for understanding the derivation and is thus not included further. Equation (2.26) is limited to $0.3 \leq n \leq 1.2$ as this gives a mean value of 0.63 with a deviation of only $\pm 3\%$ for wt and fits well with most measured polarization curves. Substituting w with f gives $f = 0.1/t$ which shows the relation between frequency and time. The resulting expression for $\varepsilon_r^{''}$ is expressed as

$$\varepsilon_r^{''} = \frac{i_p(t)t}{2\pi 0.1 C_0 U_0}. \tag{2.27}$$

Inserting equation (2.27) into equation (2.23) gives the final expression for the loss tangent, shown in equation (2.28).

$$tan(\delta)(f) \approx \frac{i_p(t)t}{\varepsilon_r 2\pi 0.1 U_0 C_0} + \frac{\sigma}{2\pi f \varepsilon_r \varepsilon_0} \tag{2.28}$$

Here, the complex permittivity is assumed $\varepsilon_r^{'} \approx \varepsilon_r$. This expression is plotted in log-log coordinates with a theoretical curve illustrated in figure 2.5.

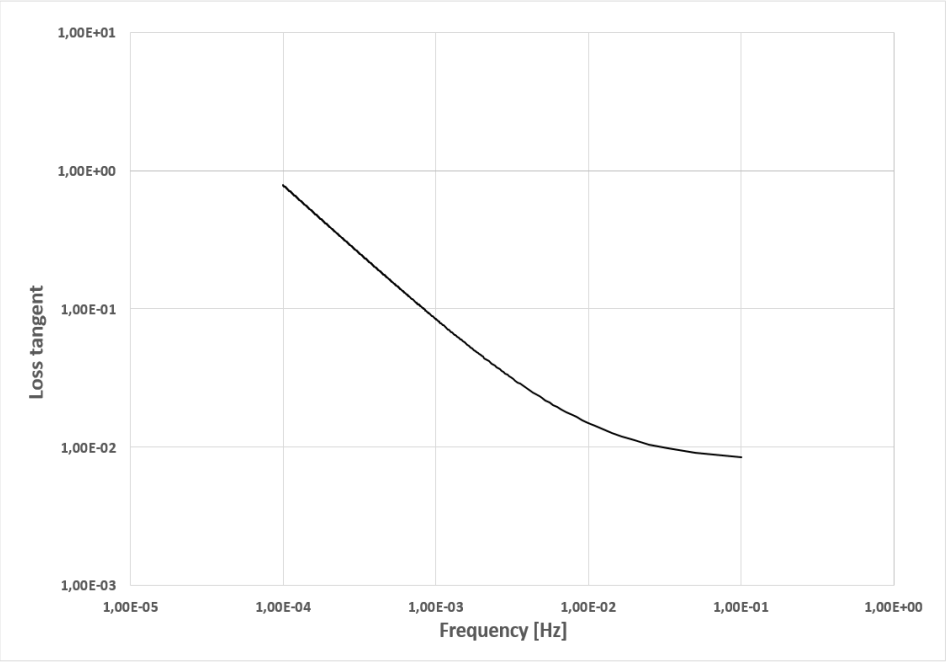

Figure 2.5: Log-log plot of a theoretical loss tangent versus frequency curve by use of the Hamon approximation.

The figure shows a near linear curve with a slight bend at the higher frequencies. As time is usually measured from 1 second the frequency is calculated from 0.1Hz and below.

In summary, the Hamon approximation is valid if the polarization current fits a 'Curie von Schweindler'-curve expressed in equation (2.25) with $0.3 \leq n \leq 1.2$. The loss tangent $tan(\delta)$ can then be expressed as equation (2.28) where $f = 0.1/t$. It is then plotted in log-log coordinates.

Chapter 3

Literature survey

This chapter presents important findings from previous studies performed on paper-oil insulation. Dependencies on temperature, field strength and pressure on paper are presented. The effect of oil gap thickness and its properties and a study of injection of homo charges are also presented.

3.1 Studies of temperature and electric field strength dependency on paper

There exist several studies of conductivity as a function of temperature and electric field strength as explained in [3]. All these studies have developed empirical formulas which presents the dependency as exponential with parameters showing the dependencies of temperature and field strength. Equation (3.1) shows the most commonly used formula with parameter values collected in table 3.1.

$$\sigma = \sigma_0 exp[\alpha T + \beta E] \tag{3.1}$$

Table 3.1: Collection of parameter values for conductivity of paper with respect to electric field strength and temperature, shown in equation (3.1).

Parameter	Value	Unit
α	0.1	$^{\circ}C^{-1}$
β	0.03	mm/kV
σ_0	10^{-6}	S/m

α and β are the constants describing the temperature and field dependency respectively and σ_0 is the conductivity at zero temperature and zero electric field strength. T is temperature in Celsius and E the electric field strength in kV/mm.

In [9], it was found that the values for the constants differed little between the paper, oil and other impregnating compounds used. It was further explained the behaviour of conductivity with temperature using Boltzmann statistical theory. Increased number and mobility of charge carriers results in a higher current and thus an increased conductivity. Greater mobility also results in faster alignment of dipoles and hence a shorter polarization time. The dependency of field strength was only deduced from experimental results. It was pointed out that the expression is applicable for electric field strengths in the range $10 \leq E \leq 40$ kV/mm, as is the range for actual cables.

In [3], it was concluded that ionic conduction was the main type of charge carrier in mass impregnated paper.

3.2 Study of injection of homo charges in successive paper layers

In the study described in [10], on charges and discharges in mass-impregnated paper insulation, the author measures the amount of space charges in successive layers of paper. Samples of one, two, three and four layers were tested under E = 20 kV/mm. Thickness of the paper used was 150-165 μm with an additional assumed 1-10 μm oil thickness between the layers. The charges were detected using a non-destructive method called Piezo Electro-Acoustic (PEA), utilizing electric and acoustic pulses.

It was concluded that homo charges were formed regardless of the oil and paper type. These charges only penetrated one layer of paper on each polarity and no more. More charges were detected at the four layered sample which was concluded to be due to surface charges.

3.3 Studies of surface pressure on dry and oil impregnated paper

The effect of applying pressure by compressing paper was studied in [11]. The author measured both permittivity and resistivity of forty pieces of 10 μm dry Kraft paper at various pressures ranging from 3 kPa to 336 kPa. The temperature was also varied from $20°C$ to $120°C$. Resulting graphs from the study of resistance is shown in figure 3.1.

The study showed a dependency of pressure for resistance. The resistance changed by about 80%.

The impact of pressure was previously studied in the specialization project [1]. The goal was to observe how much the maximum attainable pressure for the same setup as used in this thesis would affect conductivity and permittivity of oil impregnated paper as opposed to the dry paper used in [11]. The pressures tested ranged from 0 Pa to 115 kPa at $23°C$ for five layers of 90 μm paper sheets. The results showed a change of conductivity by a maximum of 16% and of permittivity by a maximum of 2%. From the results, it appeared

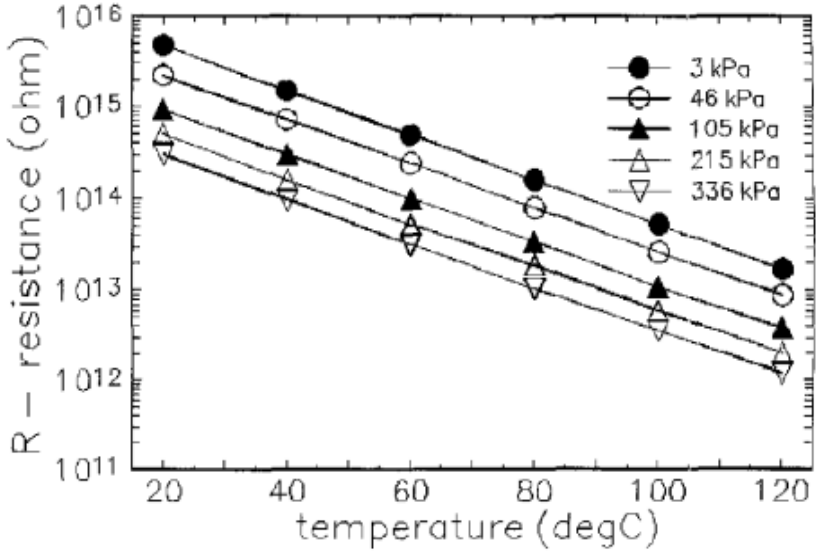

Figure 3.1: Plots of the resistance versus pressure at various temperatures studied ib [11].

that oil impregnated paper was less affected by surface pressure than dry paper.

3.4 Influence of bulk oil in series with paper

Introducing bulk oil in a system of oil impregnated paper affects the electric field distribution and thus the dielectric response. This is due to the fact that space charges accumulates in the bulk oil, distorting the field. In [5], it was conducted a study on transformer oil in series with aluminum electrodes coated with thin insulation films consisting of polyether Penton. Measurements were done with none, one and both electrodes coated for several gap thicknesses. Coating only the anode gave an exponential-like increase in currents, and coating only the cathode gave a linear increase instead. It showed that the presence of an insulting film on either electrodes gave heavy space charge accumulation which lowered the electric field strength in the bulk oil significantly.

The configuration applicable for this thesis, where both electrodes were coated, showed an increase in current as a function of voltage far greater than the cases where only one electrode was coated. Measured currents are illustrated in figure 3.2.

The measured currents had a region of slow rise before rapidly increasing at high field strengths. With a greater oil volume this region was shorter, until it appeared to be totally suppressed. With increasing bulk oil gap, the currents shifted to the left in the graph. In [5], it was suggested that the unexpected current curves came from enhanced fields and field emission at both electrodes. Hence, the field in bulk oil was reduced significantly, as with one electrode coated, almost to zero.

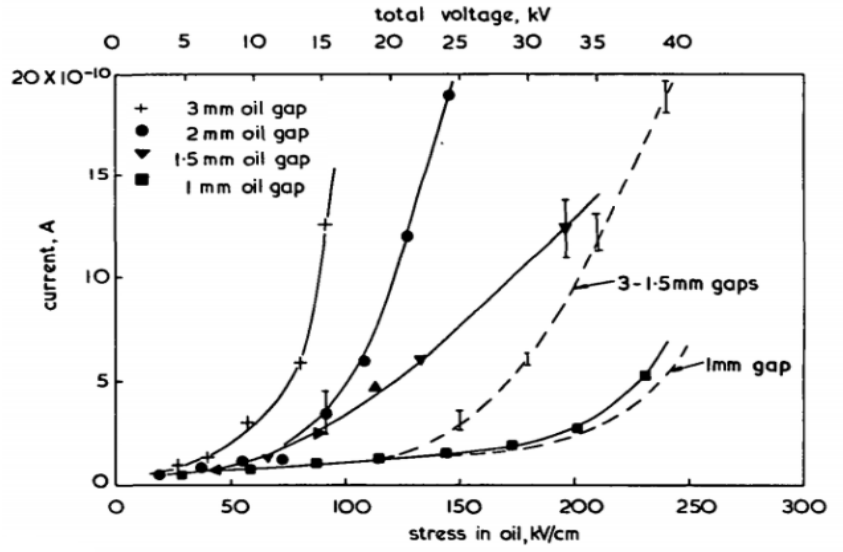

Figure 3.2: Current versus voltage for various bulk oil thicknesses in series with aluminum electrodes coated with polyether Penton insulation, as presented in [5].

In [12] and [13], it was found that the paper-oil layer interfaces tended to accumulate positive charges which increased with higher applied electric field strengths. It was suggested that these layers act as a barrier for positive charges. The applied voltage only affected the amount of space charges while the temperature affected the distribution and mobility of these charges. In [13], it was performed experiments with oil-immersed paper in series with oil bulk. Homo charges always accumulated in the oil-paper layer and positive charges accumulated in the oil bulk. This was explained in [13] as the difference in mobility between electrons and positive ions. Due to the accumulation of charges in oil-paper interfaces the electric field was distorted at the interfaces. Charges in the system increased with higher voltage but a thicker bulk oil reduced the interface charges because of recombination in oil.

3.5 Drying and impregnation process

PDC measurements were performed during the impregnation process, further shown in chapter 4.6.1. Moisture, which significantly affects the paper-oil insulation [7], is removed during the drying process.

Hence, it is of interest to investigate the durations of drying and impregnation in previous studies performed on oil-impregnated paper insulation. In [14], it was explained that drying of mass impregnated cables occurs at $120°C$. Impregnation is then performed at $110°C$ under vacuum. The durations for these processes are not mentioned. In [9], oil-impregnated paper was dried at $105°C$ under vacuum for 24 hours and then impregnated under vacuum. In [12], the paper was dried under vacuum at $120°C$ for 30 min and then impregnated for one day. In [13], the oil immersed paper was dried at $80°C$ for 24 hours. Impregnation duration and temperature was not mentioned. The study in [4] was performed with the same setup as for this thesis. The paper was dried at 100-$120°C$ for 48 hours and the oil was degassed at $100°C$ for 4 hours.

Chapter 4

Methodology

This chapter presents the methodology used for obtaining the polarization and depolarization currents investigated in this thesis. Explanations of the PDC setup and design of samples provides insight in the preparation process by the use of photographs and illustrations. Equipment used for measurements are listed and their function in the system explained. Results from all minor studies conducted throughout this thesis are presented here. Among the practical work are studies of optimal duration when impregnating the samples, change in current for long polarization and depolarization durations, time requirement for reaching thermal equilibrium after switching samples and if injection of homo charges affect the paper samples. Among the mathematical work are studies of the physical dimensions required for the design of the electrode used when measuring bulk oil samples, a method for calculating the conductivity of oil and a method for calculating the expected DC current in butt gap samples.

4.1 Method for performing Polarization Depolarization Current (PDC) measurements

The polarization and depolarization currents were measured using the method of Polarization Depolarization Current (PDC). The resulting currents had curves as shown in figure 2.3. During the polarization stage, a DC voltage was a applied to a sample. During the depolarization stage, the voltage was removed and the sample grounded. When the depolarization current had reached a satisfactory low value marked the end of one PDC measurement.

In this thesis, the ”test object” is referred to as the tank that contains all samples and oil.

4.1.1 Setup overview and procedure

Figure 4.1 shows a schematic diagram of the laboratory setup used for PDC measurements.

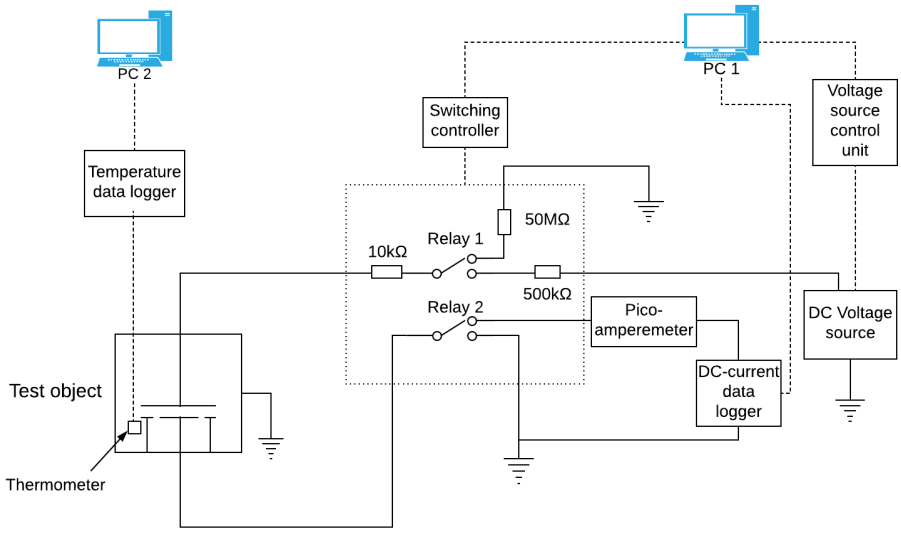

Figure 4.1: Diagram of the setup used for PDC measurements

The setup consisted of a test object, relays, voltage source, picoamperemeter, data loggers, control units, PCs. A software in PC1 controlled the voltage source and both relays through control units and received data from the picoamperemeter through the DC current data logger. PC 2 received data from the thermometer located inside the test object through the temperature data logger. Both relays were placed inside a small container also containing resistances with quantities shown in figure 4.1. The switching controller and DC current data logger functions were handled by the same instrument. The test object is further explained in the next chapter.

Before PDC measurements, noise was measured in the circuit by disconnecting the voltage source and connecting the test object to the picoamperemeter and ground.

During the polarization stage, the test object was connected to the voltage source and ground for 1 second. This was because of the initial high value of the polarization current which may damage the picamperemeter. After 1 second, relay 2 connected to the picoamperemeter.

During the depolarization stage, relay 1 was connected to ground enabling discharging of the sample within the test object.

The durations of each stage was inserted in a Labview-software in PC 1 with desired voltage levels. The components presented in figure 4.1 is collected in table 4.1.

Table 4.1: List of components in the PDC setup.

Component	Manufacturer	Type
Voltage source	FUG	HCN 140-35000
Voltage source controller	FUG	PROBUS IV IEEE 488/RS 232
Picoamperemeter	Keithley	6485
Switching controller and DC current data logger	Agilent	34972A LXI
Temperature data logger	Keysight	34972A LXI

4.1.2 Presentation of the test object

A photograph of the test object in figure 4.1 is shown in figure 4.2.

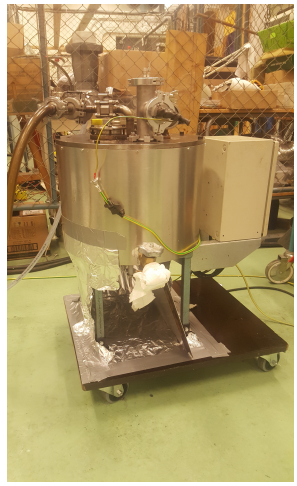

Figure 4.2: Photograph of the test object used for PDC measurements. The tank have a height of 300 mm and a diameter of 400 mm.

The test object consists of an airtight cylindrical tank with a removable cover and bushings for passing wires and tubes through. Tank height is 300 mm and diameter 400 mm. At the bottom, a heating element is placed which is controlled by a controller on the side of the tank. The high voltage (HV) electrode is mounted on the bottom of the test object[1]. A rod, connected to the HV electrode, is passed through the tank which allows for an easy connection of the voltage source. Samples were placed on the HV electrode and a removable ground electrode on top called low voltage (LV) electrode was placed on top. Figure 4.3 show a photograph of the HV and LV electrodes.

Both electrodes are made of brass. The HV electrode has a diameter of 110 mm and is mounted onto the rod in the test object. At the bottom of the LV electrode the surface area is divided into an inner and outer surface area. The inner area have a diameter of

[1] In figure 4.1, the HV electrode is drawn on the top.

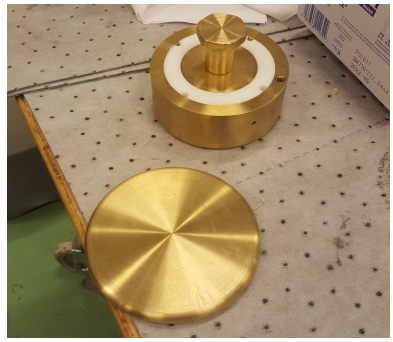

Figure 4.3: Photograph of the high voltage (bottom of the picture) and low voltage electrodes (top of the picture).

78 mm and is connected to Relay 2 and the outer area have a diameter from 80 mm to 100 mm and is connected to ground. The 2 mm gap between these areas are filled with Polytetrafluoreten (PTFE). This arrangement limits distortion from electric fields which spreads outside the measuring area, also called ”fringing effect”. The total weight of the LV electrode is 2.118 kg. An additional weight of 1.17 kg was placed on the top electrode in an attempt to squeeze any remaining oil films or cavities outside of the measuring area.

On the cover, valves connects one tube to a pressurized tank containing moisture-free Nitrogen gas[2] and one to a vacuum pump. Wires for connecting the LV electrode and thermometer to measuring equipment are passed through bushings. Two windows on the tank allows for visual inspections when the tank is closed. A valve on the bottom is used for injecting oil into the tank. Finally, the entire test object is grounded, with exception of the wires connected to the picoamperemeter.

4.2 Preparation of stacks for combining into samples

As drying and impregnating paper is a lengthy process, a flexible system was implemented. Instead of preparing one paper sample at a time several stacks of paper were prepared simultaneously which could be switched and combined to create any desired sample. This allowed for an increased number of measurements per sample in stead of preparing samples multiple times. A summary of all samples created are presented in table 4.2. Thickness of the paper sheets in paper samples were 90 μm which was also assumed for the sheets in bulk oil and butt gap samples, called ”bulk oil sheets” and ”butt gap sheets”. The nominal thicknesses of 90 μm was used for future calculations in all samples.

[2]Containing $\leq$ 99.9% Nitrogen.

4.2.1 Shaping the stacks from paper rolls

Paper sheets were taken from a paper roll and cut, glued and combined to form stacks. The glue used to combine the paper consisted of TACKIDEX C169 - DEXTRINE. All paper sheets were cut in circular shapes before making the cuts to create butt gap or bulk oil sheets. To achieve high flexibility, the stacks of paper contained no more than four-five sheets while butt gap and oil gap stacks had one paper sheet on each side. This way, the stacks could be arranged and re-arranged to easily create new samples. Stacks of paper, bulk oil and butt gaps were made in the following way.

Paper stacks contained four and five sheets with a diameter of 150 mm. The LV electrode had a diameter of 100 mm, hence the paper sheets were glued together outside this diameter on one side only. This was to avoid contaminating the measuring area. Three stacks of five sheets and five stacks of four sheets were made. Not all four-sheet stacks were assumed needed but added as a reserves. Lastly, an additional stack of five paper sheets were cut and glued together for PDC measurements during the drying and impregnation processes.

Bulk oil stacks were cut similarly as with the paper stacks but modified with a removed area which was filled with oil during impregnation. Each bulk oil stack had one unmodified paper sheets on each side. Figure 4.4a illustrates the configuration of this stack in series with paper. Figure 4.4b show a photograph of a bulk oil stack before placing the second unmodified paper sheet.

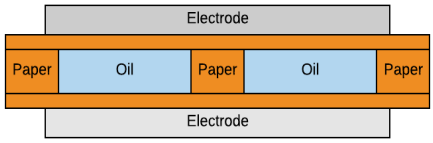

(a) Illustration of a bulk oil stack seen from the side. The middle paper serves as mechanical support.

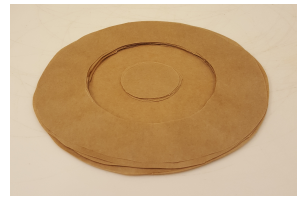

(b) Photograph of a bulk oil stack with 11 bulk oil sheets without an unmodified paper sheet on top.

Figure 4.4: Illustration and photograph of a bulk oil stack.

The oil area had an inner diameter of 40 mm and an outer diameter of 80 mm. Stacks with one, four, seven and eleven bulk oil sheets were made. All sheets were glued together with an unmodified paper sheet on each side. The total amount of sheets in the stacks were three, six, nine and thirteen. The inner circle shown in figure 4.4b was designed as mechanical support as there was a risk of collapse in the bulk oil due to pressure from the top electrode. A separate top electrode was therefore created to mirror the circle of the inner paper. This electrode is called ”bulk oil electrode” and is explained in chapter 4.6.5.

Butt gap stacks were cut in strips with a width of 20 mm. These were placed with 2 mm separation and a sheet of unmodified paper was placed on each side of the stack. Figure 4.5a illustrates the configuration of this stack in series with paper. Figure 4.5b show a photograph of a butt gap stack before placing the second unmodified paper sheet.

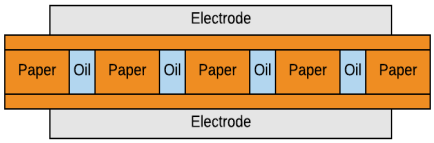

(a) Illustration of a bulk oil stack seen from the side.

(b) Photographs of a butt gap stack with 7 butt gap sheets without an unmodified paper sheet on top.

Figure 4.5: Illustration and photograph of a butt gap stack.

The strips proved difficult to combine together by only applying glue on the sides. Stacks of one and seven layers of butt gap sheets were made, totaling up to three and nine layers with the additional unmodified paper sheets.

In summary, the number of stacks from each type is collected in table 4.2.

Table 4.2: A summary of the stacks created for this thesis

Stack type	Number of sheet types per stack	Number of stacks
Paper	5	3
	4	5
Bulk oil	1	1
	4	1
	7	1
	11	1
Butt gap	1	1
	7	1

4.2.2 Positioning the stacks in the test object prior to drying and impregnation

All paper stacks were placed inside the test object in a predetermined order, as can be seen in figure 4.6.

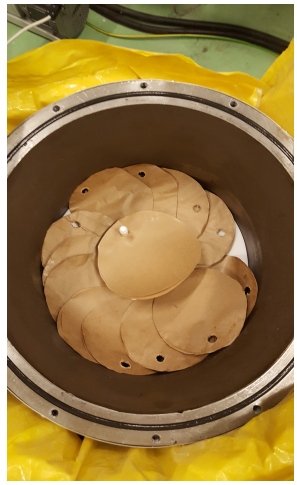

Figure 4.6: Photograph of the stacks positioned in the test object before beginning the drying and impregnation processes.

This arrangement was to have effective series of measurements to obtain as much relevant data as possible in a short amount of time. The stacks were placed as follows, starting from the top.

- One stack with five sheets of paper placed between the electrodes.
- Three stacks with five sheets of paper.
- Two butt gap stacks and two stacks with four sheets of paper.
- Four stacks with oil gap sheets.
- Three stacks with four sheets of paper as a reserve.

All stacks except the first bullet-point were placed around the bottom electrode. The procedural order was to first develop a reference with a paper sample and then study the effect of having several paper sheets under the same electric field strength. Then, butt gap stacks were studied as no new electrode was required. Lastly, oil gap stacks were studied with the bulk oil electrode.

Realizing the way all stacks was created it was critical that they be positioned correctly between the electrodes. This was not as important for paper and butt gap samples but more

so for bulk oil samples. Hence, a large teflon disk was placed at the bottom of the tank covering the entire surface area. Three small pins were attached to the disk and placed touching the HV electrode. Then, holes were cut in each paper stack to be attached to the pins. Using this method allows for an easy process of switching samples and creating new ones. The paper stack for testing during drying and impregnation was placed between the electrodes before impregnation. The electrodes were cleaned using Isopropanol.

4.2.3 Procedure for degassing the oil

The impregnating compound consisted of high viscosity mineral oil which is commonly used in paper-oil insulation. Injecting this compound strait from a barrel would include a lot of gases and moisture which could impact and distort the measurements. Hence, the compound was degassed using a separate setup, as shown in figure 4.7.

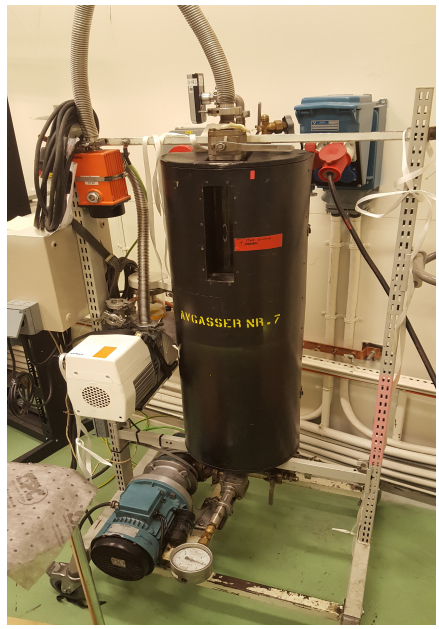

Figure 4.7: Photograph of the setup used for degassing the oil consisting of a container (black), heating elements, pressure pump (blue) and vacuum pump (white).

This setup consisted of a tank with a heating element, pressure pump and a vacuum pump connected. The procedure for degassing was to first heat the oil to 120°C while circulating it through the system using the pressure pump. Note that circulation started after the thermometer showed 70°C to avoid damaging the pressure pump. The oil was then degassed for 4 hour under constant vacuum.

4.2.4 Chosen drying and impregnation durations and temperatures

The research done in chapter 3.5 showed several options when drying and impregnating paper. With the previous studies in mind, the stacks were first dried under vacuum at 100°*C* for two days. Due to a loss of power, drying was done at room temperature for two days before drying at 100°*C*. A later measurement of moisture using the Karl Fisher method showed approximately no water content, meaning that two days at 100°*C* was sufficient.

After drying the paper and degassing the oil, the oil was injected into the test object using the pressure pump. Oil was filled to cover about half the LV electrode. The temperature was then set to 100°*C* and left constant for four days. After this time, the temperature was lowered to 50°*C* and the tank filled with moisture-free Nitrogen gas to maintain atmospheric pressure in a dry environment. Stacks were then ready to be assembled and tested. During the impregnation process measurements of the current were done which is further explained in chapter 4.6.1.

4.3 Procedure for switching samples between measurements

Re-arranging the stacks into new samples were done within two-five minutes to avoid too much humid air intrusion into the oil. The oil had a high viscosity and easily stuck to gloves and tools. Hence, a pipe wrench was used to limit the amount of oil lost when switching the samples.

A flowchart illustrating the procedure for switching samples is presented in figure 4.8.

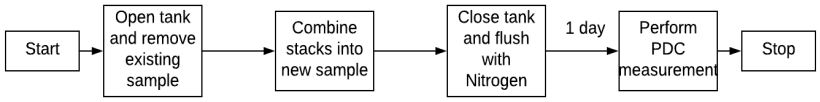

Figure 4.8: Flowchart of the procedure for switching samples between PDC measurements.

The procedure was to first open the tank and remove the top electrode and any additional weights. Then, stacks from the previous measurements were removed and placed in a designated spot on the side of the electrode. The new desired stacks were then threaded onto the teflon pins and on the bottom electrode in correct order to form a new sample. After ensuring that the stacks were placed correctly, the LV electrode and additional weight were placed on the sample. Lastly, the tank was closed and flushed with Nitrogen for about one minute to remove any remaining humid air pockets.

During each re-arrangement of samples, thermal energy would always be lost amounting to about 10°*C* in temperature drop. The temperature was regained after about two hours of reheating the oil. However, each sample did not necessarily reach thermal equilibrium during this period. Hence, the capacitance was gathered as a way of knowing when the

sample had reached its thermal equilibrium. The idea of obtaining the capacitance was that it gives an indication of the change in gap distance between the electrodes or surface area. When this expansion stops, the sample would be thermally saturated. A separate minor study was performed on this topic, shown in chapter 4.6.3. From this study, it was decided to only wait one day after changing a sample before initializing PDC measurements, otherwise the number of measurements planned would not be possible within the time restrictions of the thesis.

An important note is that capacitance measurements was utilized when positioning the bulk oil electrode, where the measured value closest to a theoretical calculated value using equation (2.3) was considered the ideal position.

4.4 Method for obtaining the sample capacitances

It was mentioned in chapter 4.3 that the capacitances of all samples were utilized as a way of knowing when they had reached thermal equilibrium after switching samples. The device used for these measurements was a Keysight U1733C impedance meter. The meter was calibrated before use. Figure 4.9 illustrates how the capacitance measuring device was connected to the test object.

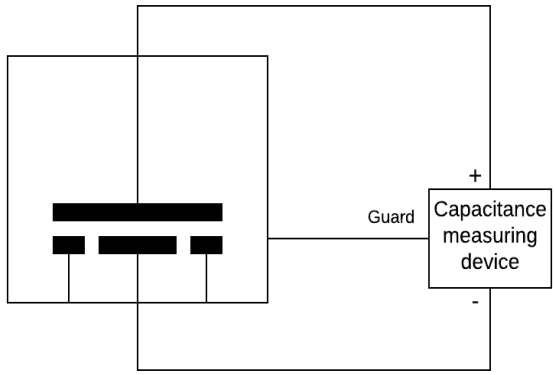

Figure 4.9: Circuit of the connections made when measuring the capacitance of the test object.

The device had positive and negative inputs and a third *guard* input for removing any stray capacitances. Positive input was connected to HV electrode and negative to the LV electrode. The guard input was connected to the test object casing to remove any stray capacitances between the tank and HV electrode. Subtraction of this additional capacitance was done automatically by the device. Measurements were performed at 100 Hz and 1 kHz and usually resulted in values in picofarad (pF).

4.5 Post processing of data

The Labview script used for PDC measurements gave *.txt* files as output files containing noise, polarization and depolarization currents. These were inserted into a Matlab script which plotted each current in an interactive graph. The Matlab script was used as a fast way of obtaining the DC current. Microsoft Excel was used for calculations, creating graphs of conductivity etc and comparisons. A curve in Excel fitting tool was used to find parameters to be used for obtaining conductivity, time constant and loss tangent.

The Matlab and Labview scripts were created and used under permission by SINTEF Energy Research [15].

4.6 Methodology development

This chapter contains the minor studies explained in the introduction of this chapter 4. Results gathered from these studies are presented here and further discussed in chapter 6.2.

4.6.1 Results of PDC measurements performed during impregnation

During impregnation, several PDC measurements were performed in order to see if this method could be used as a diagnostic tool for monitoring the impregnation duration. One measurement was performed every twelfth hour with one hour polarization and eleven hours depolarization, totaling up to four measurements. Both conductivity and time constant τ were gathered and plotted in figures 4.10 and 4.11, respectively. Graphs of the measured polarization and depolarization currents and data of the time constants are found in appendix A.2.

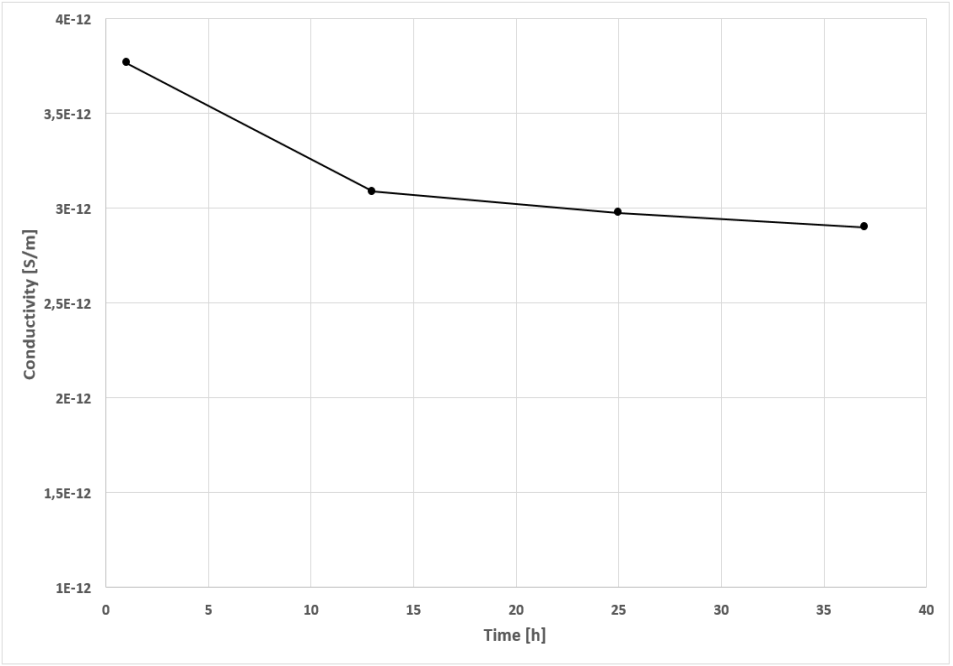

Figure 4.10: Conductivity versus time during impregnation of a sample with 5 sheets of paper. Temperature was $100°C$.

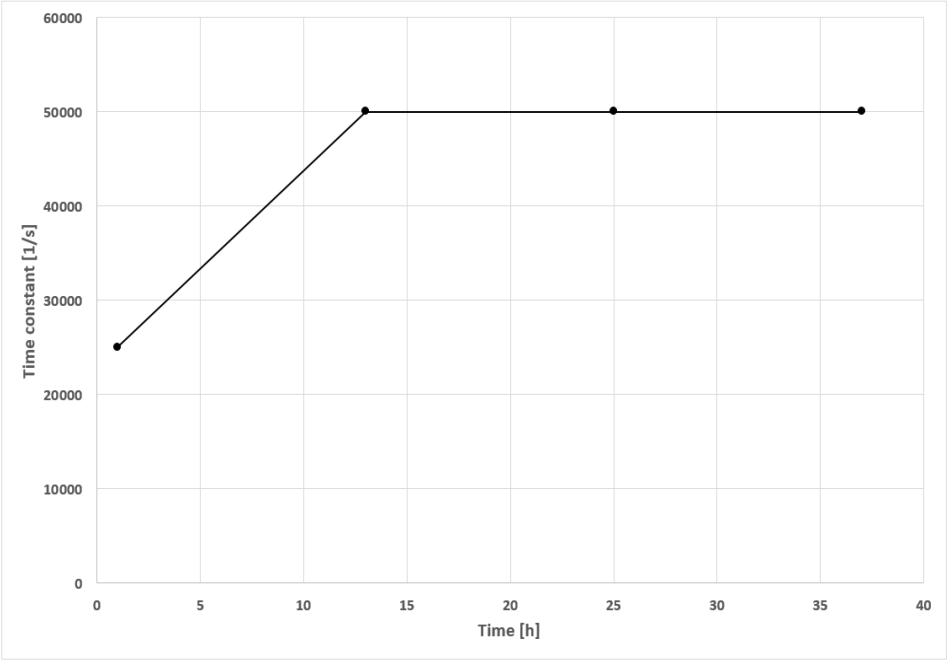

Figure 4.11: Time constant versus time during impregnation of a sample with 5 sheets of paper. Temperature was $100°C$.

The figures reveal that the region for rapid change in both conductivity and time constant occurred within the first twelve hours. Conductivity had still not reached a stable value after 36 hours but the change from 25 to 36 hours is small compared to the initial change. Time constant achieved a steady constant value after twelve hours. Investigating the figures show that most of the impregnation process was completed within twelve hours and that PDC measurement gave a clear indication of this.

The parameter n in the Hamon approximation obtained from these curves revealed to be outside the required range for the method to be applicable and were therefore not investigated any further.

4.6.2 Results of PDC measurements from prolonged polarization and depolarization durations

To achieve credible values for the conductivity, the polarization duration should be as long as possible. This also applies to the depolarization duration since emptying a sample of excess carriers and for the dipoles to regain a chaotic state takes time. In [16], it was suggested depolarization durations 10 times longer than polarization in order to achieve this. If this rule of thumb was to be followed for this thesis it would result in few measurements and it was preferable to apply several voltages with shorter durations. Hence, it was de-

cided to apply a series of increasing voltages with shorter polarization and depolarization durations. The idea behind this was that if the depolarization currents were a factor of at least 100 smaller than the polarization it would appear in the next polarization iteration as noise.

The polarization and depolarization durations chosen with each sample depended on the available time and number of voltages planned. The lowest polarization time during the major study of this thesis was at 9 000 seconds (2.5 hours) and depolarization time at 36 000 seconds (10 hours) which are rather short durations. Thus for this minor study, the current were measured for 129 000 seconds (about 36 hours) with electric field strengths of 3.33, 10, 20 and 30 kV/mm to investigate the change in current. The percentage change in current from 9 000 seconds to 129 000 seconds at multiple electric field strengths are shown in figure 4.12. Similar change for depolarization current from 36 000 to 129 000 seconds is shown in figure 4.13. Graphs of the polarization and depolarization currents are found in appendix A.3.

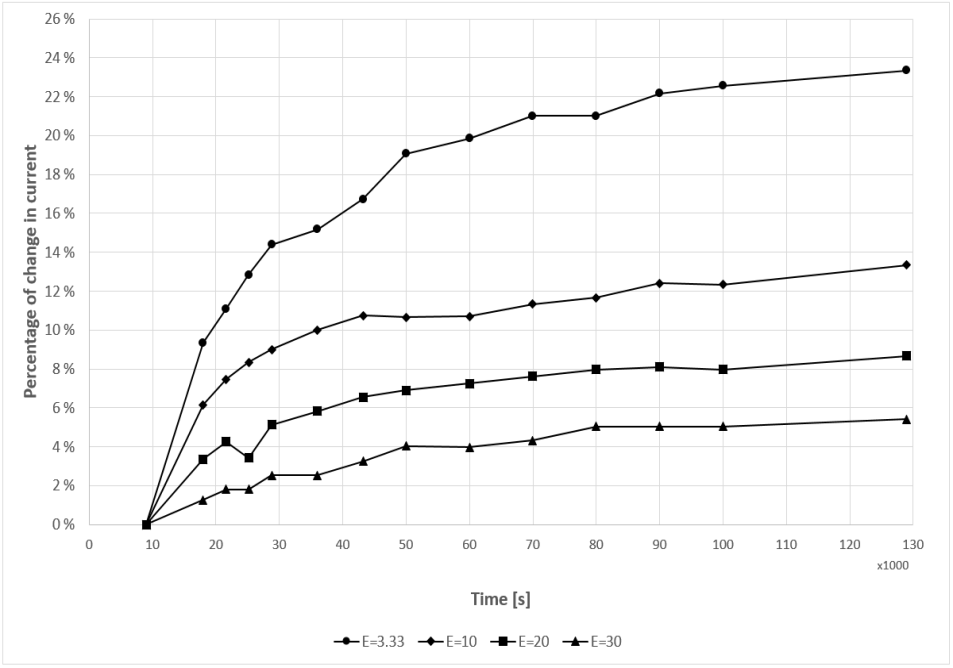

Figure 4.12: Percentage of the change in polarization current versus time from 9 000 seconds to 129 000 seconds at a sample with 10 sheets of paper for various electric field strengths. Temperature was 50 $°C$.

Figure 4.12 revealed a rate of rise in the currents which leveled out after approximately 100 000 seconds (about 27 hours). However, the current still had not reached a steady value. With increasing field strength, the rate of rise in the current decreased. The graphs show that applying a minimum of E = 10 kV/mm resulted in a maximum change of 13%.

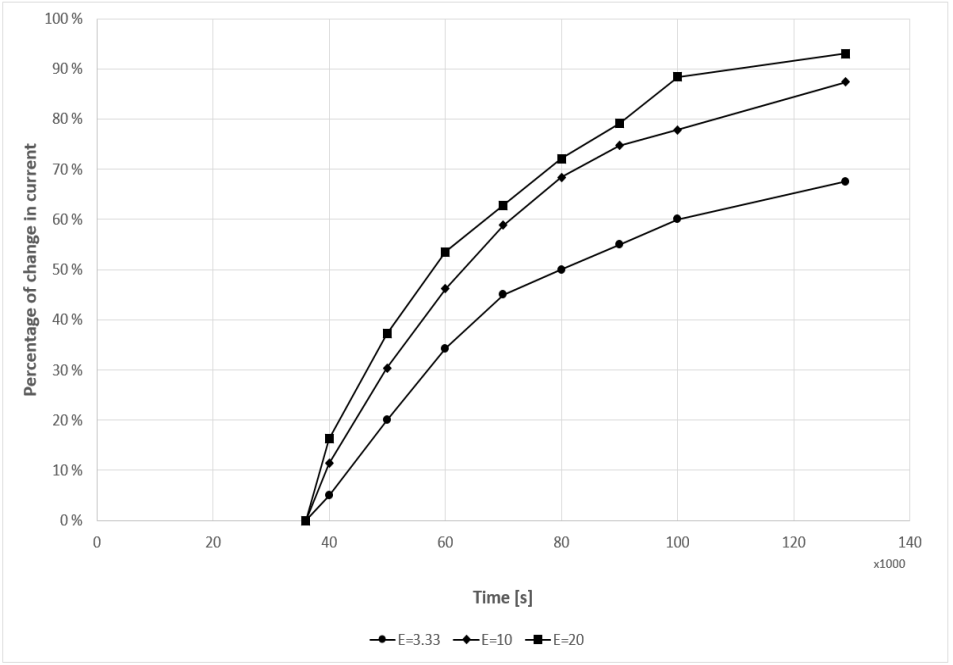

Figure 4.13: Percentage of the change in depolarization current versus time from 36 000 seconds to 129 000 seconds at a sample with 10 paper sheets for various electric field strengths. Temperature was 50 $°C$.

Figure 4.13 showed that the percentage change in depolarization current was much higher than for polarization. Note that the depolarization current was in this case unobtainable at E = 30 kV/mm due to issues with the power supply. The figure reveals a change of current from about 70% to 90% for increasing field strengths. This shows that depolarization was more affected by a short duration than polarization.

An additional study was performed on the largest bulk oil sample at 10 sheets of paper and 11 bulk oil sheets, tested at E = 6.66 kV/mm. Figure 4.14 shows the results of percentage change in polarization currents evaluated from 9 000 to 86 000 seconds and depolarization currents from 36 000 to 86 000 seconds (about 24 hours). Graphs and data of the polarization and depolarization currents are found in appendix A.4.

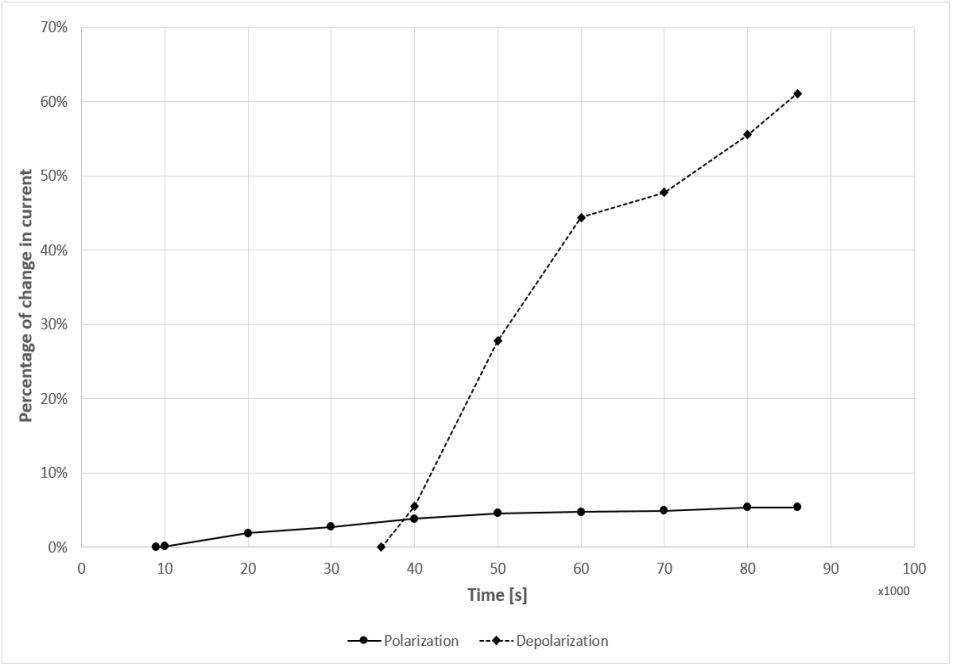

Figure 4.14: Percentage of the change in polarization and depolarization current versus time from 36 000 seconds to 129 000 seconds at a sample with 10 sheets of paper at E = 6.66. Temperature was $50^{\circ}C$.

The figure shows a slow change in polarization current which levels out to 5% after about 50 000 seconds. This was small compared to the paper samples. The depolarization current appeared to require an even longer period than 86 000 seconds to level out and amounted to a change of about 60%. If the behaviour of increasing the field strength in the bulk oil sample is equal to paper samples then the current decreases. Decreasing the bulk oil volume may increase the percentage change as the sample would then be more similar to the paper samples, but this was not studied due to time restrictions.

4.6.3 Time-requirement for obtaining thermal equilibrium in paper and bulk oil samples

Switching samples resulted in a temperature drop which was re-gained after about two hours. However, the temperatures in the samples were not believed to have reached a thermal equilibrium within this time. As temperature has a significant impact on the current measurements and thickness of the sample it was important to know the time required to reach this equilibrium. Obtaining capacitances over time gave an indication of the change in sample thickness or surface area due to the temperature drop. The capacitances were measured and compared to theoretical values using equation (2.5) with values obtained at 100 Hz and 1kHz. Permittivities used were $\varepsilon_{paper} = 4$ and $\varepsilon_{oil} = 2.5$ [7]. Values of measured capacitances showed little to no deviation between the frequencies and thus only 1 kHz were chosen for graphical representation. This data showed the time requirement to reach a stable capacitance and that thermal equilibrium in each sample had been reached. Data of the measured capacitances of all samples are found in appendix A.15.

Sample with 10 paper sheets

A sample consisting of 10 paper sheets was first observed in combination with a PDC measurement. Due to being unable to measure capacitances during the PDC measurements they were gathered directly after switching the sample and up to a week after. This process was performed twice to check its reproducibility. Results are shown in figure 4.15 plotted as capacitance versus time and compared with a theoretically calculated value.

The measured values differed from the calculated, suggesting that either the surface area had increased or gap thickness had decreased. The first measurement showed little change in capacitance over time. However, the second measurement showed a significantly lower value directly after switching the sample before rapidly increasing until the first day. Then, a smaller rate of rise occurred between one day and a week.

It appeared from the second measurement that the sample did not reach a stable capacitance until a week had passed, but the first measurement showed that the fastest rate of rise occurred until the third day.

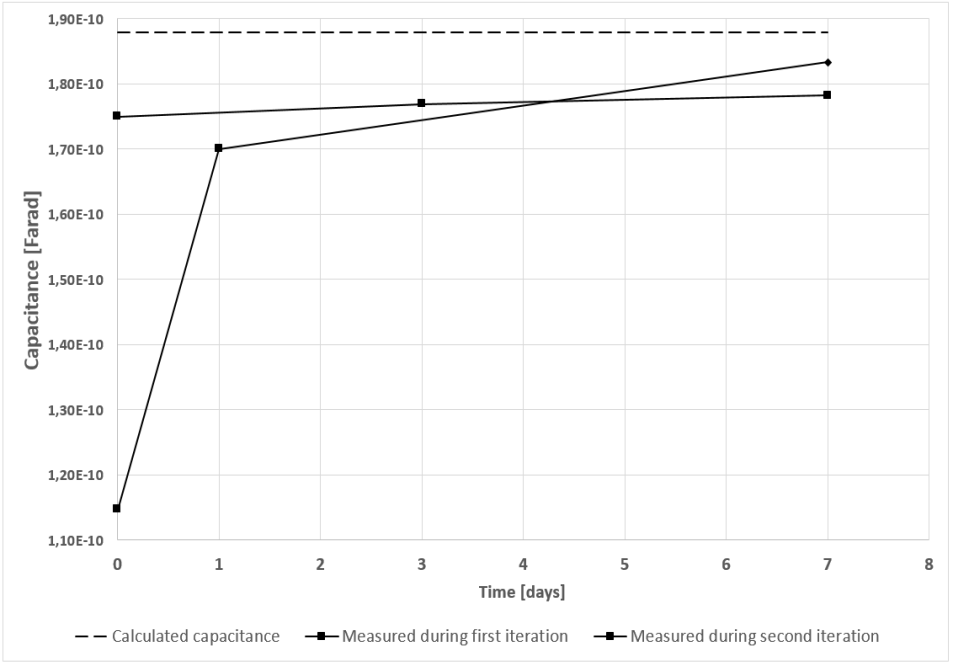

Figure 4.15: Capacitance versus time for a sample with 10 paper sheets at 100 Hz and 1kHz. Two iterations of the study were performed and compared to theoretically calculated values (plotted with dashed lines). Temperature was $50°C$.

Sample with 1 and 11 bulk oil sheets in series with 10 paper sheets.

The same process of measuring the capacitance over time for paper samples was done for bulk oil samples. This was to see if an increased oil volume would result in shorter time to reach thermal equilibrium. One measurement was performed for each of the four samples at the same frequencies. Measured capacitances for 1 and 11 sheets of bulk oil in series with 10 sheets of paper over time are presented in figure 4.16.

The figure shows that the curves reach steady values after one day, with minor increases after a week. However, the values measured from both samples differ from the theoretical values by 37%. Investigation of the samples with 4 and 7 bulk oil sheets reveal the same gap between measured and theoretical values and that the largest change in capacitance occurred after one day.

From investigating figures 4.15 and 4.16, it was decided to delay PDC measurements by one day after switching a sample. This was to cover most of the change in capacitance but also due to the time restrictions of the thesis since many PDC measurements were planned. This was also decided for the butt gap samples.

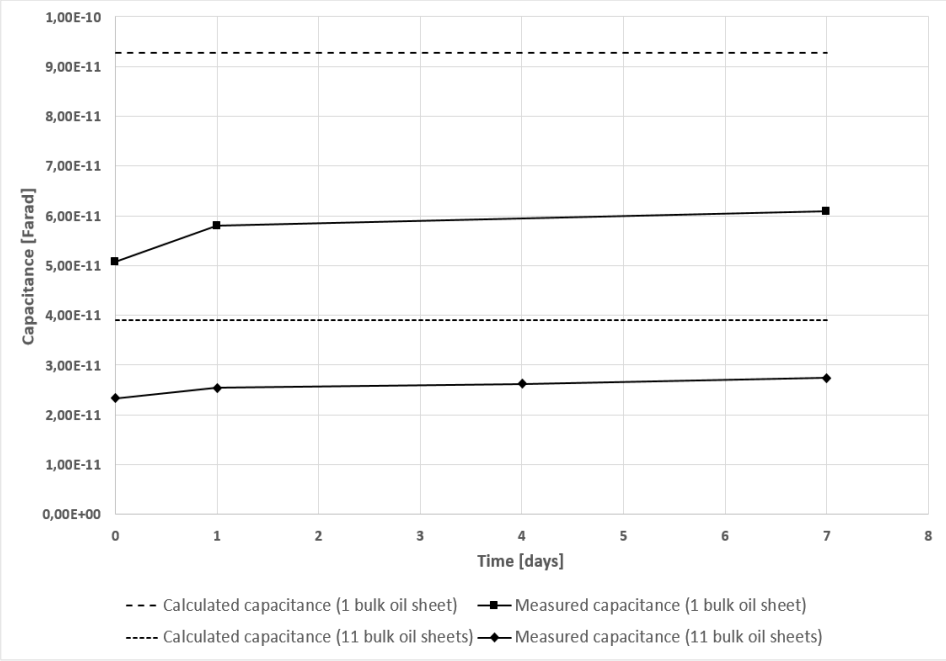

Figure 4.16: Measured capacitance versus time for samples with 1 and 11 bulk oil sheets in series with 10 paper sheets. Calculated values are plotted with dashed lines. Temperature was $50°C$.

4.6.4 Investigation of injected charges in paper samples

As explained in chapter 3.2, it was found that homo charges penetrate one sheet of paper closest to each electrode. This addition of charges may affect the results and was therefore investigated in this thesis. To avoid such impacts a study was conducted where samples of 5, 10 and 14 sheets of paper were constructed and stressed under equal field strengths. These thicknesses corresponded to 0.45, 0.9 and 1.26 mm, respectively. The field strengths were in the range of 10-40 kV/mm and temperature was set to $50°C$ for all samples. Figure 4.17 contains a plot of calculated conductivities from measured DC currents with respect to applied electric field strength for the samples. Graphs and data of measured currents are found in appendices A.6, A.7 and A.8.

The figure shows a similar rate of rise in all samples. Magnitudes between the samples with 5 and 15 sheets and the sample with 10 sheets deviate by about 10-20%. These deviations may come from small temperature differences or statistical deviations. Hence, none of the samples appeared to be affected by homo charges being injected. The sample with 10 sheets of paper was chosen as the basis for further studying the effect of electric field strength and temperature in paper.

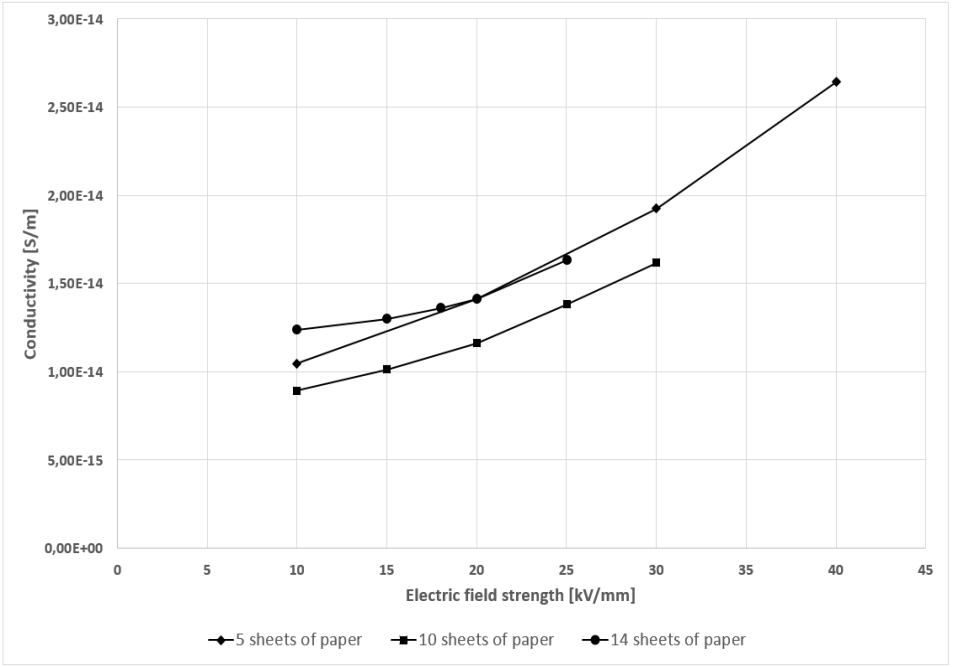

Figure 4.17: Conductivity versus field strength for samples consisting of 5, 10 and 14 sheets of paper. Temperature was 50°C for all samples.

4.6.5 Designing the electrode used for measuring the current in bulk oil samples

Designing an electrode with an inner area (guard) connected to ground that aligns with the bulk oil stacks from chapter 4.2.1 reduces the measuring area. In addition, sufficiently large inner guard area that maintains sufficient mechanical support was needed. Hence, the minimal required measuring area was calculated in the following way.

Inspecting equation (2.1) show that the lowest possible electric field strengths come from having the thickest sample and applying the lowest voltage. As the voltage is assumed to be across the paper, proposed in [5], the thickness is fixed at 10 sheets and the lowest voltage applied was 3.3 kV. The minimum electric field strength was thus

$$E_{min} = \frac{3.33}{0.09 \times 10} = 3,7\ kV/mm.$$

The temperature was fixed at T = 50°C. Inserting this into equation (3.1) with the parameters used in [3] gives the minimum attainable conductivity.

$$\sigma_{min} = 10^{-16} \times exp[0.1 \times 50 + 0.03 \times 3.7] = 1.65 \times 10^{-14}\ S/m$$

It was decided that the minimum allowable current to flow was I_{min} = 100 pA. Multiplying

ohm's law in equation (2.20) with the surface area gives an equation for current. Expressing this equation with respect to the surface area gives the minimum allowable area.

$$A_{min} = \frac{I_{min}}{\sigma_{min} \times E_{min}} = \frac{10^{-10}}{1,65 \times 10^{-14} \times 3,7} = 1638 \ \ mm^2 \tag{4.1}$$

The minimum allowable surface area of the bulk oil electrode was therefore A = 1638 mm^2. As the inner diameter of the inner guard (mechanical support) in bulk oil stacks was 40 mm it was desired to have a greater diameter in the equivalent part of the electrode. Placing the electrode after assembling a sample was expected to be difficult and thus a wider guard area in the electrode was made for creating a larger margin for error.

Considering this and the above calculations, the following dimensions were used to construct the bulk oil electrode.

- Outer diameter on outer guard = 100 mm
- Inner diameter on outer guard = 84 mm
- Outer diameter on measuring part = 80 mm
- Inner diameter on measuring part = 54 mm
- Diameter on inner guard = 50 mm
- Surface area on measuring part = 2736,32 mm^2
- Weight = 3,42 kg

As can be seen from the list, surface area for measurements was well within the calculated minimum allowable area. The inner diameter of the guard was chosen to be 50 mm^2 which was assumed to provide sufficient mechanical support. Total pressure that would result from this electrode was calculated to be P = (9,81*3,042)/2736,32 = 10,9 kPa. The electrode consisted of brass with the spaces between measuring area and guard areas filled with PTFE. A mechanical support was screwed on the top side to stabilize the electrode as the inner and outer areas were not physically attached together. Figure 4.18 show photographs of the electrode top and bottom side.

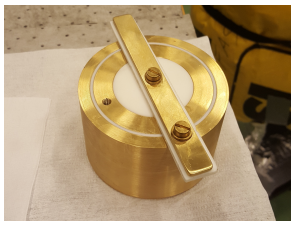

(a) Photograph of the bulk oil electrode top side.

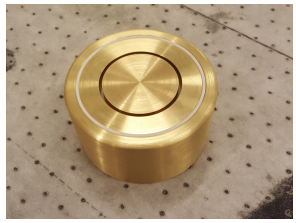

(b) Photograph of the bulk oil electrode bottom side.

Figure 4.18: Photographs of the bulk oil electrode designed for measuring the current in bulk oil samples. The white volumes in the electrode consisted of PTFE.

4.6.6 Deriving a formula for obtaining the conductivity of oil from bulk oil samples

For a series connection of paper and oil, consider figure 2.2 under DC condition where the capacitances are disregarded. The circuit then consists of two resistances in series where the applied voltage U is expressed as equation (4.2).

$$U = E_{paper}d_{paper} + E_{oil}d_{oil} \tag{4.2}$$

If no space charges are present the current density $J = \sigma E$ is equal for both dielectrics (continuity law) under steady state DC condition, such that

$$\sigma_{paper}E_{paper} = \sigma_{oil}E_{oil} \tag{4.3}$$

The conductivity of paper is calculated using equation (3.1) with the parameters from chapter 3.1. The electric field strength used to calculated the conductivity of paper is found by first assuming $U_{oil} << U_{paper}$, as suggested in [5], so that

$$U \approx E_{paper}d_{paper}. \tag{4.4}$$

After obtaining the conductivity, Ohm's Law is expressed as current and turned with respect to electric field strength to give

$$E_{paper} = \frac{I_{DC}}{\sigma_{paper}A}$$

where I_{DC} is the steady state DC current and A the surface area. The DC current is obtained from measurements, and conductivity is calculated from equation (3.1). Turning equation (4.2) with respect to electric field strength of oil gives equation (4.5).

$$E_{oil} = \frac{U - E_{paper}d_{paper}}{d_{oil}} \tag{4.5}$$

Finally, turning equation (4.3) with respect to oil conductivity and inserting equation (4.5) gives equation (4.6).

$$\sigma_{oil} = \frac{\sigma_{paper}E_{paper}d_{oil}}{U - E_{paper}d_{paper}} \tag{4.6}$$

Both equations (4.5) and (4.6) are applicable for plotting to express the DC current behaviour in bulk oil samples.

4.6.7 Deriving a formula for obtaining the DC current in butt gap samples

As butt gaps contain both paper and oil gaps, being able to calculate the expected current through a butt gap sample and compare it with measured values serves as a method for testing the derived formula for oil conductivity, shown in chapter 4.6.6. In order to calculate the current that would flow through a butt gap, the properties and dimensions of both oil and paper must be known. Conductivities of paper and oil are found in chapters 3.1 and 4.6.6, hence the physical dimensions remain. As the oil cavities and paper strips within the butt gap sheets are connected in parallel, the surface areas of each paper strip and oil channel in the butt gap sheet are needed. An illustration of a butt gap sheet is shown in figure 4.19.

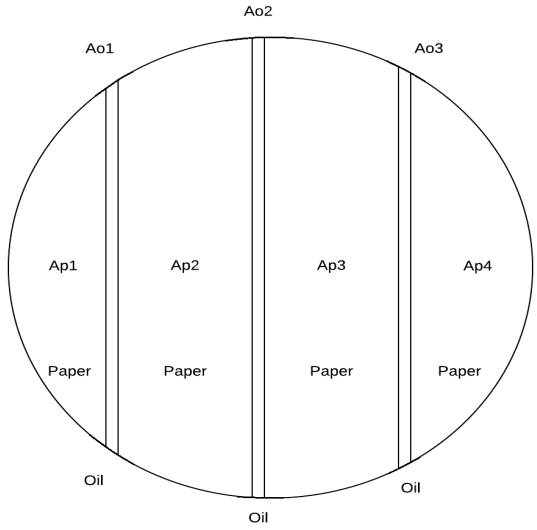

Figure 4.19: Drawing of a butt gap sheet. Subscripts *p* and *o* refer to paper and oil.

Width of the paper strips was 20 mm and oil channels 2 mm. Diameter of the sample measuring area is 78 mm. Subscripts *p* and *o* in the figure refer to paper and oil, respectively. Estimated areas of oil channels and paper strips are presented in table 4.3.

Two samples were made in this configuration consisting of 1 butt gap sheet and 7 butt gap sheets. 5 sheets of papers were placed on each side for each sample.

Converting the drawing in figure 4.19 into a mathematical model results in a circuit consisting of three components, one representing the butt gap and two representing the paper

Table 4.3: Estimated areas of oil channels and paper strips for calculating the expected DC current in butt gap samples.

Paper strips		**Oil channels**	
Area	Magnitude [mm^2]	Area	Magnitude [mm^2]
A_{p1}	434	A_{o1}	128
A_{p2}	1440	A_{o2}	160
A_{p3}	1448	A_{o3}	140
A_{p4}	680		

on each side. The butt gap consists of a parallel connection of both oil and paper. Under DC condition, the capacitances are disregarded resulting in a circuit shown in figure 4.20.

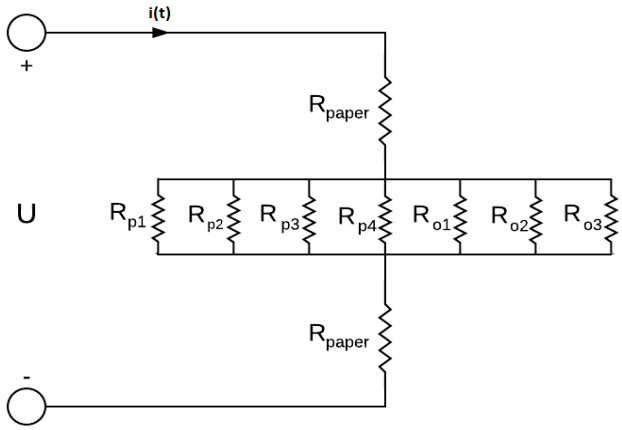

Figure 4.20: Mathematical model of butt gap sheets with paper sheets on both sides. Subscripts p and o refer to paper and oil.

Resistances for paper and oil are calculated using equation (2.17) with their respective conductivity, surface areas and gap distances. Both resistances R_{paper} are equal and can be combined by simple addition, but each branch in the parallel connection have their unique resistance which must be calculated separately. Addition of the parallel connection is done by switching the capacitances in equation (2.5) with resistances and adding the remaining branches.

Calculating the conductivity of paper is done using equation (3.1). Conductivity of oil is calculated from the formula obtained after studying bulk oil samples. Voltage is assumed to be divided equally among each paper and butt gap sheet allowing calculation of conductivity in paper.

After all resistances in the parallel connection are calculated, a circuit of two resistances in series remain which are added together. Then, Ohm's law is used to calculated the DC current which is further plotted with respect to the total applied voltage.

Chapter 5

Results

This chapter contains results of DC current measurements obtained from stressing various samples. Samples with paper, paper with bulk oil and paper with butt gaps are subjected to various voltages and temperatures. Only the sample with paper is stressed with different temperatures, all other samples are at a constant temperature of T = 50°C. Measured currents are plotted versus applied voltage or electric field strength. The loss tangent from equation (2.28) is presented in a log-log plot versus frequency. None of the polarization current curves in bulk oil and butt gap samples fulfilled the requirement of the Hamon approximation. As this requirement is only a recommendation, the calculations from studying the sample with 1 butt gap sheet was chosen to be investigated.

5.1 Steady state DC current and loss tangent from studying paper samples

A sample of 10 paper sheets, combined from two 5-sheet stacks, was selected as the sample for obtaining the temperature and electric field strength dependency of paper. These dependencies were investigated separately by applying a constant temperature or electric field and varying the other. Polarization time was set to 18 000 seconds (or 5 hours) and depolarization time to 36 000 seconds (10 hours). To confirm the validity of using the obtained polarization current curves in the Hamon approximation to obtain the loss tangent $\tan(\delta)$, each data set was curve fitted in Excel to obtain its parameter n. This parameter had to be in the range of $0.3 \leq n \leq 1.2$, as was explained in chapter 2.5. A relative permittivity for paper of $\varepsilon_{paper} = 4$ was used for these calculations.

5.1.1 Measured steady state DC currents from applying temperatures and electric field strengths

Figure 5.1 present the measured DC currents when different temperatures were applied. Temperatures ranged from T = 23 - 83 $^{\circ}C$ at a constant electric field strength of E = 20 kV/mm. DC current is plotted in logarithmic coordinates from 10^{-11} to 10^{-6} A. Graphs and data of the measured polarization and depolarization currents are found in appendix A.5.

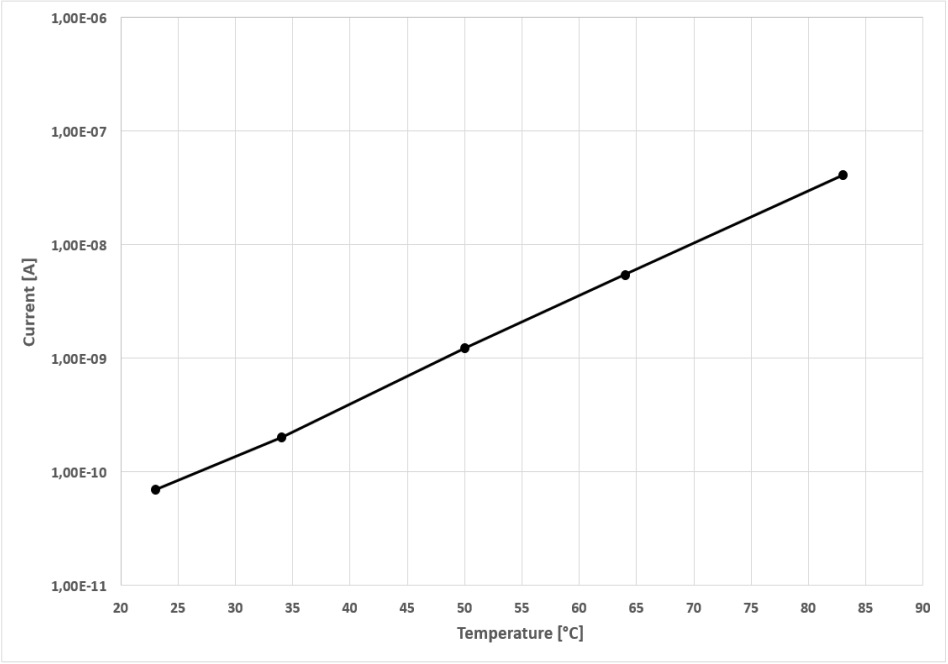

Figure 5.1: Logarithmic plot of measured DC current versus temperature at a constant electric field strength of 20 kV/mm. A sample containing 10 sheets of paper was used for this measurement.

The graph in figure 5.1 reveal a linear curve which shows that the current is exponentially dependent on temperature. Measured current at room temperature was 70 pA and at 1.24 nA with 50 $^{\circ}C$. At the highest temperature of 83 $^{\circ}C$, measured DC current was at 0.415 μA.

Figure 5.2 presents the obtained DC currents from applying various mean electric field strengths in the range of 10 - 30 kV/mm. A constant temperature of T = 50 $^{\circ}C$ was applied for all field strengths. DC current is plotted with the same logarithmic scale as with temperature, ranging from 10^{-11} to 10^{-6} A. Graphs of the measured polarization and depolarization currents are found in appendix A.7.

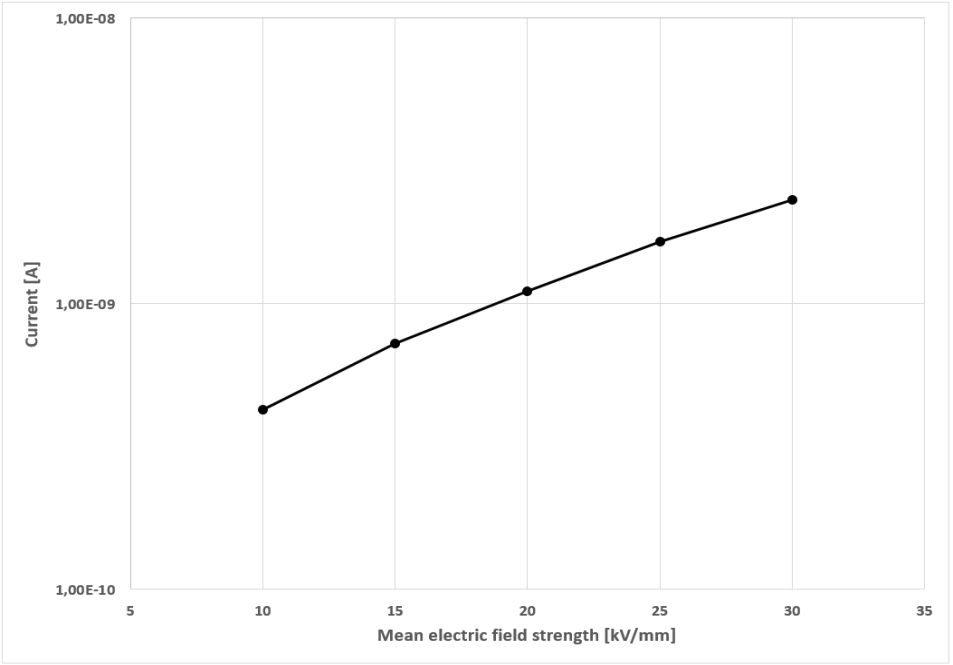

Figure 5.2: Logarithmic plot of measured DC current versus applied mean electric field strength at a constant temperature of T = 50 $^{\circ}C$. A sample containing 10 sheets of paper was used for this measurement.

The plot in figure 5.2 reveals an approximately linear curve which show that the current is exponentially dependent on electric field strength. However, the rate of rise from electric field strength is smaller compared to temperature. Current at E = 10 kV/mm is measured to be 0.426 pA, at E = 20 kV/mm to be 1.11 pA and for the highest field strength of E = 30 kV/mm at 2.32 pA.

5.1.2 Obtained loss tangents by use of Hamon approximation at various temperatures and electric field strengths

Varying the temperature

Obtained values for parameter *n* are collected in table 5.1 at various temperatures. Geometric capacitance is calculated to be 47 pF. Additionally, the apparent conductivities, using equation (2.21), used for calculating the loss tangent are collected here.

Table 5.1: Parameter n, required for the Hamon approximation, obtained from polarization currents under various temperature at a sample with 10 paper sheets. Temperature was 50°*C*.

Temperature [°*C*]	n	Conductivity [S/m]
23	0.771	$7.33\ 10^{-16}$
34	0.804	$2.05\ 10^{-15}$
50	0.958	$1.3\ 10^{-14}$
64	1.023	$5.71\ 10^{-14}$
83	1.082	$4.34\ 10^{-13}$

The table shows that all polarization curves are applicable for the approximation. Resulting curves from calculating the loss tangent $\tan(\delta)$ is presented in figure 5.3. The loss tangent is plotted versus frequency in log-log coordinates. Frequency axis ranges from 1 Hz to 1μHz while loss tangent axis ranges from 10^{-3} to 10^{3}.

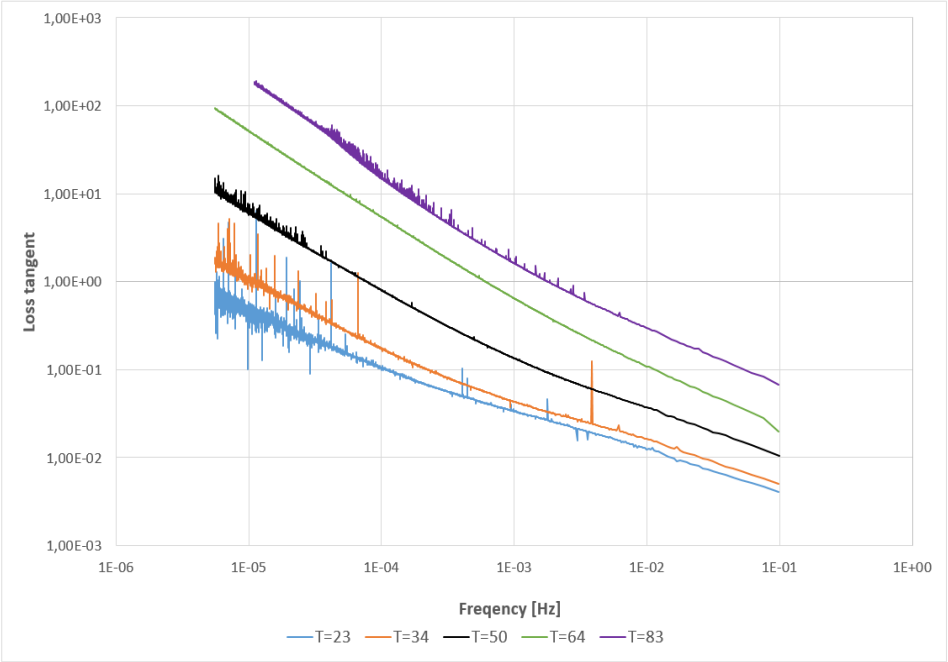

Figure 5.3: Log-log plot of loss tangent tan(δ) versus frequency at various temperatures and with an electric field strength at 20 kV/mm and 10 sheets of paper.

The figure reveals a clear difference in tan(δ) with the various temperatures at all frequencies. The curves are linear below 1 mHz for temperatures below 50 $^{\circ}C$ while above this frequency, the loss tangents show a slight bend. At T = 64 and T = 83 $^{\circ}C$, the curves are linear for all frequencies.

Varying the electric field strength

Obtained values for parameter n and conductivities are collected in table 5.2. The same geometric capacitance of 47 pF were used for these calculations.

Table 5.2: Parameter n, required for the Hamon approximation, obtained from polarization currents under various field strengths at a sample with 10 paper sheets. Temperature was 50$^{\circ}C$.

Electric field strength [kV/mm]	n	Conductivity [S/m]
10	1.03	$8.91\ 10^{-15}$
15	1.002	$1.01\ 10^{-14}$
20	0.954	$1.16\ 10^{-14}$
25	0.945	$1.38\ 10^{-14}$
30	0.915	$1.62\ 10^{-14}$

The table shows that all polarization curves are applicable for the approximation. Figure

5.4 presents the resulting loss tangent tan(δ) for various electric field strengths versus frequency, plotted in log-log coordinates. Frequency axis ranges from 1 Hz to 1μHz while loss tangent axis ranges from 10^{-3} to 10^{2}.

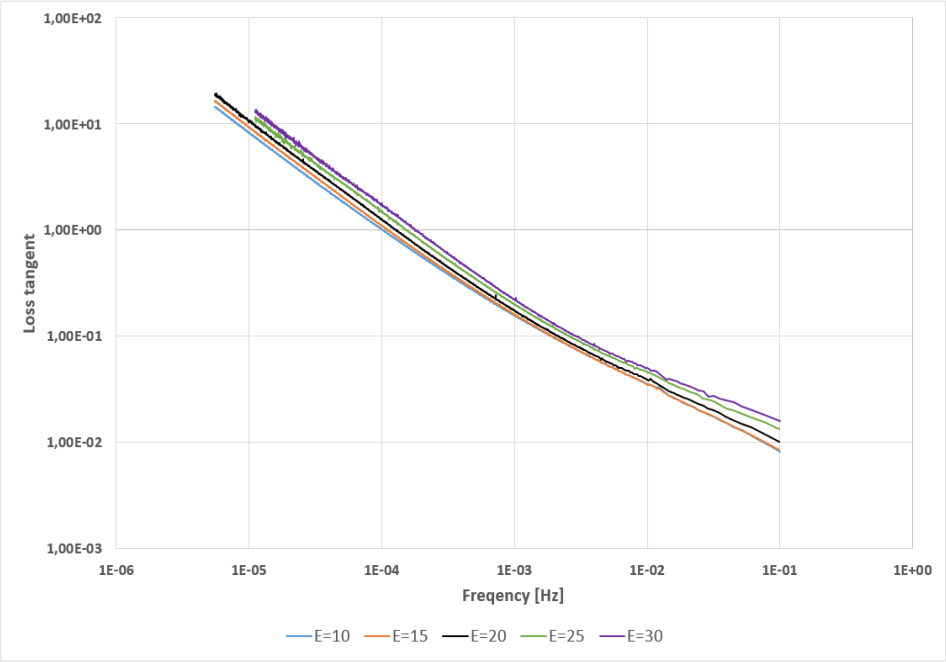

Figure 5.4: Log-log plot of loss tangent tan(δ) versus frequency at various electric field strength with a constant temperature of 50°C. A sample of 10 paper sheets was used.

Figure 5.4 show small differences between tan(δ) of the various electric field strengths at all frequencies. The graph shows two regions, linear curves below 1 mHz and a slight bend above 1 mHz for all field strengths.

5.2 Measurements of steady state DC current from studying bulk oil samples

All bulk oil samples had 10 layers of paper, constructed from two 4-sheet paper stacks and with 1, 4, 7 and 11 bulk oil sheets. Temperature was constant at $50°C$ and total applied voltage were in the range 4-32 kV. Both polarization and depolarization durations were set to 36 000 seconds (10 hours).

Figure 5.5 shows the measured DC current for voltages ranging from 4 kV to 32 kV. Results from samples with 1, 4 and 7 bulk oil sheets are plotted in the figure. Graphs of the measured polarization and depolarization currents are found in appendices A.9, A.10, A.11 and A.12. The sample with 11 bulk oil sheets gave unintelligible curves and were thus excluded from this plot.

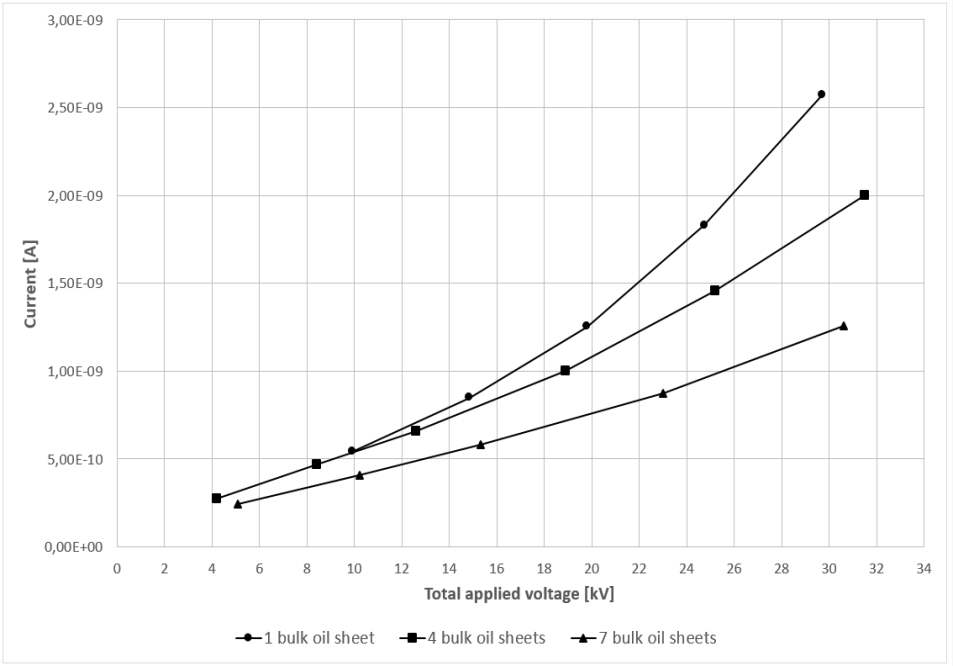

Figure 5.5: A plot of the measured DC current versus total applied voltage for different bulk oil thicknesses in series with 10 paper sheets. Temperature was T = $50°C$.

The measured current ranges from $2 * 10^{-10}$A to $2.5 * 10^{-9}$A. The curves reveal a region of linear rate of rise at low voltages and a rapidly growing current at higher voltages. With more bulk oil present in the samples this region of rapid increase in current appear to become totally suppressed until only a linear rate of rise remain.

5.3 Steady state DC current and loss tangent from studying butt gap samples

Two samples were used to study butt gaps at a constant temperature of T = 50°*C*. The first sample consisted of a 1 bulk oil sheet stack and two 4-sheet paper stacks to simulate a single butt gap. The second sample consisted of only a 7 bulk oil sheet stack with 2 paper sheets to observe the effect of significantly increasing oil volume. Polarization time was set to 9 000 seconds (2.5 hours) for the sample with 1 butt gap sheet and 12 000 seconds (3.33 hours) for the 7 butt gap sheet sample. Depolarization times were set to 25 200 seconds (7 hours) and 18 000 seconds (5 hours) respectively.

5.3.1 Investigating measured steady state DC currents from various applied electric field strengths

Figure 5.6 presents the measured DC currents when applying electric field strengths in the range 10 - 30 kV/mm for both samples. The current-axis is plotted in logarithmic coordinates and ranges from 10^{-11} to 10^{-6}A. Graphs of the measured polarization and depolarization currents are found in appendices A.13 and A.14.

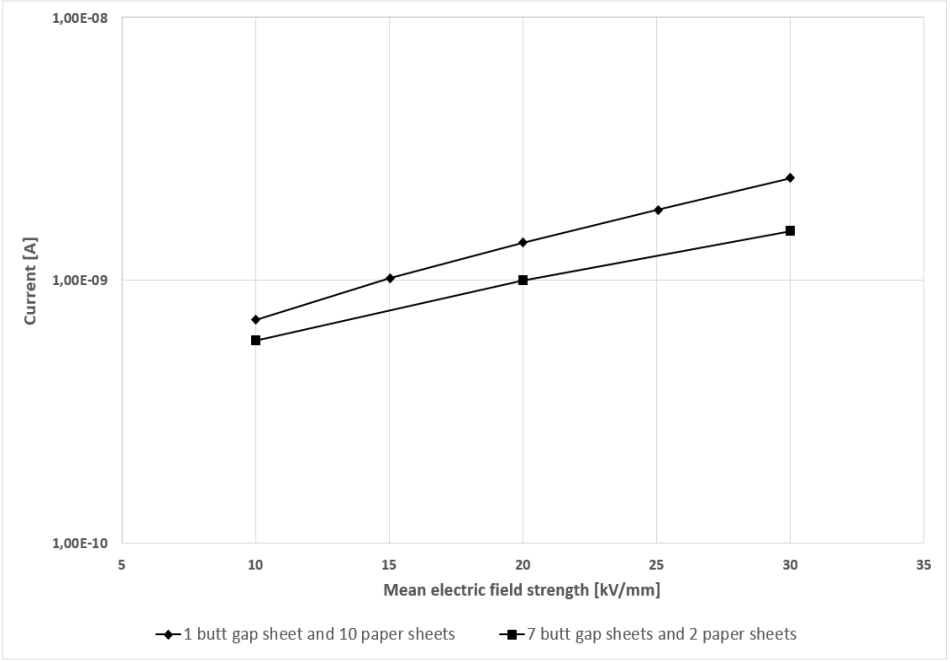

Figure 5.6: Logarithmic plot of DC current versus mean electric field strengths applied to butt gap samples consisting of 1 butt gap sheet with 10 paper sheets and 7 butt gap sheets with 2 paper sheets. Temperature was T = 50°*C*.

Figure 5.6 show approximately linear curves for both samples revealing an exponential dependency. There are small current differences between the samples and both show about the same rate of rise. The measured currents range from 0.7 nA to 2.45 nA for the 1 butt gap sample and 0.6 nA to 1.54 nA for the 7 butt gap sample.

5.3.2 Investigation of obtained loss tangents by use of Hamon approximation at various applied electric field strengths

Values obtained for parameter n are collected in table 5.3. The relative permittivity was assumed to be dominated by paper and the geometric capacitance was calculated to be 42.7 pF. The apparent conductivity was obtained from using equation (2.21) with corresponding measured DC currents.

Table 5.3: Collection of values of parameter n and conductivities for various electric field strength used in the Hamon approximation for the 1 butt gap sheet sample.

Electric field strength [kV/mm]	n	Conductivity [S/m]
10	0.244	$1.48\ 10^{-14}$
15	0.232	$1.41\ 10^{-14}$
20	0.222	$1.45\ 10^{-14}$
25	0.213	$1.54\ 10^{-14}$
30	0.203	$1.71\ 10^{-14}$

The table shows that none of the parameters n are within the range $0.3 \leq n \leq 1.2$. This range is only a recommendation, hence the loss tangent is still plotted as it is of interest to observe $\tan(\delta)$ behaviour with a single butt gap, thus a larger percentage of error is to be expected.

Figure 5.7 present the loss tangent tan(δ) versus frequency plotted in log-log coordinates. Frequency axis ranges from 1 Hz to 1μHz while loss tangent axis ranges from 10^{-2} to 10.

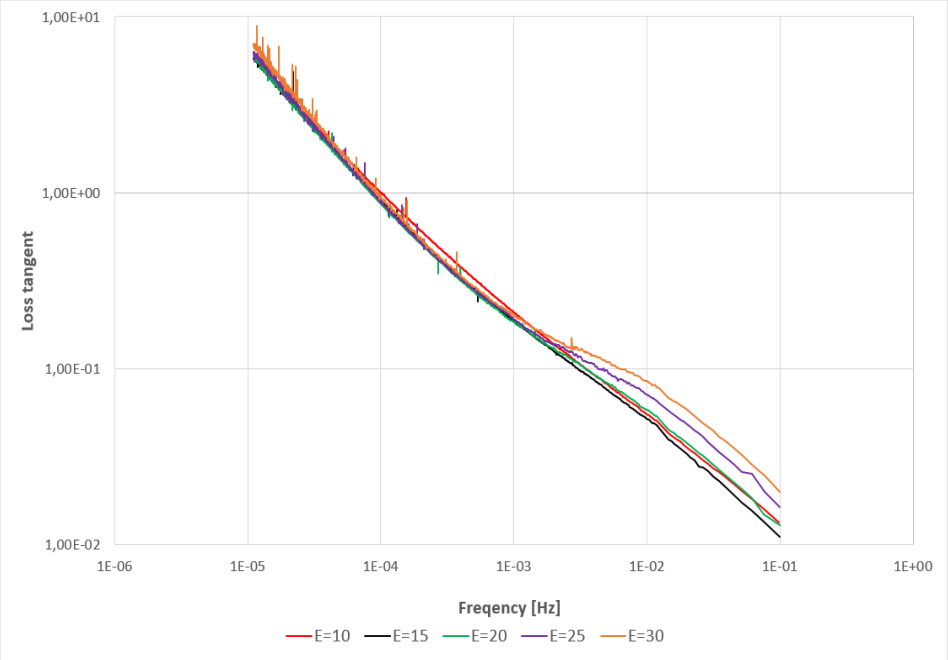

Figure 5.7: Log-log plot of loss tangent tan(δ) versus frequency at various electric field strengths at a constant temperature of 50 $^{\circ}C$. The sample used consisted of 1 butt gap sheet and 10 paper sheets.

Figure 5.7 show near linear curves for field strength below E = 20 kV/mm. At E $\geq$ 20, the curves bend upwards at frequencies above 1 mHz while slightly bending downwards below this frequency. An interesting observation is that tan(δ) for E = 10 kV/mm is equal to E = 20 kV/mm and greater than E = 15 kV/mm at f $\geq$ 1 mHz. At f $\leq$ 1 mHz, E = 10 has a greater tan(δ) than all other field strengths. The curve shows no clear dependency of electric field strength which can also be seen in table 5.3 when observing the change in conductivity with increasing applied field strength.

Chapter 6

Discussion

This chapter contains the thoughts, reflections and findings of the work in this thesis. Three sub-chapters presents the discussion of work prior to and after PDC measurements as well as the methodology. The contents are presented by text, graphical figures and tables.

6.1 Reflections of preparations prior to the main study

6.1.1 Creation of paper stacks and preparation of oil

Shaping the various stacks was done by drawing their shapes with a marker, then the paper was hand cut with a knife. The sheets were cut with a diameter greater than the electrodes so measurements would be less affected by poor cutting. However, this approach does not give perfect cuts regarding the bulk oil and butt gap sheets. Uneven cuts between layers may create some edge effects which enhances the electric field locally. It is uncertain how much this would affect the field distribution but [17] showed that butt gaps, which are no more than 2 mm wide, create local field enhancements. Although this may cause an effect on the measurements, it was disregarded along with any other edge effect in this thesis. To improve the method, a compass could be used to give smoother circles. In addition, several sheets of paper could be cut simultaneously to improve the effectiveness.

To attach the sheets to form stacks, special made powder called TACKIDEX C169 - DEXTRINE was used. Combining the powder with water created the glue, but no clear mixture rate guide was available. From trial and error, small amounts of water with a moderate portion of powder was found to be suitable. The glue was only used to combine small areas in the paper stacks but was required more frequently in both bulk oil and butt gap stacks. The glue was also used within the measuring area of the butt gap stacks to attach the strips properly. It is uncertain as to how this could affect the dielectric response of the samples. However, this glue is a cellulose compound and basically extends the paper

thickness when attaching two sheets together. This may have created thicker samples than the nominal thickness.

A separate setup, presented in chapter 4.2.3, was used to degas the oil before impregnation. While the oil was degassed for four hours under close observation the container, pipes and valves were not completely airtight. This also applied to the pipes used to transfer the oil from the degassing device to the test object. Hence, some air may have been injected into the oil during transfer. This would result in small air bubbles which, if infiltrated into the samples, could distort the measurements. This was kept in mind when opening the test object to switch samples and no visible bubbles were ever found.

6.1.2 Drying and impregnation of paper and findings from PDC measurements during these processes

All samples were dried and impregnated simultaneously as these processes require time. A power loss occurred shortly after the drying process had begun which was not discovered until two days after. The temperature was then increased to $100°C$ and dried for additional two days. As was presented in chapter 3.5, some authors in previous studies only dried for 24 hours and even below $100°C$. Furthermore, impregnation durations was usually about 24 hours at $120°C$. The impregnation process in this thesis was performed over the weekend at $100°C$, giving a total of four impregnation days. Due to the current being obtained during impregnation, this process was far longer than in previous studies. A measurement of the moisture content in the paper using Karl Fisher was done where the resulting moisture content was below the devices threshold. Hence, it was concluded that the drying and impregnation processes were successfully performed.

As explained previously, a PDC study during impregnation was conducted, shown in chapter 4.6.1, to see if this type of technique could be used as a diagnostic tool for the impregnation process. From this minor study, the largest change in current occurred after the first 12 hours and had minor changes the following 24 hours. The results from looking at the time constant also reveal that most of the impregnation had occurred during the first 12 hours. As opposed to all other stacks, the sample used for this study was compressed by the electrode and additional weight which slowed the absorption of oil in the paper. The other stacks then had an easier time absorbing oil which strengthen the possibility that 12 hours was a sufficient impregnation duration. The technique of PDC measurement for assessing the impregnation state showed promise, as the steady state currents and time constants appeared to reach constant values, which gave an indication that the impregnation was completed.

A PDC measurement of the paper sample before any injected oil was also performed. The results here showed a higher current by a factor of 10 which suggests that the oil enhances the insulating properties by blocking certain conduction channels previously present. This is opposite of what was previously perceived as conductivity of oil has been found to be higher than paper and effectively reduces the insulating capability [7].

6.2 Reflections upon the methodology

A flexible system where stacks can be switched to form samples is an effective method for obtaining large quantities of data over a short duration of time. Being able to dry and impregnate all sample simultaneously is advantageous in this regard but it also carries new factors of uncertainties. Every time the test object is opened for more than 5-10 minutes air may be injected into the oil and create bubbles. These bubbles may be small but if this process is repeated multiple times, they could accumulate to impact the results. Hence, the test object was never opened for longer than 5 minutes and flushed with moisture-free Nitrogen gas each time to remove any eventual humid air pockets that had infiltrated the tank. Due to the high viscosity of the oil, small quantities were lost every time a sample was switched meaning that there was a finite number of times the samples could be switched. Although only one batch of oil was needed for this thesis, a solution to this problem would be to refill the tank by degassing the oil under the same temperature and for the same duration.

The voltage source used had a maximum level of 35 kV. However, at the highest voltages (typically 33 kV and above) the measuring software had problems switching from polarization to depolarization resulting in a long polarization and no depolarization. As a safety margin the voltage never exceeded 33 kV. The samples had a resistance R in the range of $10^{10} - 10^{13}\Omega$ while resistances in the circuit had a maximum of 50 MΩ, as seen in figure 4.1. A quick circuit analysis shows that virtually all voltage would be across the sample and any voltage drop across the circuit can be disregarded.

6.2.1 Time-requirement to reach thermal equilibrium in samples after a temperature drop

Switching samples always resulted in temperature drops which were regained after a few hours, as explained in chapter 4.6.3. As oil impregnated paper is heavily dependent on temperature it was important to ensure that the sample had reached its thermal equilibrium. This is difficult to measure, but obtaining the capacitance gives an indication of how the surface area, thickness and permittivity behave, see equation (2.3). The sample thickness might change due to increased temperature after a sudden drop and this could also occur with the electrode surface area. An indication that the surface area had changed was that the screws used to attach the circuit-wires were difficult to unscrew after the electrode had been used for measurements, which indicated an expansion of the metals. The total relative permittivity might also change due to the expansion of oil films between paper sheets. Having more oil in the sample lowers the total capacitance such that the theoretical relative permittivity of 4 might actually be lower. This is indicated from the study in chapter 4.6.3, were the capacitance was found to be lower than the theoretically calculated values. It also showed that the capacitance stabilized after about one week of switching a sample, with the highest change occurring after one day. However, waiting one week before stressing a sample was never an option since it would significantly reduce the number of measurements possible within the time restriction of the thesis. Results in chapter 4.6.3 indicated that the capacitance only changed by a few percentages between one day

and one week and would not result in any major impact on PDC measurements.

6.2.2 Study of prolonged polarization and depolarization durations

Polarization and depolarization durations varied depending on the available time with regard to holidays and planned outages in the laboratory. Due to the large quantity of measurements, the number of applied voltages was prioritized rather than their durations. The minor study in chapter 4.6.2 revealed that both polarization and depolarization currents continued to decrease long after the chosen durations. The polarization current change ranged from 23% to about 5% from the lowest to highest voltages. The chosen electric field strengths applied in this thesis were thus rarely below E = 10 kV/mm as this gave a maximum deviation of 13%, which was acceptable. The change in depolarization current was much higher than polarization with a change of 70% to 90%. The same study was performed for the largest bulk oil sample, 10 paper sheets and 11 bulk oil sheets, were the change in polarization and depolarization current were 5% and 60%, respectively. The idea behind choosing the largest sample was that more oil would require longer time to polarize as the number of paper sheets were the same as with paper samples. These studies revealed that depolarization was more affected by a short duration than polarization. However, the depolarization currents were always a factor of 100 times lower than polarization currents and only appeared as noise in the next measurement. Additionally, equation (2.21) and (2.22) were compared which revealed that the samples had be sufficiently discharged.

6.2.3 Minimum sample thickness to avoid the effect of injected homo charges

The study of paper sample thickness in chapter 4.6.4 was conducted to see if eventual injected homo charges would affect any measurement, as was presented in [10]. The results presented in figure 4.17 showed that the conductivities between paper thicknesses had no major differences. All samples had similar rate of rise, and samples with 5 and 14 sheets of paper had similar magnitudes that were higher than the 10 sheet sample. This may come from statistical deviations. It appears from these graphs that a sample with at least 5 sheets of paper is viable as it appears to not suffer from any injected homo charges. The sample with 10 sheets of paper was chosen due to the realistic thickness compared to actual cable insulation and because of the limitations of the voltage source.

6.3 Investigation of the results

This chapter investigates the results obtained in chapter 5. Conductivities are calculated using measured DC currents and compared with literature. Additional calculations performed in this chapter consist of obtaining the voltage distribution in bulk oil samples, conductivity of oil and expected DC current in butt gap samples. The latter calculations contains a sensitivity analysis of the parameters of conductivity in oil and paper. Previously, the assumption of conductivity in oil has been that it is far greater than paper [7].

6.3.1 Study of paper samples with respect to electric field strength and temperature

Plots of calculated conductivities using equation (2.21) with the DC currents from figures 5.1 and 5.2 are compared with calculated conductivities using equation (3.1). Figures 6.1 and 6.2 show this comparison in a logarithmic plot of the conductivities. Conductivity obtained from measured DC current are referred to as ”measured conductivity” and conductivity using equation (3.1) is referred to as ”calculated conductivity”.

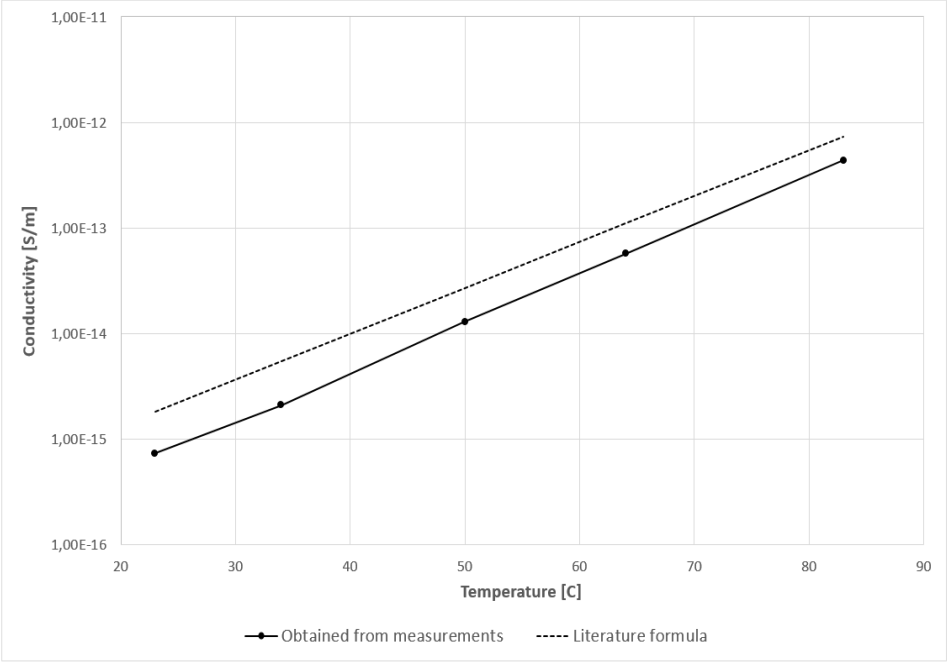

Figure 6.1: Comparison of calculated conductivities obtained from measured DC current and literature formula using equation (2.21). The figure contain a logarithmic plot of conductivity versus temperature with a constant electric field strength of E = 20 kV/mm.

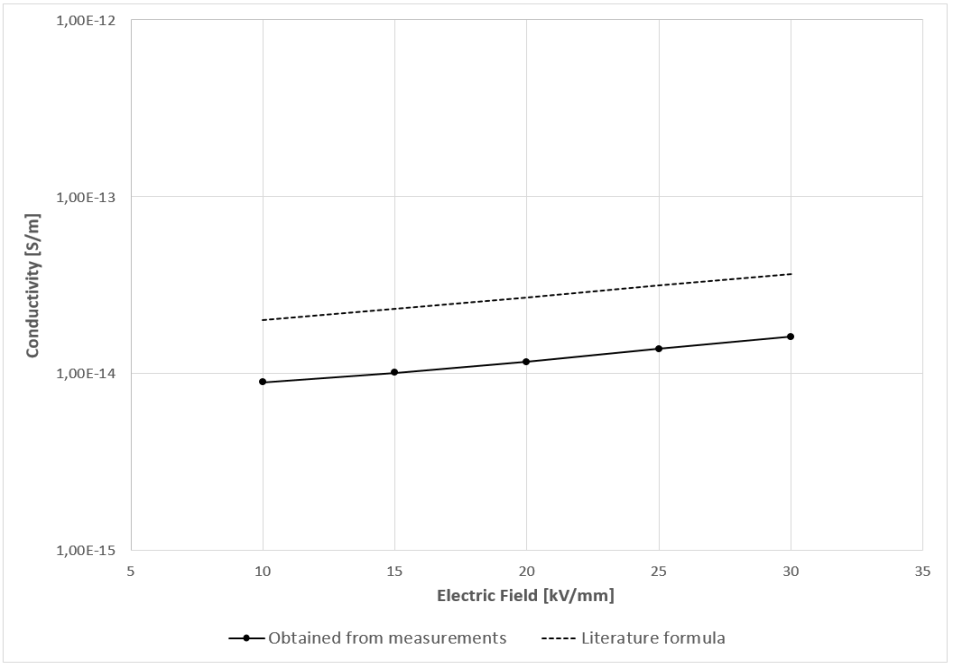

Figure 6.2: Comparison of calculated conductivities obtained from measured DC current and literature formula using equation (2.21). The figure contain a logarithmic plot of conductivity versus electric field strength at a constant temperature of T = 50°C.

It is apparent from the figures that the measured conductivity curves match the calculated ones with regard to their behaviour, having approximately the same slopes in the semi logarithmic plots. The measured conductivities were curve fitted to give the field and temperature dependency parameters α and β used in equation (3.1), respectively. These parameters were found to be $\alpha = 0.1°C^{-1}$ and $\beta = 0.03$ mm/kV which is in accordance with the literature, as shown in chapter 3.1. Parameter σ_0 was calculated to be $0.33*10^{-16}$ and $0.47*10^{-16}$ S/m which is about 50% to 70% lower than the literature. This deviation may come from statistical deviations, different preparation techniques in the studies or aged oil. The value from literature of $\sigma_0 = 10^{-16}$ S/m was used for future calculations. From the figures, the method used in this thesis is viable to study paper samples and has good prerequisites for providing credible results with regard to bulk oil and butt gap samples.

The study of loss tangents tan(δ) in chapter 5.1.2 reveals that the Hamon approximation is applicable when studying paper samples. Calculated values presented in figures 5.3 and 5.4 show a greater dependency of temperature than electric field strengths, also seen in figures 6.1 and 6.2. A linear rate of rise was observed in both loss tangent curves which suggests that the latter part of equation (2.28), governed by conductivity, is dominating. The slight bend observed at lower electric field strength and frequencies above 1 mHz are due to the contribution of AC, from the first part of the equation, as this region of frequencies comes from the transient region of the polarization curve. Hence, if the loss

tangent is measured at frequencies f $\leq$ 1 mHz, and given a known permittivity, it may serve as a fast method for obtaining the conductivity.

6.3.2 Measured steady state DC currents and voltage distribution in bulk oil samples

The study of bulk oil samples in chapter 5.5 contained several bulk oil thicknesses in series with paper. Curves of current versus voltage in figure 5.5 showed regions with different rate of rises that differed with bulk oil thickness. At low voltages the current was linear for all thicknesses but at 15 kV and above the rate appeared to become more exponential with decreasing oil volume. This suggested that the effect of bulk oil in the system was overshadowed by the amount of paper. With more oil in the system the region of rapid increase appears to be totally suppressed.

The current in bulk oil samples in figure 5.5 decreased with increasing oil volume. Studying figure 3.2 presented in [5] revealed an opposite behaviour where the current increases with a thicker oil sample. However in the same study, aluminum electrodes and polyether Penton insulation were used as opposed to brass electrodes and oil impregnated paper insulation in this study. The electrode-insulation interface plays an important part in field distribution as explained in chapter 3.4 and could affect this current behaviour. In [5], it was also used a thin insulation film meaning that the oil played a dominant role and that the region of suppressed current increase never occurred. An important note is that capacitance measurements were used to position the bulk oil electrode. The electrode was positioned where the highest capacitance was measured, but this did not guarantee that the bulk oil electrode aligned with the sample which could give incorrect current behaviour and/or magnitudes.

In [5], it was suggested that the voltage across bulk oil was approximately zero in an insulation-"bulk oil"-insulation configuration. This assumption was made in combination with the measured DC current in order to calculated the conductivity of oil, as presented in chapter 4.6.6. To verify this assumption, the voltage across the bulk oil was calculated and compared to the voltage in paper. Figure 6.3 presents the ratio of U_{oil}/U_{total} versus the total applied voltage for samples with various bulk oil thicknesses at temperature of T = 50°C.

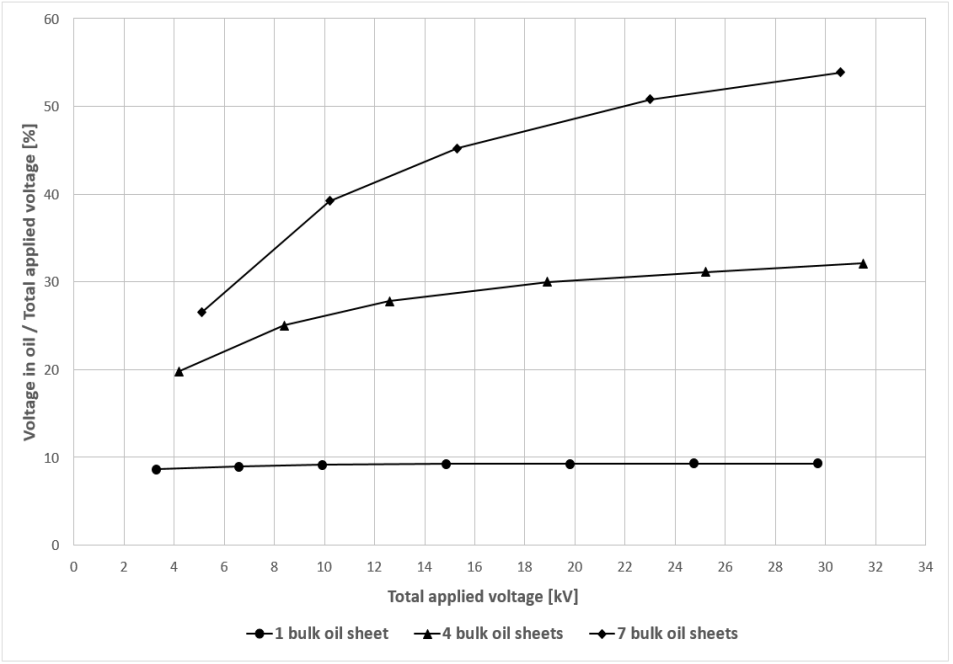

Figure 6.3: Ratio of voltage drop across the bulk oil in multiple bulk oil samples. The samples had 10 sheets of paper in series with various amount of bulk oil sheets. Temperature was T = 50°C.

At the lowest bulk oil volume, voltage drop in the bulk oil is stable at 10% of the drop in paper for all voltages. With increasing bulk oil volume, up to about 55% of the voltage drop appears to move to the oil. It also appears that the voltage distribution reaches stable values at the highest applied voltages. This suggests that the conductivity of oil may be close to that of paper and thus the mobility μ of charge carriers. Recall that ions are regarded as the dominant charge carrier in both oil impregnated paper and the bulk oil [3].

It is apparent that the voltage drop across the bulk oil differs from zero, as opposed to the suggestion in [5]. The voltage drop in bulk oil can therefore not be disregarded which makes the assumption in chapter 4.6.6 less credible. Hence, the percentages of voltage distribution in figure 6.3 are utilized to obtain the voltage in paper and oil and to further calculate the conductivity of oil. An important note is that the findings in figure 6.3 affects the bulk electrode design, as this was based on the assumption of zero voltage across the bulk oil. This is not further investigated in the thesis.

6.3.3 Obtaining a formula for conductivity of oil with respect to electric field strength

The conductivity of oil is calculated using the derivation presented in chapter 4.6.6 and with the voltage distribution in figure 6.3. Hence, calculations are made for the samples with 1, 4 and 7 bulk oil sheets. Conductivity of paper is obtained from equation (3.1) with a temperature T = 50°*C*. Figure 6.4 presents the calculated conductivity of oil versus calculated electric field strength in the oil.

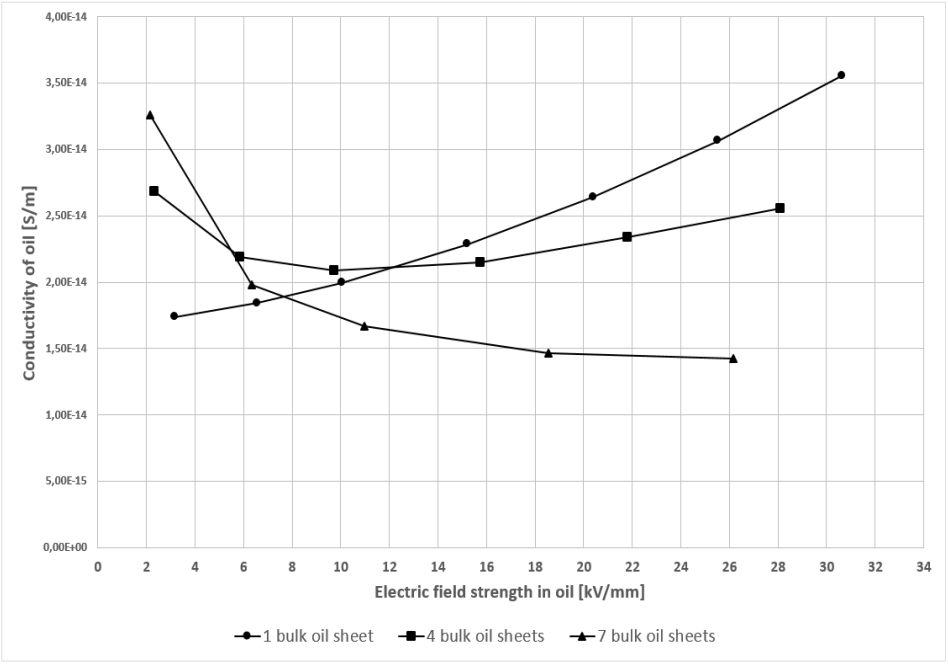

Figure 6.4: Conductivity of oil versus electric field strength in bulk oil for 1, 4 and 7 bulk oil sheets in series with 10 paper sheets. Temperature was T = 50°*C*.

The figure reveals different curves for each bulk oil thickness with conductivities in the range of 1.5×10^{-14} S/m to 3.5×10^{-14} S/m. 1 bulk oil sheet sample shows a clear exponential dependency of electric field strength and is thus used for further calculations. Increasing the bulk oil volume appears to create a region of initial high DC current which declines at the lowest field strengths before increasing at an exponential rate, resulting in U-shaped curves. The minima of this U-shape appears to occur at higher field strength when increasing the oil volume. A region of exponential rate of rise is clear in the samples with 1 and 4 bulk oil sheets but appears to require higher voltages to be visible for the 7 bulk oil sheet curve.

The U-shape may be explained from the findings in chapter 4.6.2 where the change in current due to polarization durations was studied. At lower field strengths the change in

current is higher which suggests that the DC currents in the initial region of figure 6.4 is lower. In order to confirm this theory, the study in chapter 4.6.2 must be performed on all bulk oil samples. This was not done for this thesis due to time restrictions.

Considering the exponential regions in samples with 1 and 4 bulk oil sheets, the electric field dependency in conductivity of oil appear to decline with increased oil volume. This suggests that fewer ions are conducted in the bulk oil, likely due to recombination in the oil volume which reduces the number of surface charges at the paper-bulk oil interfaces [13].

Considering the sample with 1 bulk oil sheet, an equation expressing the electric field strength dependency of oil is extracted from curve fitting of figure 6.4. The expression is presented in equation 6.1.

$$\sigma_{oil} = Aexp(BE) \tag{6.1}$$

Constants are A = 2*10^{-14} S/m and B = 0.0265 mm/kV. This expression is similar to paper in equation (3.1) but with a lower electric field strength dependency, where the equivalent parameter was β = 0.03. The magnitude parameter A is not comparable with σ_0 as this requires a study of the temperature dependency of oil.

6.3.4 Investigation of steady state current in butt gap samples

Investigating figure 5.6 show that the current in the sample with 7 butt gap sheets and 2 paper sheets are lower than 1 butt gap sheet with 10 paper sheets. The increased presence of oil in this parallel configuration reduces the number of total charges being conducted in the sample, suggesting that the oil enhances the insulation. As the width of the oil channels are equal in both samples, an increased channel height provides a longer longitudinal paper-oil interface. A possibility for the decrease in current is that surfaces charges may accumulate at these interfaces creating local field enhancements that affect the conductivity in oil. Another possibility is that the oil has a lower conductivity than paper in this configuration from local temperature differences.

Comparing calculated and measured DC currents in a sample with 1 butt gap sheet and 10 paper sheets

As a way of testing the validity of equation (6.1) the method explained in chapter 4.6.7 is utilized to calculate the expected current that would flow in the sample with 1 butt gap sheet. Equation (3.1) with parameter values from chapter 3.1 is used for obtaining the conductivity of paper while the parameters obtained in chapter 4.6.7 is used for oil. The expected DC currents for 1 butt gap sheet sample are calculated and compared to the measured values. In addition, both these curves are compared with the measured DC current from the 10 paper sheet sample. This comparison illustrates the effect of replacing a paper sheet with a butt gap sheet. Figure 6.5 presents this comparison plotted in logarithmic coordinates of conductivity versus mean applied electric field strength.

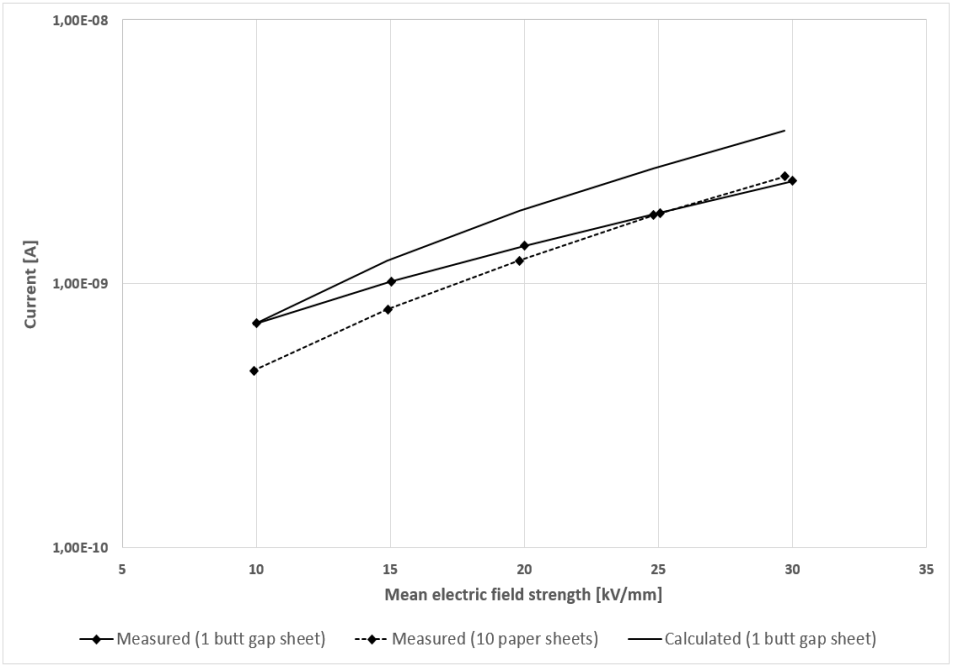

Figure 6.5: Logarithm of DC current versus applied mean electric field strength. The straight lines mark measured and calculated values for a sample with 1 butt gap sheets in series with 10 paper sheets. The dashed line represents measured values for a sample with 10 paper sheets. Temperature was T = $50^{\circ}C$.

From inspecting figure 6.5, it is clear that the measured values deviate little from the calculated ones[1]. All curves are approximately linear which shows an exponential dependency. Calculated values for 1 butt gap sheet sample have the same magnitudes as the measured values for the same sample at low field strengths. At higher field strengths, the rate of rise in measured values decline as opposed to the calculated ones. Both butt gap curves have greater magnitudes than the sample with paper, but only the calculated butt gap curve shows the same rate of rise.

The measured butt gap curve declines with increasing field strength to a point where it approximates the paper sample. By extrapolation the measured butt gap curve appears to reach lower values than the paper sample at E $\geq$ 30 kV/mm. This suggests that oil reduces the total electric field dependency of the sample when connected in parallel with paper.

[1] A difference by a factor of 10 would have been considered as large.

Sensitivity analysis of parameters in formulas for conductivity of paper and oil

To evaluate the impact each parameter in equations (3.1) and (6.1) has on the calculated DC current in figure 6.5, a sensitivity analysis of the parameters is conducted. The procedure for analyzing each parameter is to change one parameter value by a certain percentage and calculate the percentage change in output DC current. Percentage change of input ranges from 1% to 100% for all parameters. Changes in output DC current by change in input parameters are collected in table 6.1. Parameters α, β and B are exponential parameters and expected to be sensitive while σ_0 and A are linear parameters and expected to be less sensitive.

Table 6.1: Sensitivity analysis of positive and negative percentage change in input parameters α, β and σ_0 of equation (3.1) and A and B of equation (6.1) versus percentage change in DC current. Electric field strength is set to E = 20 kV/mm and temperature to T = 50°C for a sample with 1 butt gap sheet and 10 paper sheets.

	% change in DC current				
% change in parameter	α	β	σ_0	A	B
1 %	8 %	0 %	1 %	0 %	0 %
5 %	22 %	2 %	4 %	1 %	1 %
10 %	50 %	5 %	8 %	2 %	1 %
20 %	128 %	10 %	16 %	4 %	1 %
50 %	786 %	27 %	39 %	8 %	2 %
100 %	10161 %	63 %	76 %	14 %	11 %
-1 %	-4 %	0 %	-1 %	-0 %	-0 %
-5 %	-18 %	-2 %	-4 %	-1 %	-1 %
-10 %	-33 %	-5 %	-8 %	-2 %	-1 %
-20 %	-56 %	-9 %	-16 %	-4 %	-2 %
-50 %	-88 %	-21 %	-43 %	-12 %	-5 %
-100 %	-99 %	-38 %	- %	- %	-9 %

The same observations are made when changing the input values in positive and negative directions. Data in table 6.1 show that α is by far the most sensitive parameter and A and B the least sensitive. Parameters β and σ_0 are noticeably sensitive at $\pm$ 20% change in input value. It is clear from table 6.1 that the parameters in conductivity of paper are significantly more sensitive than the parameters in conductivity of oil. Parameters representing the oil affect the DC current by a noticeable amount when increasing the value by at least 100 %. Having increased oil volume in the butt gaps may alter this sensitivity but this is not investigated further in this thesis.

6.3.5 Investigation of the calculated loss tangents in bulk oil and butt gap samples

As was explained in the introduction in chapter 5.3.2, none of the polarization current curves when stressing bulk oil and butt gap samples were applicable for the Hamon ap-

proximation. All values for parameter *n* were below 0.3. As this is only a recommendation the loss tangent for the 1 butt gap sample was still plotted in figure 5.7. A consequence of ignoring this recommendation is that the product of wt, explained in chapter 2.5, may deviate more than $\pm 3\%$, and cause less accurate results.

The plot in figure 5.7 showed that the butt gap sample was dominated by the latter part of equation (2.28), governed by the conductivity, at $f \leq 1$ mHz. At $f \geq 1$ mHz, the first part of the equation representing the AC contribution appeared to have a greater impact. All loss tangents had linear curves and with slight bends at $f \geq 1$ mHz. The only exception was for the curve at E = 20 kV/mm which was linear at all frequencies. An interesting note is that the loss tangents at $f \geq 1$ mHz had approximately equal values at E = 10 and E = 20 kV/mm which were higher than at E = 15 kV/mm. This can also be seen with the apparent conductivity in table 5.3.

6.4 Suggestions for further work

A majority of the work in this thesis was spent developing the methodology and researching literature during PDC measurements. Obtaining currents for the various samples is a lengthy process which limits the amount of data possible to obtain. For further work the following is suggested.

- Performing several PDC measurements on bulk oil with sufficiently long polarization and depolarization durations.
- Construing realistic butt gap samples that replicates the butt gap positioning of multiple butt gaps as in actual cables.
- Studying the temperature dependency of bulk oil and butt gap samples.
- Obtaining the conductivity of oil with respect to temperature.

Chapter 7

Conclusion

The work in this thesis consisted of gathering data which facilitates design improvements of oil-impregnated paper insulation used in HVDC cables. Steady state currents, conductivities and loss tangents of samples with paper, bulk oil and butt gaps were studied under various voltages and temperatures. Minor studies for improving the methodology was also conducted. From the main study of this thesis, the following conclusions are made.

- Electric field strength and temperature dependency of conductivity in paper were in accordance with the literature.
- Voltage across the oil in bulk oil samples differed significantly from zero. Hence, results of the voltage distribution between paper and oil opposed previous assumptions [5].
- DC current in bulk oil samples had exponential rate of rise with applied voltage which became linear with increasing bulk oil volume.
- The magnitude of conductivity in oil was similar to paper, at about 10^{-14} S/m.
- A method for calculating the expected steady state current in butt gap samples was derived from the conductivities of paper and oil. Comparison with measured DC currents of a sample with a single butt gap showed equal magnitudes at low voltages but the measured curve had a lower rate of rise.
- A sensitivity analysis of the method for calculating steady state DC current in butt gap samples showed that the parameters in conductivity of paper are by far the most sensitive. Parameters in conductivity of oil are expected to have a larger impact with increased oil volume.
- Paper samples were applicable for the Hamon approximation but neither bulk oil nor butt gap samples were applicable. Plots of the loss tangent in paper and butt gap samples revealed curves dominated by conductivity at frequencies below 1 mHz.

From the methodology development of the thesis, the following conclusions are made.

- Polarization Depolarization Current measurements was an efficient method for monitoring the impregnation state of paper during this process. Results of current and time constants gave clear indications that most of the absorption in paper occurred during the first 12 hours.
- Current in impregnated paper was lower than dried paper by a factor of 10. This suggested that the oil blocks certain conduction channels previously present.
- Insufficient polarization durations significantly affects the DC currents at low field strengths. Depolarization currents are more sensitive to short durations but have magnitudes that are only regarded as noise in the polarization currents.
- After a temperature drop from switching samples in the test object, at least one day was needed for the samples to reach thermal equilibrium.
- None of the paper samples suffered from injected charges, as was suggested in [10]. Samples with at least 5 sheets of paper are applicable for PDC measurements.

Bibliography

[1] L. E. Pettersen. *"A study of dielectric parameters in oil-impregnated paper insulation for HVDC cables", specialization project*. Trondheim, Norway, NTNU Department of Electric Power Engineering, Dec 2017.

[2] T. Worzyk. *"Submarine Power Cables: Design, Installation, Repair, Environmental Aspects"*. Berlin, Germany, Springer Science Business Media, 2009. ISBN: 978-3-642-01270-9.

[3] M.J.P. Jeroense and F.H. Kreuger. "*Electrical Conduction in HVDC Mass-impregnated Paper Cable*". In: 2.5 (Oct 1995), pp. 718–723. DOI: 10.1109/94.469968.

[4] G. Håkonseth and E. Ildstad. *Steady-State Electric Field and Conductivity in Mass-Impregnated HVDC Cable Insulation*. To be presented at 2nd IEEE International Conference on Dielectrics, 2018.

[5] M.E. Zein Eldine; A.A. Zaky; R. Hawley; M.C. Cullingford. "*Influence of insulating films on conduction*". In: 112.3 (March 1965), pp. 580–585. DOI: 10.1049/piee.1965.0098.

[6] B.V. Hamon. "*An approximate method for deducing dielectric loss factor from direct-current measurements*". In: 99.69 (June 1952), pp. 291–293. DOI: 10.1049/pi-2.1952.0076.

[7] E. Ildstad. *"TET4160 Insulating Materials for High Voltage Applications"*. Trondheim, Norway, NTNU Department of Electric Power Engineering, 2016.

[8] F.H. Kreuger. *"Industrial High DC Voltage"*. Delft, The Netherlands, Delft University Press, 1995. ISBN: 90-407-1110-0.

[9] E. Occhini and G. Maschio. "*Electrical Characteristics of Oil-Impregnated Paper as Insulation for HV DC Cables*". In: PAS-86.3 (March 1967), pp. 312–326. DOI: 10.1109/TPAS.1967.291959.

[10] M.J.P. Jeroense. *"Charges and discharges in HVDC cables", Ph.D. dissertation*. Delft, The Netherlands, Delft University Press, 1997. ISBN: 90-407-1438-X.

[11] V. T. Morgan. "*Effects of Frequency Temperature, Compression, and Air Pressure on the Dielectric Properties of a Multilayer Stack of Dry Kraft Paper*". In: 5.1 (Feb 1998), pp. 125–131. DOI: 10.1109/94.660818.

[12] C. Tang; G. Chen; M. Fu ; R.J. Liao. "*Space Charge Behavior in Multi-layer Oil-paper Insulation under Different DC Voltages and Temperatures*". In: 17.3 (June 2010), pp. 775–784. DOI: 10.1109/TDEI.2010.5492250.

[13] K. Wu; Q. Zhu; H. Wang; X. Wang; S. Li. "*Space Charge Behavior in the Sample with Two Layers of Oil-immersed-paper and Oil*". In: 21.4 (August 2014), pp. 1857–1865. DOI: 10.1109/TDEI.2014.004241.

[14] M. Runde; R. Hegerberg; N. Magnusson; E. Ildstad; T. Ytrehus. "*Cavity Formation in Mass-Impregnated HVDC Subsea Cables Mechanisms and Critical Parameters*". In: 30.2 (March-April 2014), pp. 22–33. DOI: 10.1109/MEI.2014.6749570.

[15] T. Andersen Ve. *private communication*. SINTEF Energy Research, 2018.

[16] A. Jonscher. *"Dielectric relaxation in solids"*. Chelsea Dielectrics Press Limited, 1983. ISBN: 978-0-950-8-7110-3.

[17] G. Håkonseth. *"Local Electric Field in Mass-Impregnated HVDC Cables"*. Trondheim, Norway, NTNU Department of Electric Power Engineering, 2017.

Appendix A

Raw data of measured currents and capacitances

This appendix contains graphs of raw data from all measurements obtained throughout the thesis. Values of DC currents and currents at the end of depolarization period, called ”end of depol”-currents, are collected in tables. Capacitances for the study of thermal equilibrium is also included.

A.1 Measured currents of dried paper sample

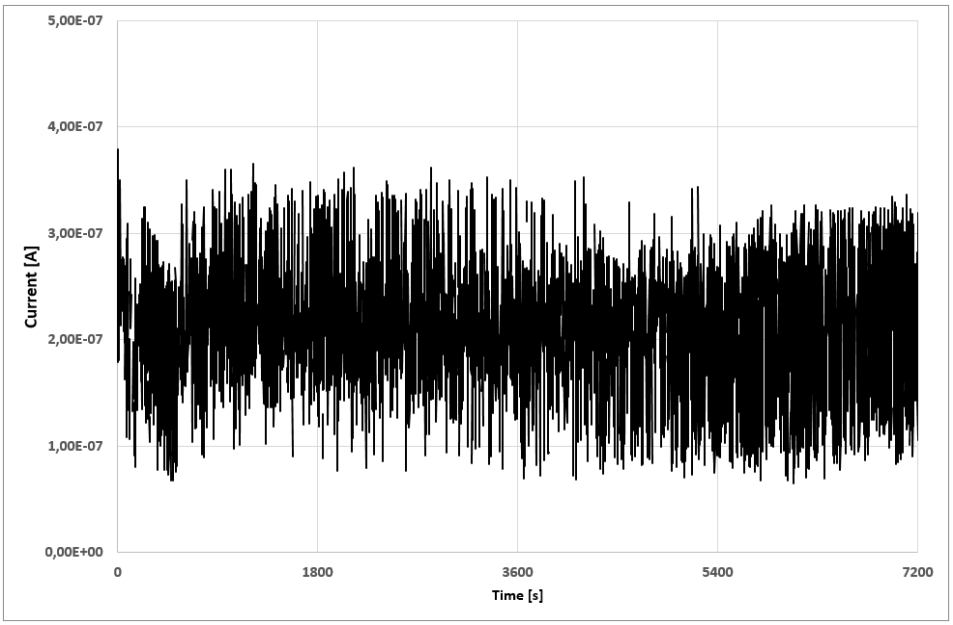

Figure A.1: Measured polarization current of a dried sample with 5 paper sheets at U = 1kV and T = 100°C.

Table A.1: Data of measured DC current of a dried sample with 5 paper sheets at U = 1kV and T = 100°C.

Voltage [kV]	DC current [A]
1	2×10^{-7}

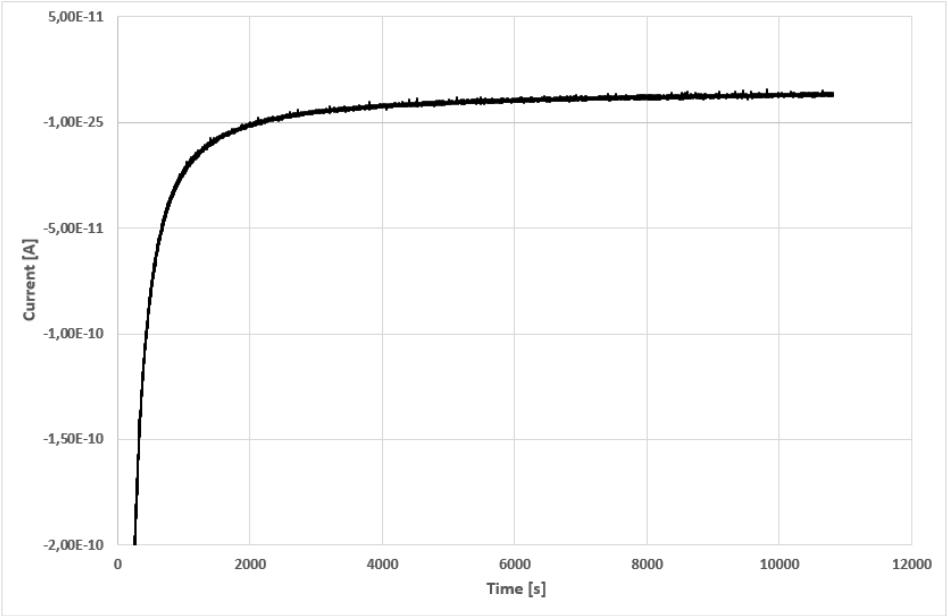

Figure A.2: Measured depolarization current of a dried sample with 5 paper sheets at U = 1kV and T = 100°*C*.

Table A.2: Data of measured 'end of depol' current of a dried sample with 5 paper sheets at U = 1kV and T = 100°*C*.

Voltage [kV]	**'End of depol'-current [A]**
1	1×10^{-11}

A.2 Measured currents of paper sample during impregnation

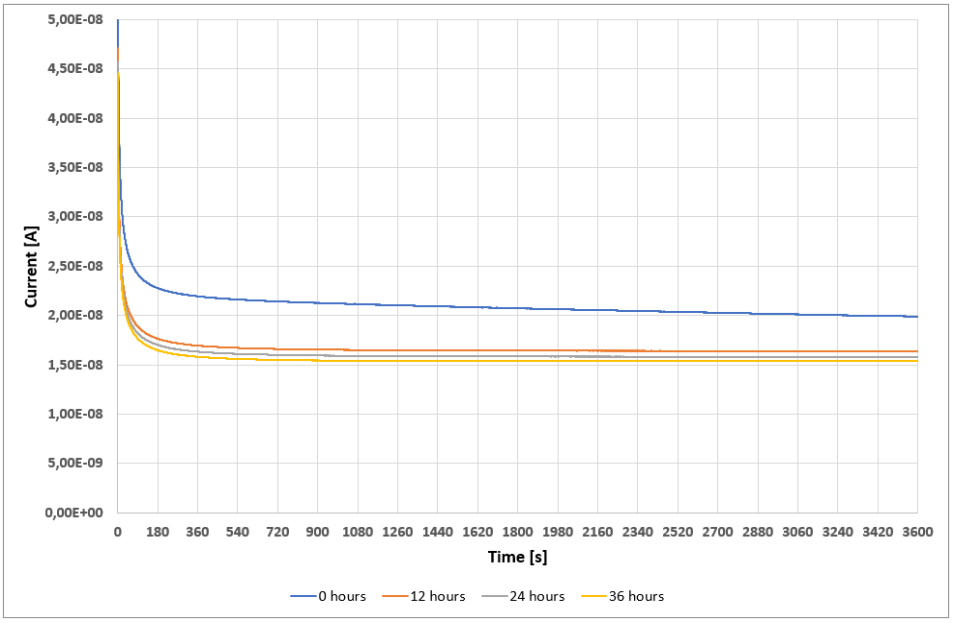

Figure A.3: Measured polarization current during impregnation of a sample with 10 paper sheets at U = 1kV and T = 100°C.

Table A.3: Data of measured DC currents during impregnation of a sample with 5 paper sheets at U = 1kV and T = 100°C.

Time [h]	DC current [A]	Time constant [seconds]
0	2×10^{-8}	25 000
12	1.64×10^{-8}	50 000
24	1.54×10^{-8}	50 000
36	1.54×10^{-8}	50 000

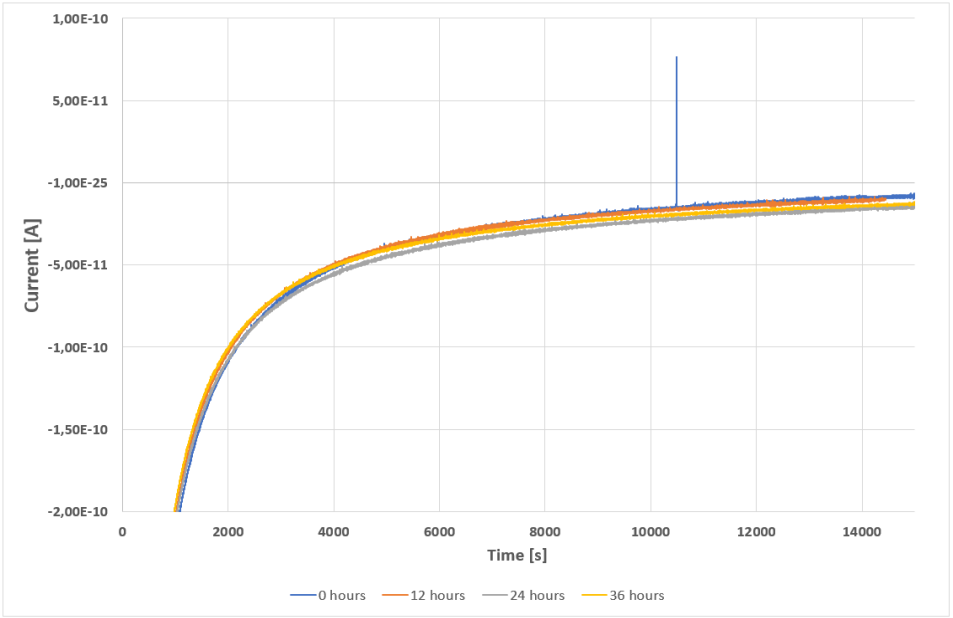

Figure A.4: Measured depolarization current during impregnation of a sample with 10 paper sheets at U = 1kV and T = 100°C.

Table A.4: Data of measured current at the end of depolarization duration during impregnation of a sample with 5 paper sheets at U = 1kV and T = 100°C.

Time [h]	”End of depol”-current [A]
0	-7.18×10^{-12}
12	-8.5×10^{-12}
24	-1.39×10^{-12}
36	-1.35×10^{-12}

A.3 Measured currents at prolonged polarization and depolarization durations of a paper sample

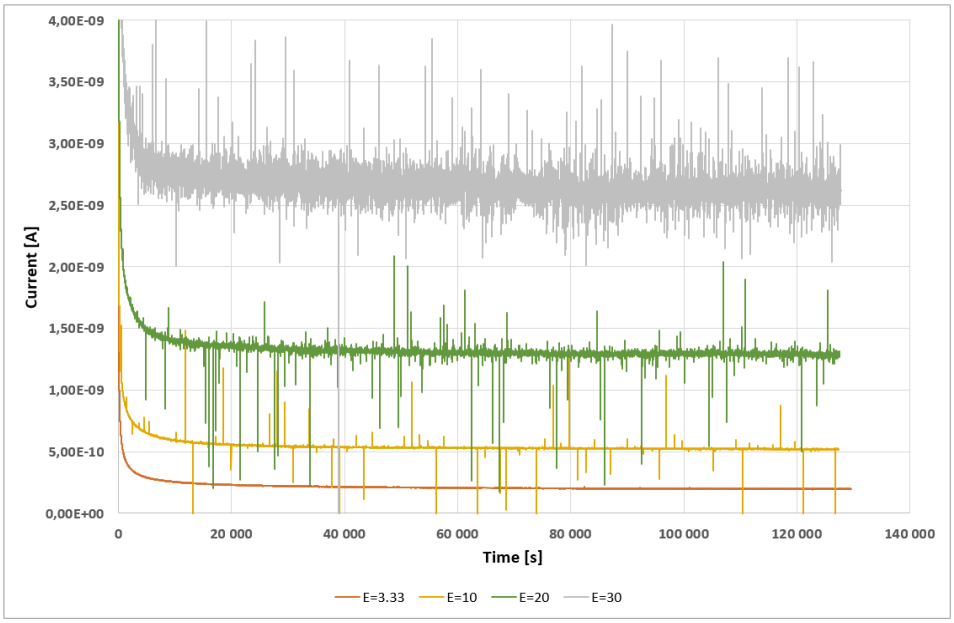

Figure A.5: Measured current at long polarization durations of a sample with 10 paper sheets at various electric field strengths and T = 50°C.

Table A.5: Data of measured DC currents at long polarization durations of a sample with 10 paper sheets at various electric field strengths and T = 50°C.

Electric field strength [kV/mm]	DC current [A]
3.33	1.98×10^{-10}
10	5.18×10^{-10}
20	1.28×10^{-9}
30	2.6×10^{-9}

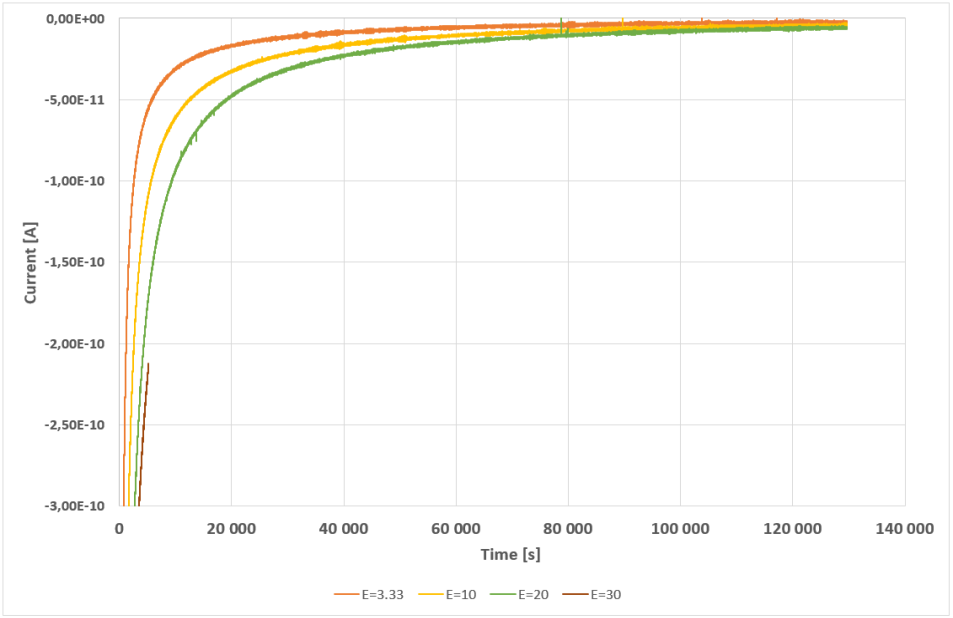

Figure A.6: Measured current at long depolarization duration of a sample with 10 paper sheets at various electric field strengths and T = 50°C.

Table A.6: Data of measured ”end of depol”-currents at long depolarization durations of a sample with 10 paper sheets at various electric field strengths and T = 50°C.

Electric field strength [kV/mm]	”End of depol”-current [A]
3.33	-2.6×10^{-12}
10	-5×10^{-12}
20	-6.8×10^{-12}
30	-2.14×10^{-10}

A.4 Measured currents at long polarization and depolarization periods of a bulk oil sample

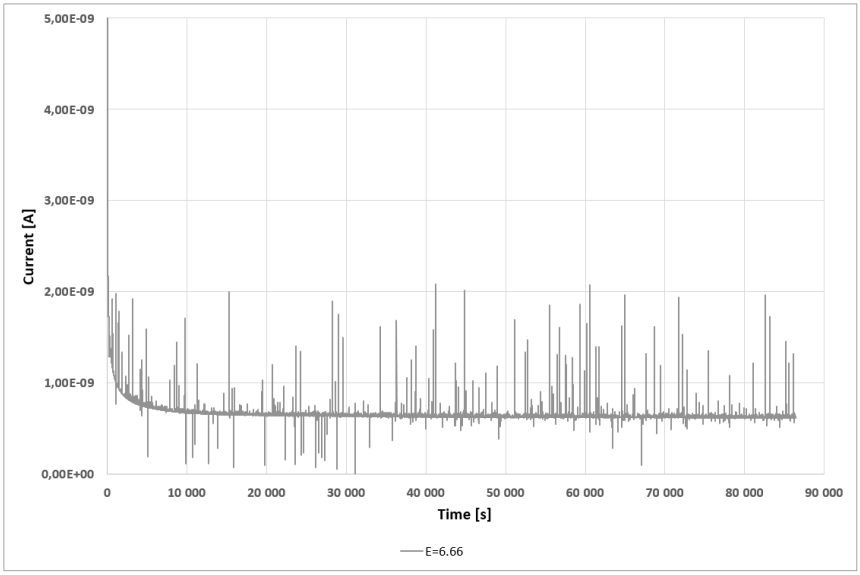

Figure A.7: Measured current at long polarization durations of a sample with 10 paper sheets and 11 bulk oil sheets at various electric field strengths and T = 50°*C*.

Table A.7: Data of measured DC currents at long polarization durations of a sample with 10 paper sheets and 11 bulk oil sheets at various electric field strengths and T = 50°*C*.

Electric field strength [kV/mm]	DC current [A]
6.66	6.17×10^{-10}

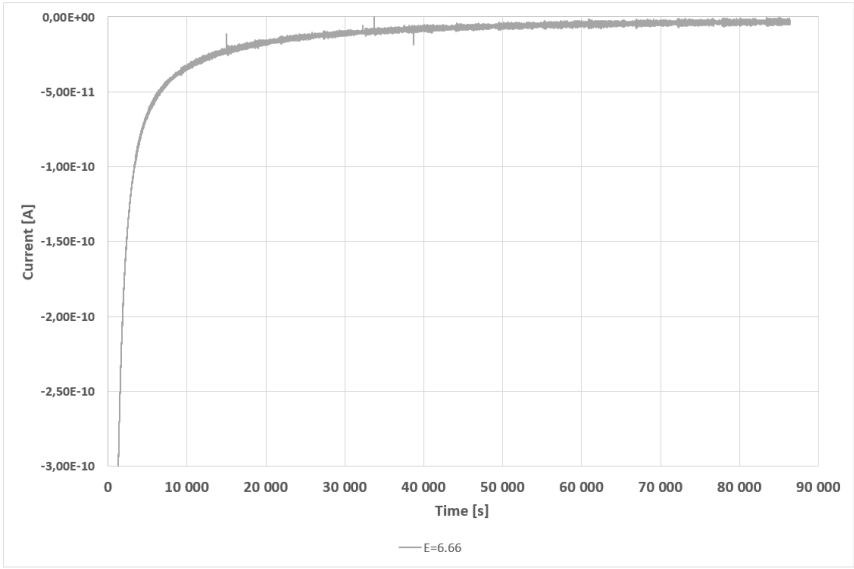

Figure A.8: Measured current at long depolarization duration of a sample with 10 paper sheets and 11 bulk oil sheets at various electric field strengths and T = 50°C.

Table A.8: Data of measured 'end of depol' currents at long depolarization durations of a sample with 10 paper sheets and 11 bulk oil sheets at various electric field strengths and T = 50°C.

Electric field strength [kV/mm]	**"End of depol"-current [A]**
6.66	-3.82×10^{-12}

A.5 Measured currents of a sample with 10 paper sheets varying the applied temperature

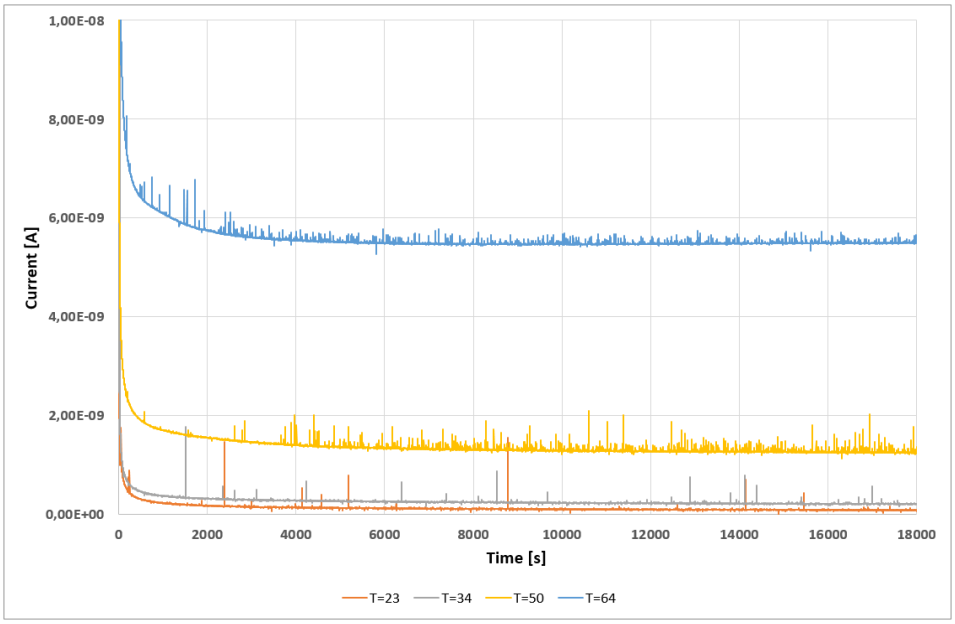

Figure A.9: Measured polarization current of a sample with 10 paper sheets at T = 23°*C* to T = 64°*C* and E = 20 kV/mm.

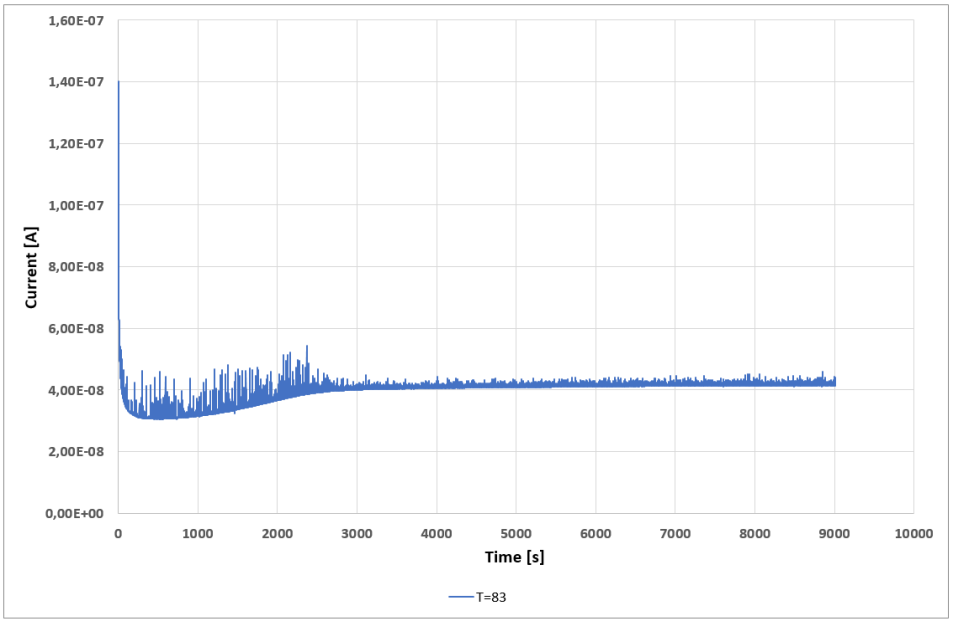

Figure A.10: Measured polarization current of a sample with 10 paper sheets at T = 83°C and E = 20 kV/mm.

Table A.9: Data of measured DC currents of a sample with 10 paper sheets at various temperatures and E = 20 kV/mm.

Temperature [°C]	**DC current [A]**
23	7×10^{-11}
34	2×10^{-10}
50	1.24×10^{-9}
64	5.46×10^{-9}
83	4.15×10^{-8}

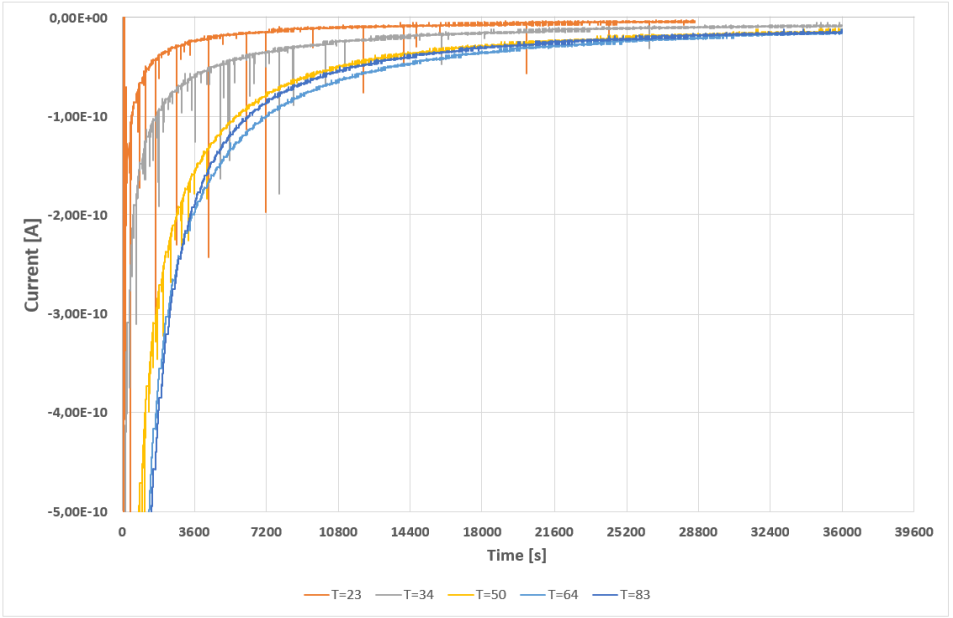

Figure A.11: Measured depolarization current of a sample with 10 paper sheets at various temperatures in Celsius and E = 20 kV/mm.

Table A.10: Data of measured 'end of depol' currents of a sample with 10 paper sheets various temperatures and E = 20 kV/mm.

Temperature [$^{\circ}C$]	**"End of depol"-current [A]**
23	-4.93×10^{-12}
34	-8×10^{-12}
50	-1.4×10^{-11}
64	-1.5×10^{-11}
83	-1.54×10^{-11}

A.6 Measured currents of a sample with 5 paper sheets varying the applied electric field strength

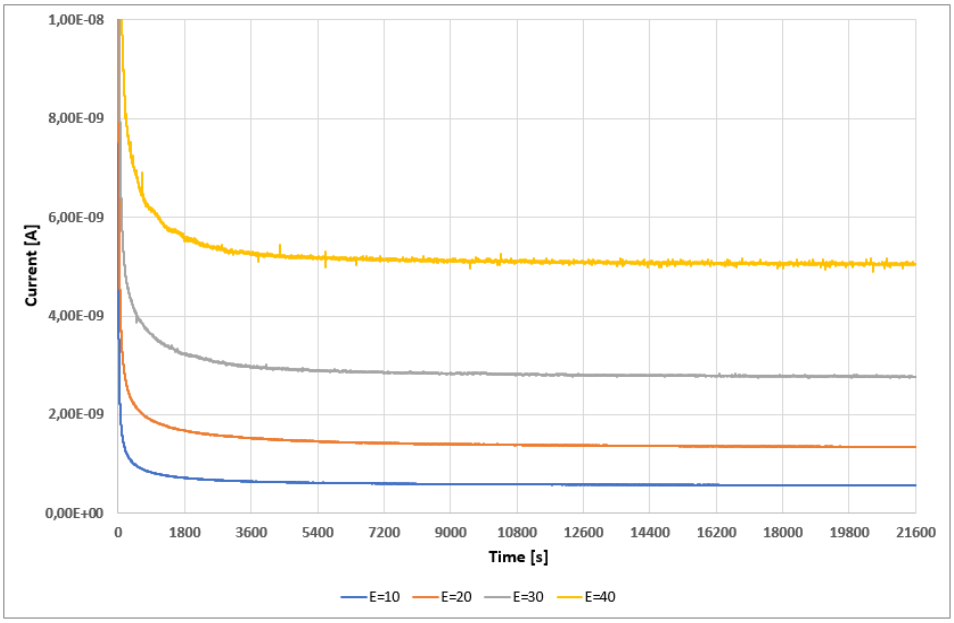

Figure A.12: Measured polarization current of a sample with 5 paper sheets at various electric field strengths and T = 50°*C*.

Table A.11: Data of measured DC currents of a sample with 5 paper sheets at various electric field strengths and T = 50°*C*.

Electric field strength [kV/mm]	DC current [A]
10	5×10^{-10}
20	1.35×10^{-9}
30	2.76×10^{-9}
40	5.05×10^{-9}

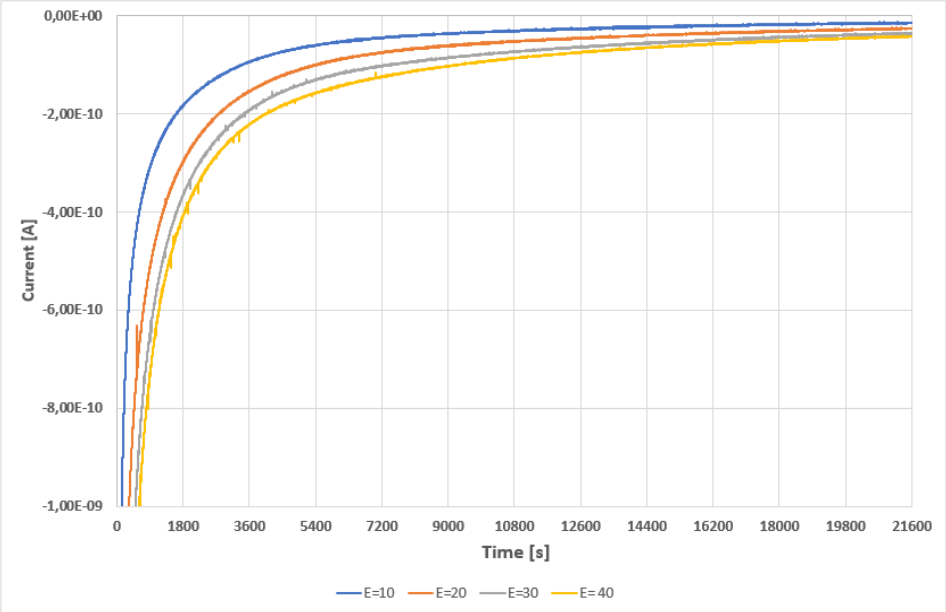

Figure A.13: Measured polarization current of a sample with 5 paper sheets at various electric field strengths and T = 50°C.

Table A.12: Data of measured 'end of depol' currents of a sample with 5 paper sheets at various electric field strengths and T = 50°C.

Electric field strength [kV/mm]	"End of depol"-current [A]
10	-1.17×10^{-11}
20	-3.46×10^{-11}
30	-4.1×10^{-11}
40	-4.2×10^{-11}

A.7 Measured currents of a sample with 10 paper sheets varying the applied electric field strength

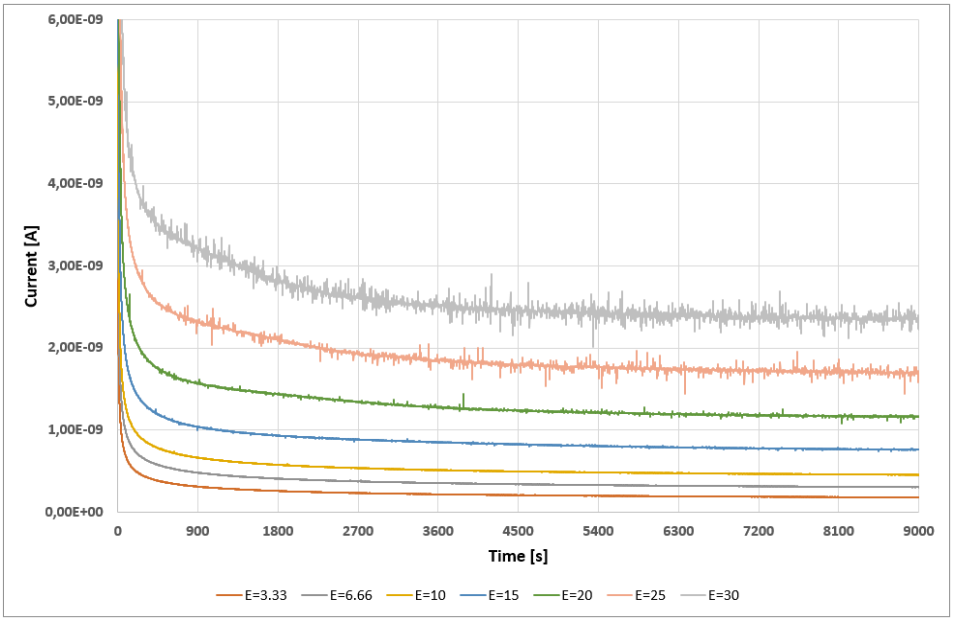

Figure A.14: Measured polarization current of a sample with 10 paper sheets at various electric field strengths and T = 50°*C*.

Table A.13: Data of measured DC currents of a sample with 10 paper sheets at various electric field strengths and T = 50°*C*.

Electric field strength [kV/mm]	DC current [A]
3.33	1.6×10^{-10}
6.66	2.8×10^{-10}
10	4.26×10^{-10}
15	7.26×10^{-10}
20	1.11×10^{-9}
25	1.65×10^{-9}
30	2.32×10^{-9}

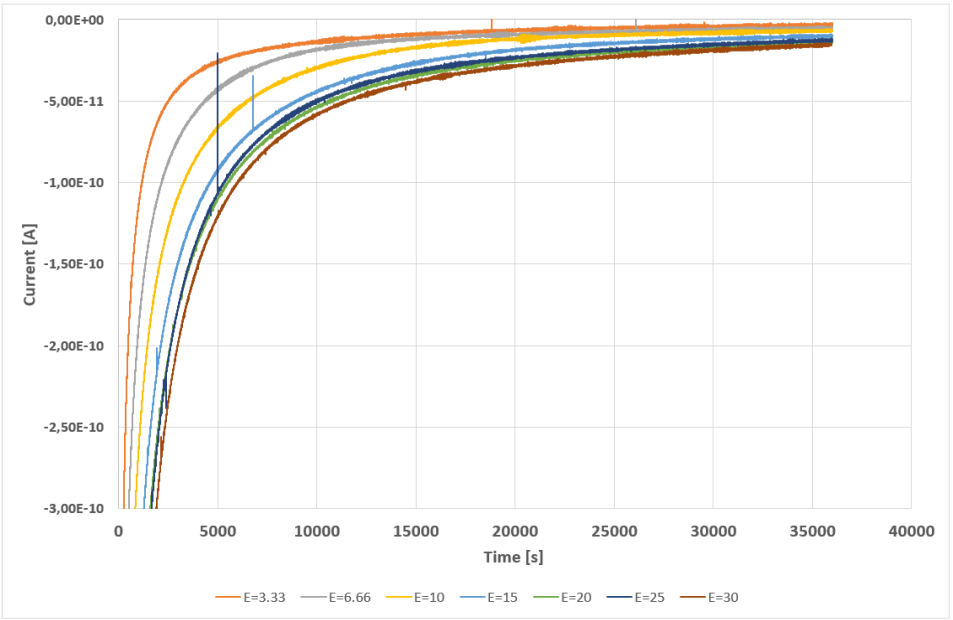

Figure A.15: Measured depolarization current of a sample with 10 paper sheets at various electric field strengths and T = 50°C.

Table A.14: Data of measured 'end of depol' currents of a sample with 10 paper sheets at various electric field strengths and T = 50°C.

Electric field strength [kV/mm]	End of 'depol' current [A]
3.33	-2.18×10^{-12}
6.66	-5.2×10^{-12}
10	-6.77×10^{-12}
15	-1×10^{-11}
20	-1.46×10^{-11}
25	-1.28×10^{-11}
30	-1.58×10^{-11}

A.8 Measured currents of a sample with 14 paper sheets varying the applied electric field strength

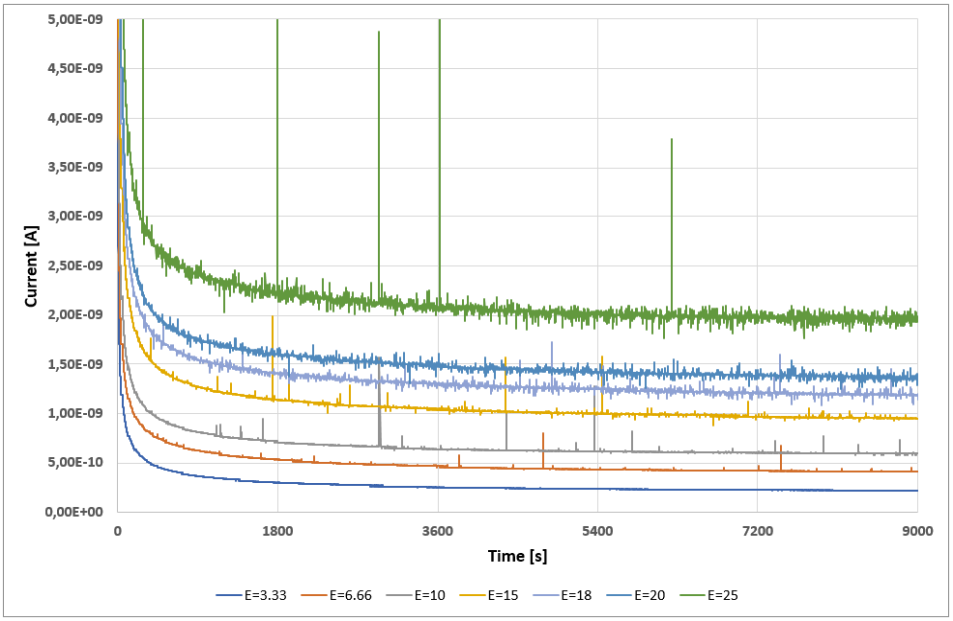

Figure A.16: Measured polarization current of a sample with 14 paper sheets at various electric field strengths and T = 50°*C*.

Table A.15: Data of measured DC currents at of a sample with 14 paper sheets at various electric field strengths and T = 50°*C*.

Electric field strength [kV/mm]	DC current [A]
3.33	2.16×10^{-10}
6.66	4.07×10^{-10}
10	5.92×10^{-10}
15	9.31×10^{-10}
18	1.17×10^{-9}
20	1.35×10^{-9}
25	1.95×10^{-9}

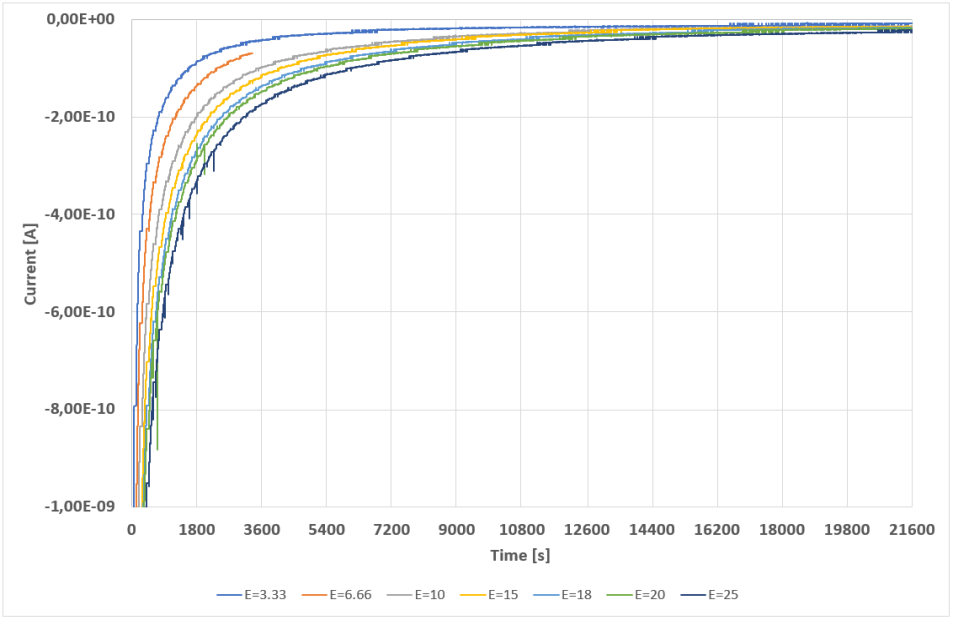

Figure A.17: Measured depolarization current of a sample with 14 paper sheets at various electric field strengths and T = 50°C.

Table A.16: Data of measured 'end of depol' currents of a sample with 14 paper sheets at various electric field strengths and T = 50°C.

Electric field strength [kV/mm]	"End of depol"-current [A]
3.33	-7.95×10^{-12}
6.66	-6.85×10^{-11}
10	-1.19×10^{-11}
15	-1.52×10^{-11}
18	-1.74×10^{-11}
20	-1.88×10^{-11}
25	-2.4×10^{-11}

A.9 Measured currents of a sample with 10 paper sheets and 1 bulk oil sheet varying the mean electric field strength

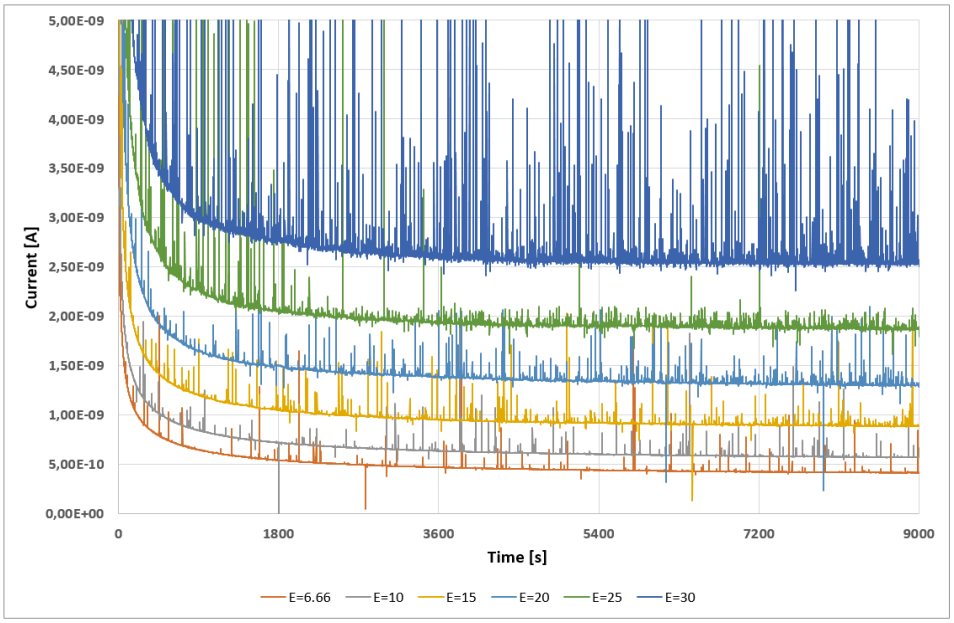

Figure A.18: Measured polarization current of a sample with 10 paper sheets and 1 bulk oil sheet at various electric field strengths and T = 50°C.

Table A.17: Data of measured DC currents of a sample with 10 paper sheets and 1 bulk oil sheet at various electric field strengths and T = 50°C.

Electric field strength [kV/mm]	DC current [A]
6.66	3.87×10^{-10}
10	5.42×10^{-10}
15	8.5×10^{-10}
20	1.26×10^{-9}
25	1.83×10^{-9}
30	2.57×10^{-9}

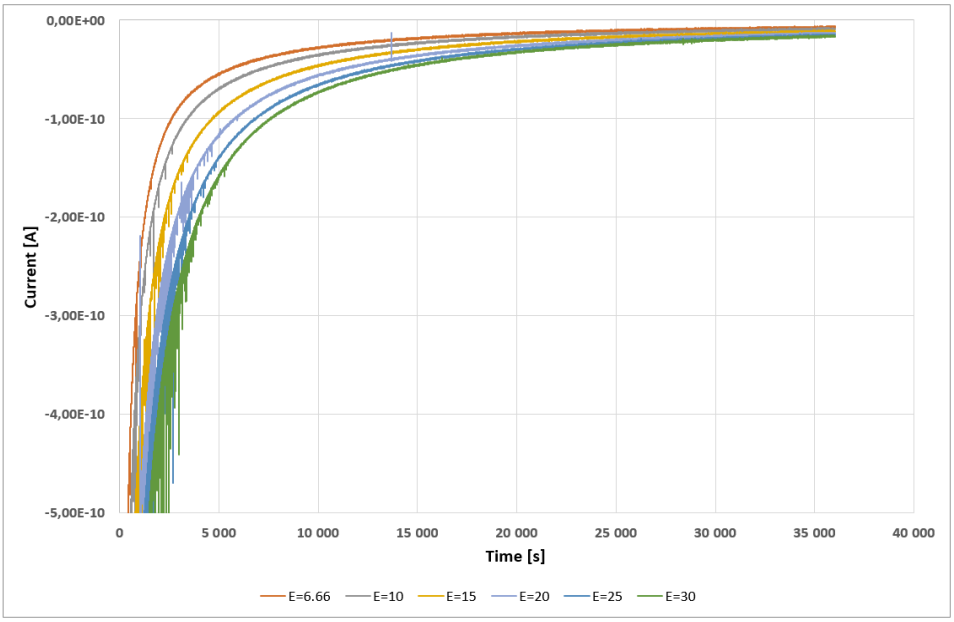

Figure A.19: Measured polarization current of a sample with 10 paper sheets and 1 bulk oil sheet at various electric field strengths and T = 50°C.

Table A.18: Data of measured 'end of depol' currents of a sample with 10 paper sheets and 1 bulk oil sheet at various electric field strengths and T = 50°C.

Electric field strength [kV/mm]	"End of depol"-current [A]
6.66	-7.97×10^{-12}
10	-8.75×10^{-12}
15	-1×10^{-11}
20	-1.41×10^{-11}
25	1.57×10^{-11}
30	1.66×10^{-11}

A.10 Measured currents of a sample with 10 paper sheets and 4 bulk oil sheet varying the mean electric field strength

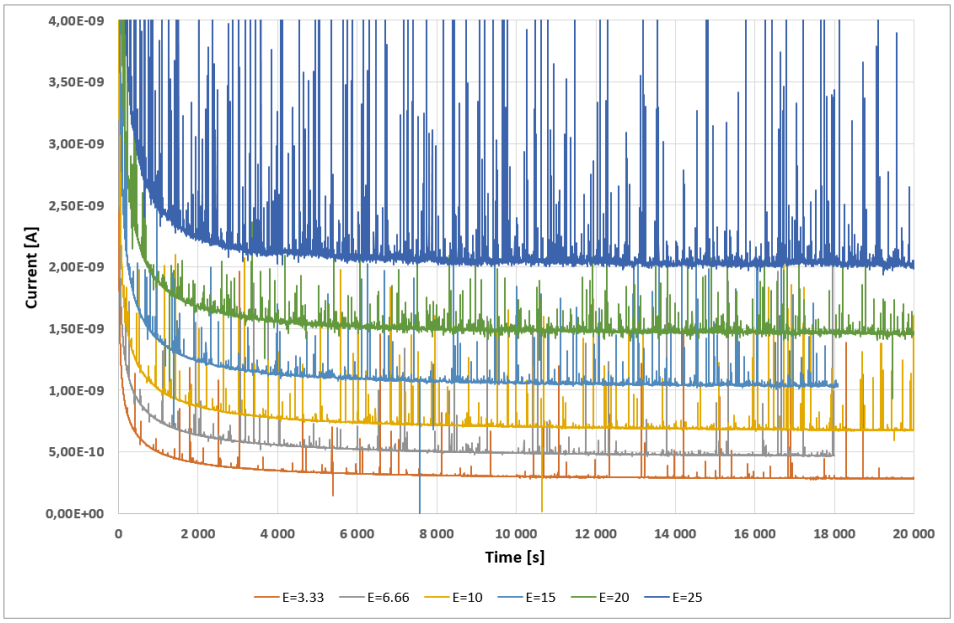

Figure A.20: Measured polarization current of a sample with 10 paper sheets and 4 bulk oil sheet at various electric field strengths and T = 50°C.

Table A.19: Data of measured DC currents of a sample with 10 paper sheets and 4 bulk oil sheet at various electric field strengths and T = 50°C.

Electric field strength [kV/mm]	DC current [A]
3.33	1.7×10^{-10}
6.66	4.69×10^{-10}
10	6.6×10^{-10}
15	1×10^{-9}
20	1.46×10^{-9}
25	2×10^{-9}

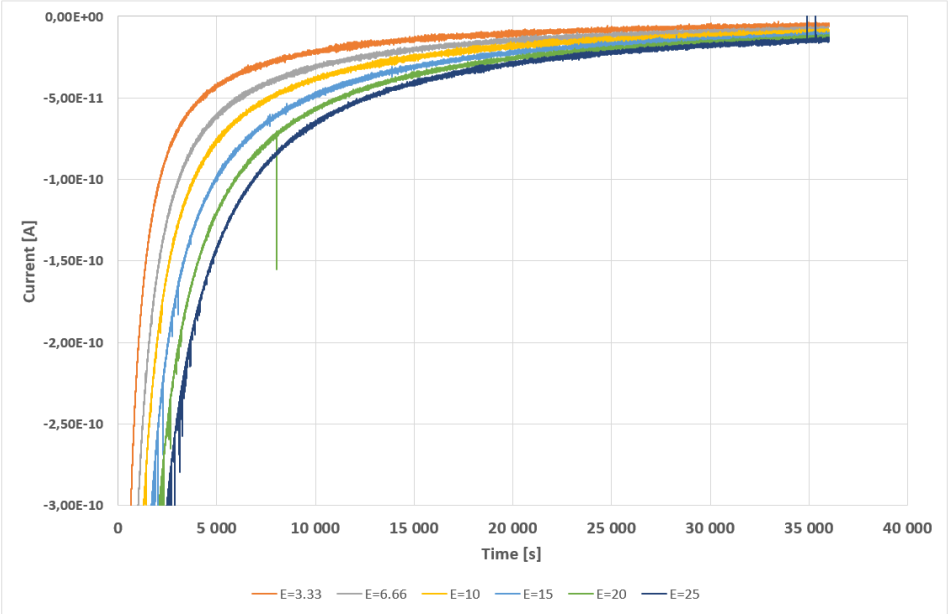

Figure A.21: Measured polarization current of a sample with 10 paper sheets and 4 bulk oil sheet at various electric field strengths and T = 50°C.

Table A.20: Data of measured 'end of depol' currents of a sample with 10 paper sheets and 4 bulk oil sheet at various electric field strengths and T = 50°C.

Electric field strength [kV/mm]	"End of depol"-current [A]
3.33	-5.25×10^{-12}
6.66	-2.13×10^{-12}
10	-8.57×10^{-12}
15	-6.15×10^{-11}
20	-1.27×10^{-11}
25	1.48×10^{-11}

A.11 Measured currents of a sample with 10 paper sheets and 7 bulk oil sheet varying the mean electric field strength

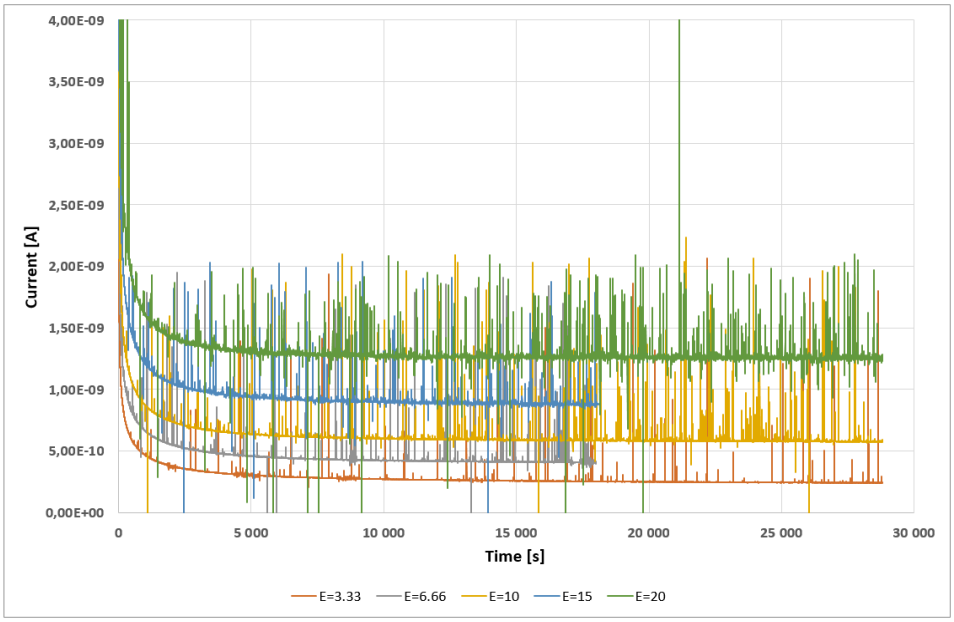

Figure A.22: Measured polarization current of a sample with 10 paper sheets and 7 bulk oil sheet at various electric field strengths and T = 50°C.

Table A.21: Data of measured DC currents of a sample with 10 paper sheets and 7 bulk oil sheet at various electric field strengths and T = 50°C.

Electric field strength [kV/mm]	DC current [A]
3.33	2.42×10^{-10}
6.66	4.06×10^{-10}
10	5.82×10^{-10}
15	8.75×10^{-10}
20	1.26×10^{-9}

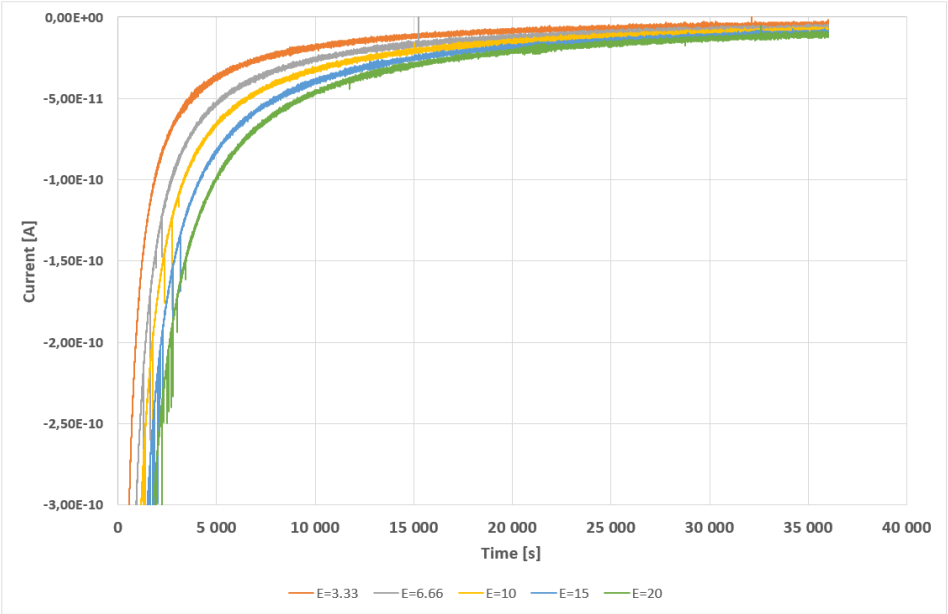

Figure A.23: Measured polarization current of a sample with 10 paper sheets and 7 bulk oil sheet at various electric field strengths and T = 50°C.

Table A.22: Data of measured 'end of depol' currents of a sample with 10 paper sheets and 7 bulk oil sheet at various electric field strengths and T = 50°C.

Electric field strength [kV/mm]	"End of depol"-current [A]
3.33	-4.6×10^{-12}
6.66	-5.13×10^{-12}
10	-7.26×10^{-12}
15	-8.9×10^{-12}
20	-1.1×10^{-11}

A.12 Measured currents of a sample with 10 paper sheets and 11 bulk oil sheet varying the mean electric field strength

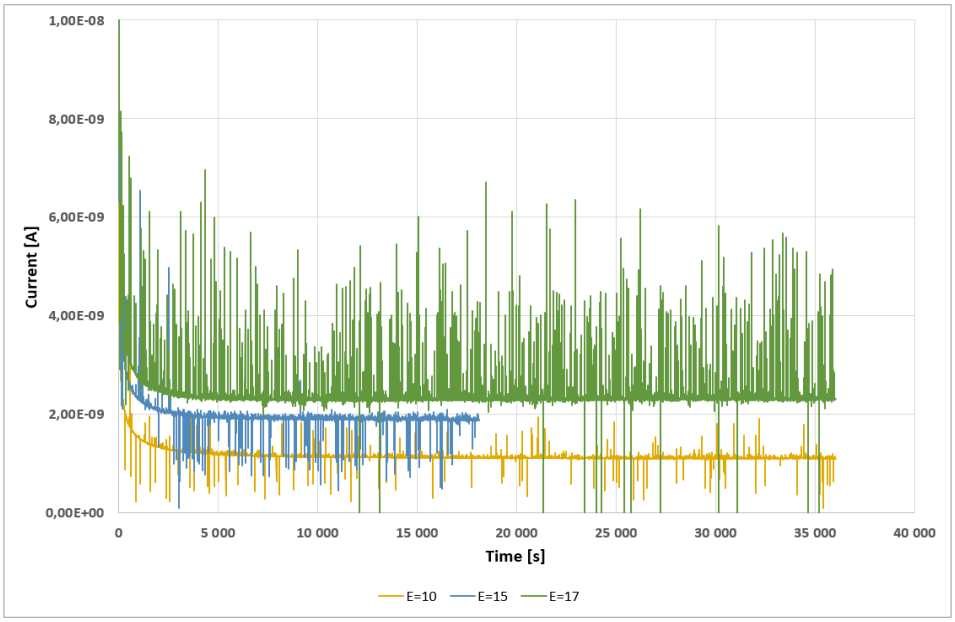

Figure A.24: Measured polarization current of a sample with 10 paper sheets and 11 bulk oil sheet at various mean electric field strengths and T = 50°*C*.

Table A.23: Data of measured DC currents of a sample with 10 paper sheets and 11 bulk oil sheet at various electric field strengths and T = 50°*C*.

Electric field strength [kV/mm]	DC current [A]
10	1.1×10^{-9}
15	1.88×10^{-9}
17	2.31×10^{-9}

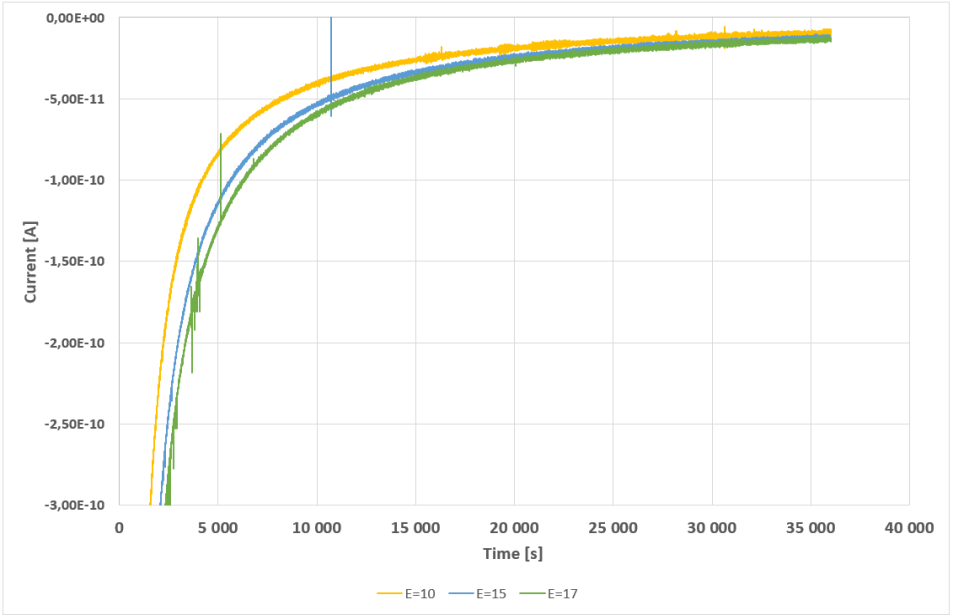

Figure A.25: Measured polarization current of a sample with 10 paper sheets and 11 bulk oil sheet at various mean electric field strengths and T = 50°C.

Table A.24: Data of measured 'end of depol' currents of a sample with 10 paper sheets and 11 bulk oil sheet at various electric field strengths and T = 50°C.

Electric field strength [kV/mm]	"End of depol"-current [A]
10	-1×10^{-11}
15	-1.2×10^{-11}
20	$-1.1.4 \times 10^{-11}$

A.13 Measured currents of a sample with 10 paper sheets and 1 butt gap sheet varying the mean electric field strength

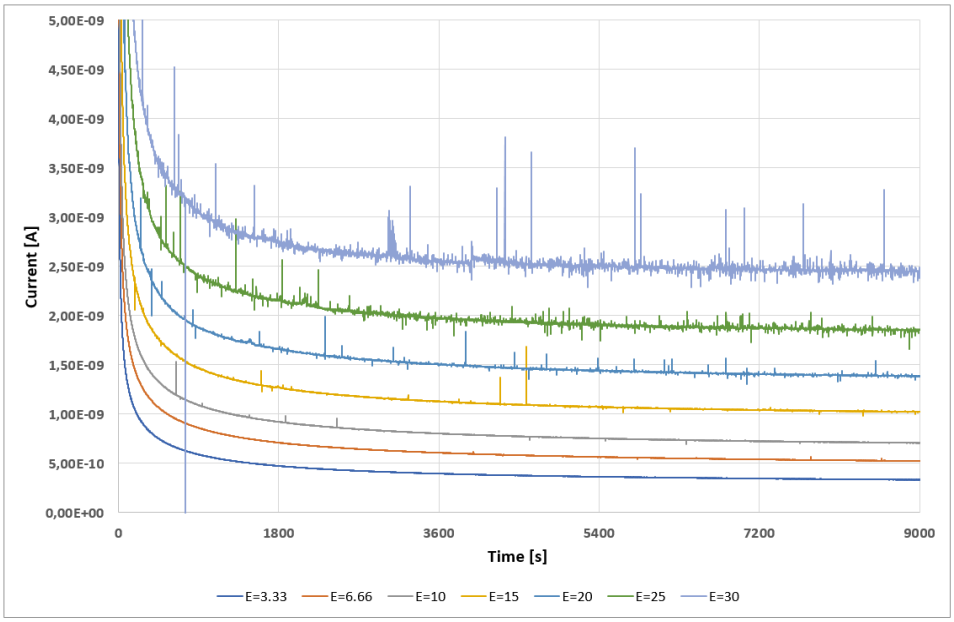

Figure A.26: Measured polarization current of a sample with 10 paper sheets and 1 butt gap sheet at various mean electric field strengths and T = 50°*C*.

Table A.25: Data of measured DC currents of a sample with 10 paper sheets and 1 butt gap sheet at various electric field strengths and T = 50°*C*.

Electric field strength [kV/mm]	DC current [A]
3.33	3.4×10^{-10}
6.66	5.248×10^{-10}
10	7.08×10^{-10}
15	1.02×10^{-9}
20	1.39×10^{-9}
25	1.85×10^{-9}
30	2.45×10^{-9}

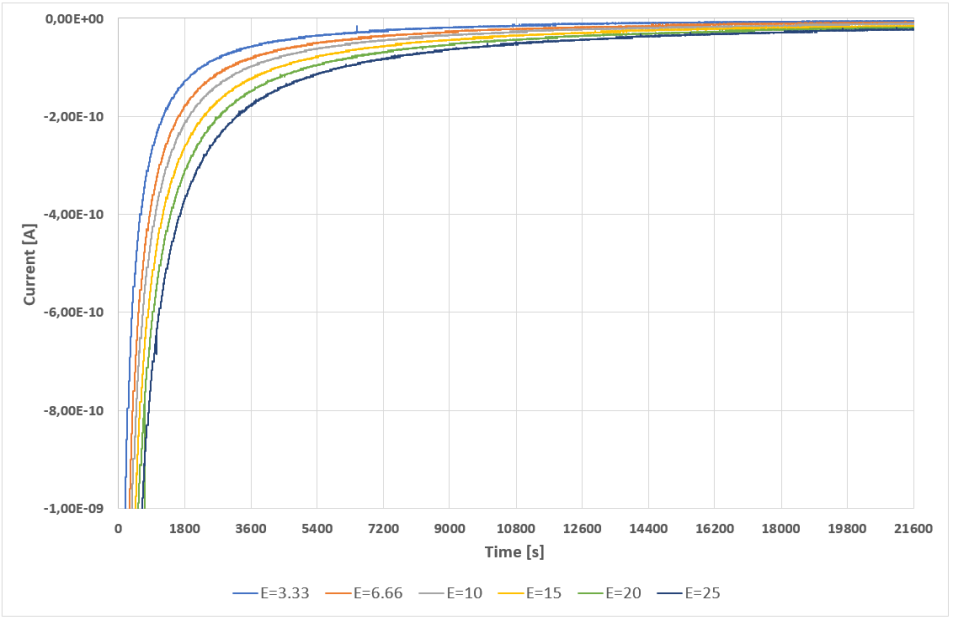

Figure A.27: Measured polarization current of a sample with 10 paper sheets and 1 butt gap sheet at various mean electric field strengths and T = 50°C.

Table A.26: Data of measured 'end of depol' currents of a sample with 10 paper sheets and 1 butt gap sheet at various electric field strengths and T = 50°C.

Electric field strength [kV/mm]	"End of depol"-current [A]
3.33	-5.72×10^{-12}
6.66	-9.56×10^{-12}
10	-1.21×10^{-11}
15	-1.6×10^{-11}
20	-1.94×10^{-11}
25	-2.32×10^{-11}
30	-2.72×10^{-11}

A.14 Measured currents of a sample with 2 paper sheets and 7 butt gap sheet varying the mean electric field strength

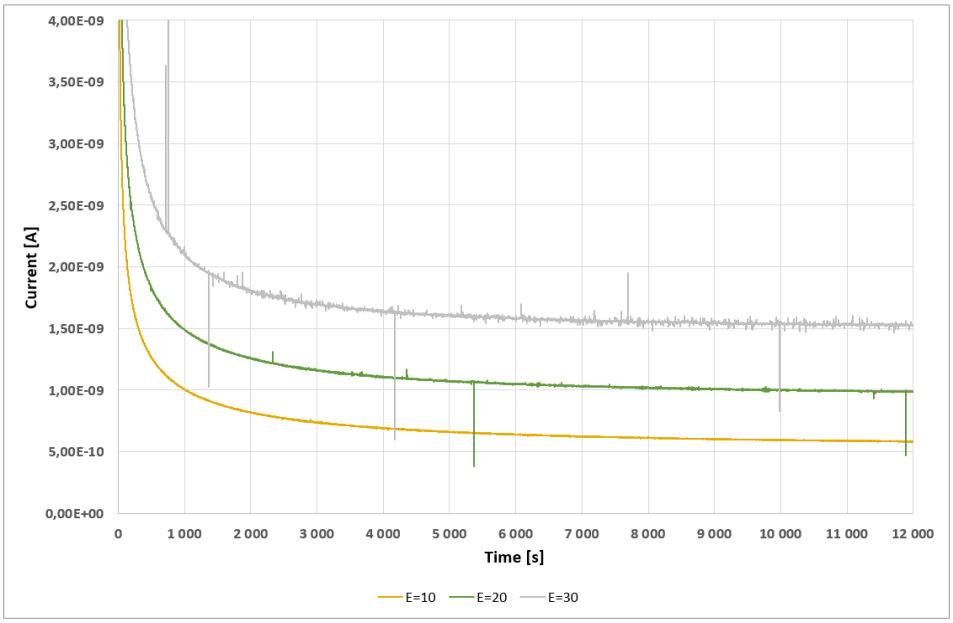

Figure A.28: Measured polarization current of a sample with 2 paper sheets and 7 butt gap sheet at various mean electric field strengths and T = 50°C.

Table A.27: Data of measured DC currents of a sample with 2 paper sheets and 7 butt gap sheet at various electric field strengths and T = 50°C.

Electric field strength [kV/mm]	DC current [A]
10	5.9×10^{-10}
20	1×10^{-9}
30	1.54×10^{-9}

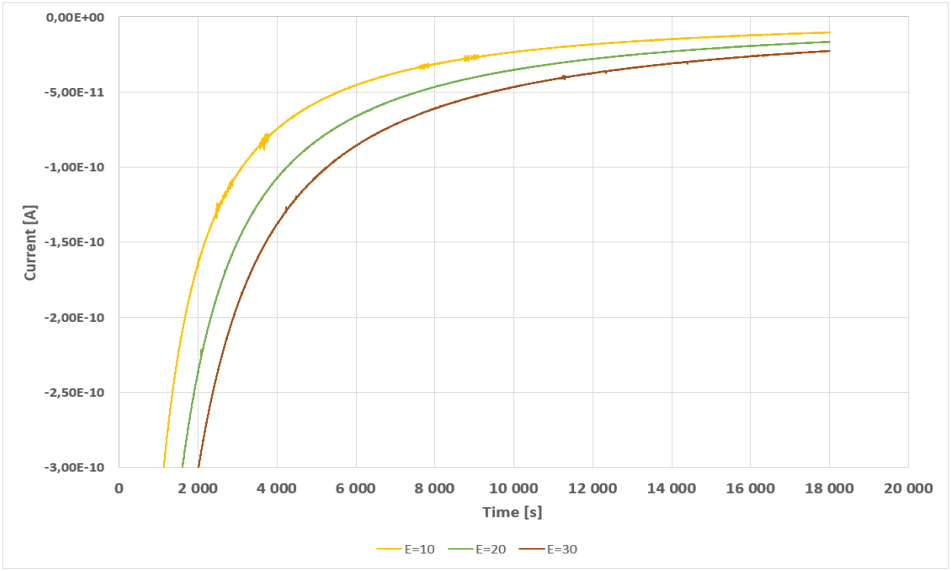

Figure A.29: Measured polarization current of a sample with 2 paper sheets and 7 butt gap sheet at various mean electric field strengths and T = 50°C.

Table A.28: Data of measured 'end of depol' currents of a sample with 2 paper sheets and 7 butt gap sheet at various electric field strengths and T = 50°C.

Electric field strength [kV/mm]	"End of depol"-current [A]
10	-1.05×10^{-11}
20	-1.68×10^{-11}
30	-2.28×10^{-11}

A.15 Measured capacitances for the study of thermal equilibrium in all samples

Table A.29: Collection of all capacitances measured for all samples used to study thermal equilibrium in all samples. Temperature was 50 $°C$.

Sample			Capacitance			
Paper sheets	**Butt gap sheets**	**Oil sheets**	**0 day**	**1 day**	**3 days**	**7 days**
10 (first iteration)	0	0	1,75E-10		1,77E-10	1,78E-10
10 (second iteration)	0	0	1,15E-10	1,70E-10		1,83E-10
10	0	1	5,08E-11	5,80E-11		6,09E-11
10	0	4	3,43E-11	3,63E-11		4,43E-11
10	0	7	2,20E-11	2,27E-11		2,39E-11
10	0	11	2,34E-11	2,54E-11		2,74E-11
10	1	0	5,98E-11	7,53E-11	7,61E-11	
2	7	0	4,91E-11	5,10E-11		